Thesis submitted for a
Doctor of Philosophy Degree

FLOW IN CENTRIFUGAL PUMPS WORKING AT PART CAPACITY

by

FRANC SCHWEIGER, Dipl. Ing.

Special Research Fellow
at the University of Glasgow

December, 1965

Department of Aeronautics and Fluid Mechanics
The University
Glasgow

Summary

The thesis attempts to analyse the flow and energy condition at zero discharge for a simplified radial impeller fitted in a cylindrical casing.

Considerable inward and outward flow was observed passing through the impeller and extending along the suction pipe. The discharge area was shared equally between inward and outward flow.

Two hydraulic systems were found to exist in the impeller, namely, those corresponding to a pump and a turbine. Part of the impeller was found to act as a pump and part as a turbine. The turbining effect was fairly large and had the effect of reducing the input power considerably. A linear relationship was found between the head and the power coefficients.

The geometry of the pump played an important role and had a great effect on the energy and flow conditions at the suction and discharge sides of the pump.

Decay of recirculatory flow along the suction pipe was very rapid and depended on the geometry of the pump and on viscous forces.

Theoretical results based on ideal fluid motion did not give sufficient information about the head reduction coefficient.

General behaviour of the head coefficient given by theory was found to follow the experimental results.

Acknowledgements

The author would like to thank the University of Glasgow for appointing him a Special Research Fellow to the Department of Aeronautics and Fluid Mechanics.

The author wishes to express his gratitude to the Head of the Department of Aeronautics and Fluid Mechanics, Professor T.R.F. Nonweiler, and to Dr. A.S. Thom for their technical assistance and advice.

Many thanks are also extended to Dr. A.W. Babister, Mr. F.H. Kelling, Mr. P.H. Tanner, Mr. D.A. Pirie and Miss A. Milne all of whom made my stay very pleasant by the friendly atmosphere they created.

Thanks are due to the Staff of the Workshop of the Faculty of Engineering without whose help the work could not have been satisfactorily completed.

The author wishes to express his sincere gratitude to the Ministry of Technology, London (D.S.I.R.) for their financial support in awarding to the University of Glasgow the contract which enabled him to undertake this research work.

Sincere thanks are given to the Director of the National Engineering Laboratory, and particularly to Dr. E.A. Spencer, Head of the Mechanics of Fluids Division, N.E.L., not only for accepting and supporting his candidature, but also for his personal attention.

The author thanks Dr. F.A.L. Winternitz, Director of Sigmund Pulsometer Pumps Limited for his kindness and understanding in every respect, and Dr. D.S. Myles and Mr. R.A. Nixon of N.E.L. for their valuable discussions and suggestions on the problem undertaken.

Last, but not least, thanks are due to all innumerous friends and former colleagues at the National Engineering Laboratory, who, in the friendliness they displayed, undoubtedly made valuable contributions to the work undertaken.

Contents

List of figures

List of Appendices

List of Plates

List of References

1. Reddy K.R.

   Relative eddy and its effects on the performance of a radial bladed centrifugal impeller.

   Journal of the Royal Aeronautical Society August 1954

2. Busemann A.

   Das Forderhohenverhaltnis radialer Kreiselpumpen mit logaritmische spiralen Schaufeln.

   Zeitschrift für Angewandte Mathematik and Mechanik Band 8, Heft 5, 1928

3. Fischer K. and Thoma D.

   Investigation of the flow conditions in a centrifugal pump.

   A.S.M.E. 1932; Vol.54; HYD - 54 - 8

4. Wislicenus G.F.

   Fluid mechanics of turbomachinery, 1947

5. Winternitz F.A.L.

   Probe measurements in three-dimensional flow

   Aircraft Engineering, August 1956

6. Winternitz F.A.L.
   Ramsay W.J.

   A cantilever Pitot cylinder for three-dimensional flow survey

   N.E.L. Report No.77

7. Worster R.G.

The flow in volutes and its effect on centrifugal pump performance.

Proceedings of the investigation of Mechanical Engineers

1963 - Vol.177 No.31

8. Stepanoff A.I.

Centrifugal and axial flow pumps. Page 39.

2nd edition 1957

9. Eckert B.

Axialkompressoren und Radialkompressoren, 1953

10. Kearton W.J.

The influence of the number of impeller blades on the pressure generated in a centrifugal compressor and on its general performance.

Proc. Mech. Eng. April 1933; Vol.124

11. Tognola S.

Further development of high-head storage pumps.

Escher Wyss News, No. 1/2/3/ Vol.33; 1960

12. Young L.
Nixon R.A.

Power, flow and pressure measurement in pump testing.

The Inst. of Mech. Engineers, 1960

13. Nixon R.A.

Eliminating rotation errors from pump head measurement.

Water and Water Engineering, Jan.1959 Vol.63

14. Nixon R.A.

Problems of Pump Head Measurement.

N.E.L. Report No.113 Sept. 1963

15. Worster R.C.
Zanker K.
Campbell I.A.
Fellermann L.

A comparison of air and water tests on centrifugal pumps.

B.H.R.A. SP 663 Oct. 1960

16. Myles D.J.

An investigation of the pressure and velocity distribution in centrifugal pumping machines, and the effect on this of varying the exit angles and number of rotor blades.

Ph.D. Thesis 1959

17. Pfleiderer C.

Die Kreiselpumpen, 1955

18. Stodola A.

Dampf und Gas Turbinen, 1926

19. Spannhake W.

Eine stromungstechnische Aufgabe der Kreiselradforschung und ein Satz zu ihrer Losung.

Mitt. d. Inst. f. Stromungsmaschinen Karlsruhe, 1930

20. Whitaker
Jones M.R.

Air flowmeter calibration equations for dence computer programme.

N.E.L. Fluid Mech. No.174 July, 1963

21. Rashed M.I.I.

Die Druckschwankungen in einer Zentrifugalpumpe und die rechnerische Bestimmung der Pumpencharakteristiken.

Mitteilungen aus dem Institut fur Hydraulik und Hydraulische Maschinen, Zurich.

22. Stahler A.F.

The slip factor of a Radial Bladed Centrifugal Compressor.

Journal of Engineering for Power, 1965

23. Eck. B.

Ventilatoren, 1953 Springer

Nomenclature

Symbols which are not listed below are defined in the text:

- H – head
- Q – volumetric flow rate
- N – power applied to the shaft
- u – peripheral velocity at discharge
- w – relative velocity
- C – absolute velocity
- C_m – meridional velocity
- C_u – tangential component of absolute velocity
- C_{u_z} – tangential component of absolute velocity at impeller outlet with z – blades
- C_{u_∞} – tangential component of absolute velocity at impeller outlet with infinite number of blades
- C_x – circumferential velocity
- C_y – velocity of flow
- β_2 – outlet angle
- z – number of blades
- D_1 – inlet diameter of impeller
- D_2 – outlet diameter of impeller
- D_3 – volute ring diameter
- b – width of casing
- b_2 – width of impeller
- ω – angular velocity
- n – number of revolutions

φ - flow coefficient

ψ - head coefficient

λ - power coefficient

σ - specific speed

ρ - specific density

1. INTRODUCTION

1.1 General

For many years successful design of centrifugal pumps has been based on the Euler theory. Theoretical knowledge combined with experimental data and designer's experience successfully proved that a predicted duty point i.e. point of maximum efficiency can be achieved in most cases. Pumps generate a head which is fairly close to predicted head and power consumption is no more than would be expected.

At points in the range where Q=o or less than, say 10% of Q normal the predicted values could give unreasonable and misleading results. It is believed that at low flow rates flow patterns through the suction pipe, entrance of the impeller, outlet of the impeller, through the impeller and in the casing gradually change their intermediate position and take a shape which is almost impossible to predict. Change of flow patterns is immediately indicated by the two main parameters concerned with the hydraulic research i.e. head and power. The behaviour of head and power characteristics becomes very uncertain and at flow rate Q=o difficult to understand.

It appears that the head is less than that predicted by theory and power consumption is more than expected. See figure 1. In

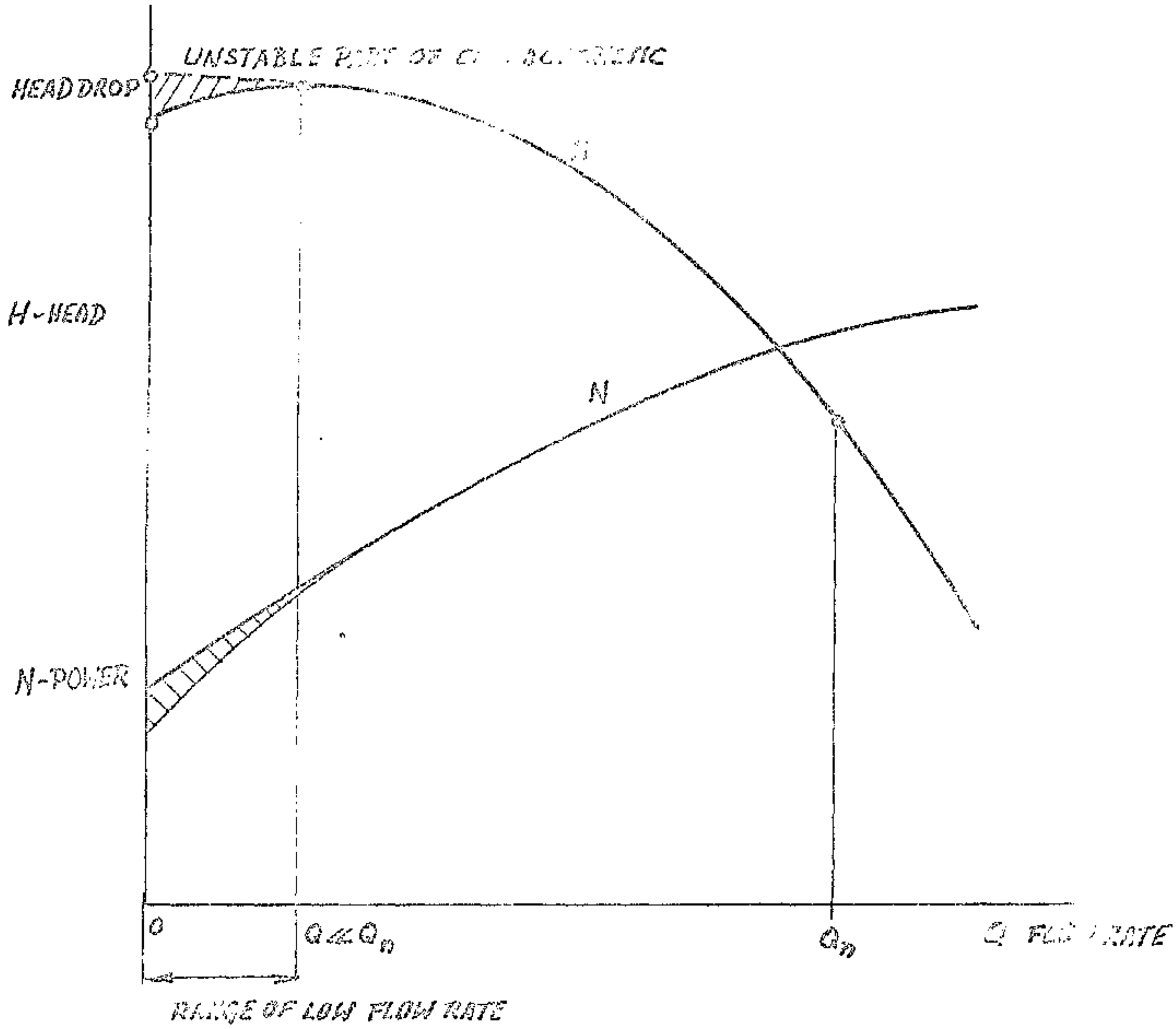

FIG. I Q–H CHARACTERISTIC

most cases the head and power characteristic curves have a peculiar shape with unexplained bumps and kinks. This may be due to a swirl which is developed along the suction pipe, at the inlet of the impeller as well as the flow conditions at the discharge of the impeller. See figure 2.

Any prediction of the head or power characteristics at low delivery is fruitless without substantial knowledge of what actually happens in a pump.

At the present time there is almost no information available which could throw any light on this problem.

The problem itself is most interesting and has a particular application in boiler-feed pumps, storage pumps etc. which require a stable (positive pressure gradient) flow head characteristic without bumps and loops. Actually it is desirable that any pumps or fan characteristic should be stable to avoid head-capacity fluctuations at start-off.

1.2 Introduction of the problem

A general idea of the problem at flow-rate Q=o has been given above.

All anomalies which occur in pumps within the range Q=normal (duty point) and Q=o could be split into two main causes:

a) prerotation

b) recirculation

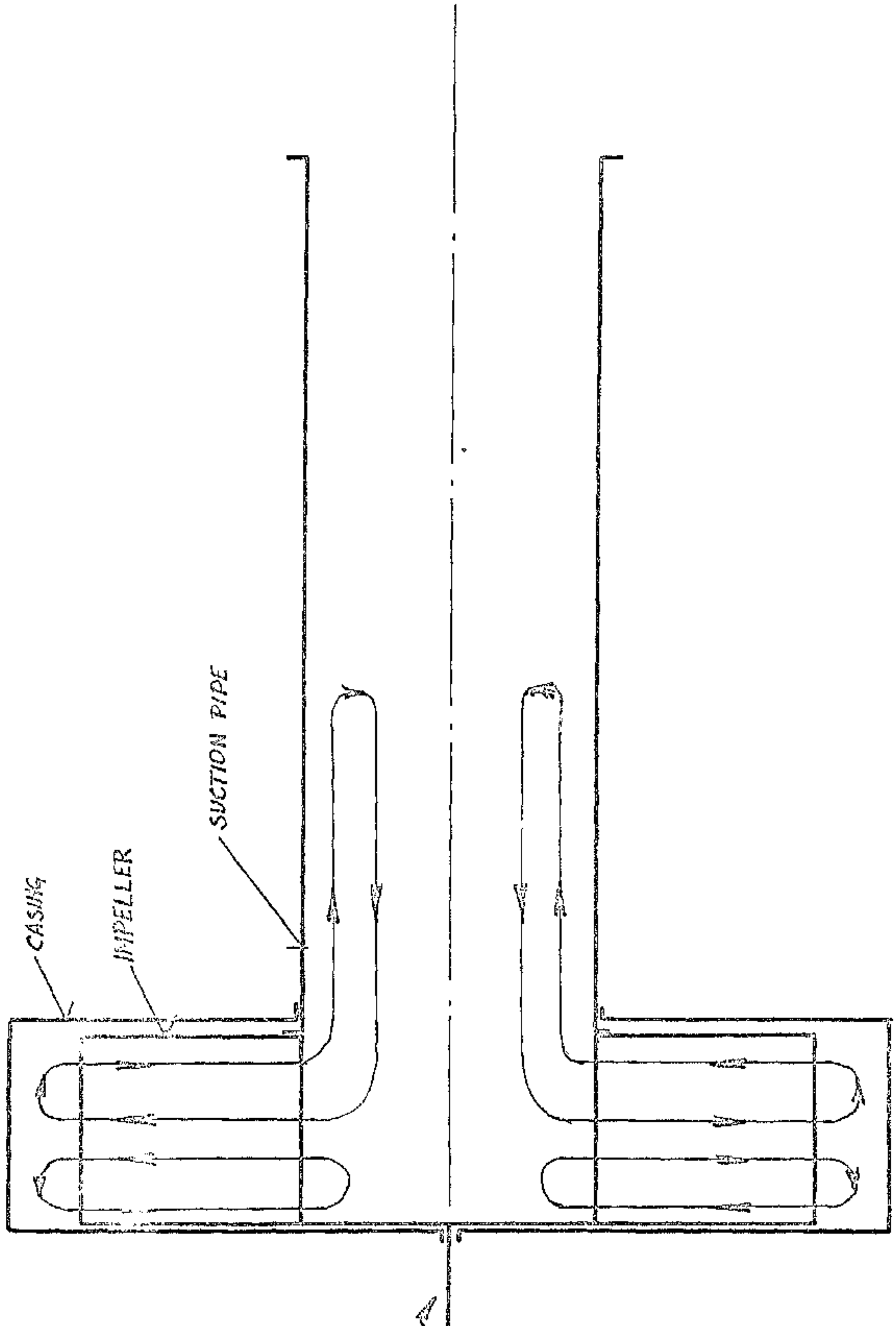

FIG. 2 FLOW PATTERN IN THE PUMP

It is obvious that resistance to flow is a minimum if the liquid enters the impeller at an angle which is very close or equal to the vane entrance angle. Differences in the angle of approach or in capacity indicate the magnitude of prerotation. From the velocity triangles it can be seen that only at one capacity (duty point) is the prerotation zero. At capacities smaller than normal the liquid should acquire prerotation to be able to enter with the minimum resistance. Steward (Ref.8) was one of the first investigators who established that prerotation existed in the suction pipe.

Strong back-flow or recirculation has been observed when the flow rate Q is reduced to zero. Similarly strong recirculation has been noticed at the discharge side.

The author believes that both the above mentioned phenomena depend mainly on the flow rate and on the geometry of the machine.

Present investigations have been concerned with the hydraulic conditions at zero flow rate.

As the geometry of machine is believed to be the main variable which influences the hydraulic parameters extensive theoretical and experimental studies have been carried out.

The first part of this thesis gives a short survey of basic theory of fluid motion at zero flow.

The second part extends curent theory and shows the influence of the geometry of the impeller on hydraulic parameters.

The third part gives analysis of experimental data and discusses theoretical results. In addition a more comprehensive survey is given of flow phenomena at shut-off valve condition.

2. FLOW AND ENERGY CONDITIONS IN CENTRIFUGAL PUMPS

2.1 Euler equation

The purpose of a centrifugal pump is to energize the fluid passing through it. Euler originally derived the simple theory which is generally applied to rotodynamic machines.

According to Kearton, Euler made the following assumptions: (Ref.10)

a) the velocities of fluid particles on different flow lines are equal to one another

b) the relative outlet velocities of all fluid particles are parallel to the tangents to the vanes.

c) the impeller passages are completely filled with the fluid

It is also assumed that the fluid enters the impeller without a tangential component, i.e. the absolute velocity at inlet is radial.

Thus the Euler equation becomes:

$$H = \frac{u_2\, c_{u_2}}{g} \tag{2.1}$$

This equation shows that all head is produced by circular motion around an axis. Transformation of equation 2.1 with reference to fig.3 leads to:

$$H = \frac{u_2^{\,2}}{g} - \frac{u_2\, c_{m_2}}{g\, \mathrm{tg}\beta_2} \tag{2.2}$$

When the flow approaches zero C_{u_2} becomes u_2. At zero flow equation 2.2 will be:

$$H = \frac{u_2^2}{g} \qquad 2.3$$

Plotting the equation 2.2 as $H = f\ (Q)$ a straight line is obtained which intersects the head axis at $\frac{u_2^2}{g}$

The actual characteristics of centrifugal machines do not match with Euler's theoretical performance. Total head as given by Euler's infinite blade theory is never obtained. The fluid in passing through the channels does not receive from the rotating blades the required design tangential velocity. This results in the fluid leaving the baldes at a smaller angle. Other phenomena which are entirely ignored in Euler's equation are relative eddies of the fluid within the impeller channel (see 2.2) and break away from the curved boundaries of the blade passage. In addition, friction losses and shock losses take place.

2.2 Relative eddy

Velocity distribution in the impeller channel is affected by relative circulation of the liquid. Consider a particle of the fluid in the impeller channel, see fig.4. At a certain time and position the particle will be pointing radially outward from the centre. The particle following the rotation of the impeller fails to turn with the impeller. This means, that a

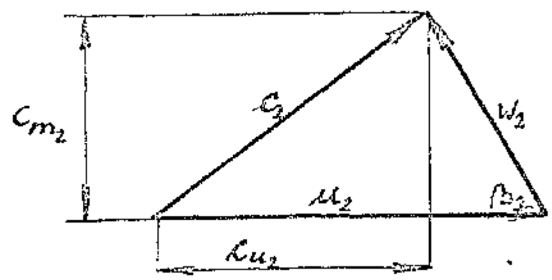

FIG. 3 DISCHARGE VELOCITY TRIANGLE

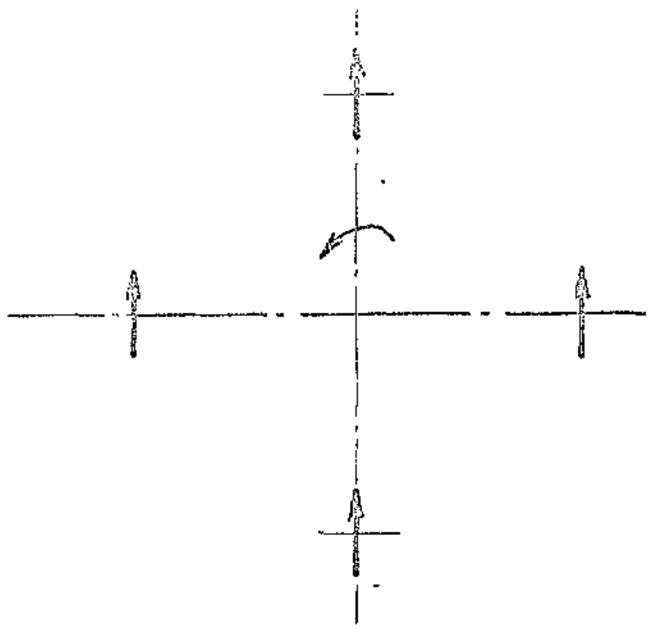

FIG. 4 ROTATION OF FLUID PARTICLE

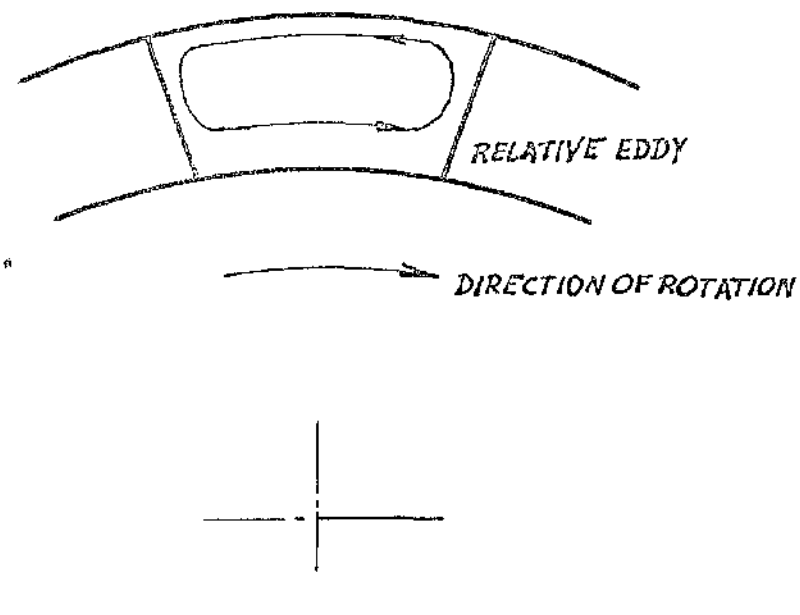

FIG. 5 RELATIVE EDDY

particle keeps its orientation while following the translatory movement around the shaft. It can be seen that during one revolution of the shaft the particle will have to rotate by one revolution about its own axis in the opposite direction. This results in relative eddy, see fig.5, which by superposition of flow through the impeller increases the velocities along the trailing face and reduces the velocities along the leading face. See fig.6.

The same conclusions are found taking into account supposition "a" and Bernoulli's equation. Supposition "a" implies that there is no difference in pressure across the blade channel and furthermore that the impeller does no work on the fluid. Since that is not true the necessary condition is that a pressure difference between leading and trailing face must exist. The latter statement requires similar velocity distribution (as shown in fig.6) and confirms the invalidity of the first Euler assumption. This conclusion was confirmed in practice by Uchimaru (Ref.8) who estimated the pressure differences between front and back of the vane.

The superposition of relative eddy on through flow at the outlet affects the Euler velocity triangle. See fig.7. The actual relative velocity W_2 is obtained by adding the tangential velocity σ_e due to relative eddy to the relative velocity w^1 which is tangential to the blade angle. Consequently the other

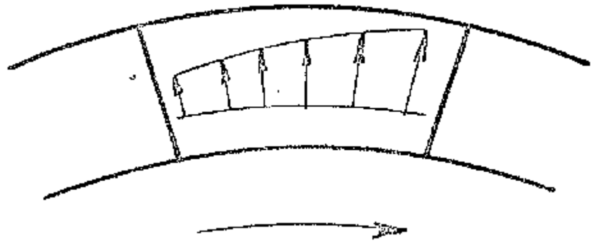

FIG. 6 VELOCITY DISTRIBUTION IN THE IMPELLER CHANNEL

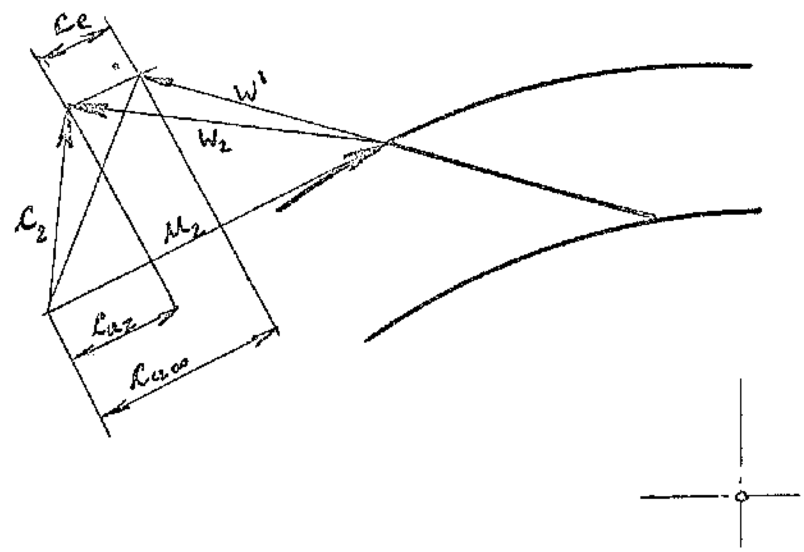

FIG. 7 SLIP EFFECT

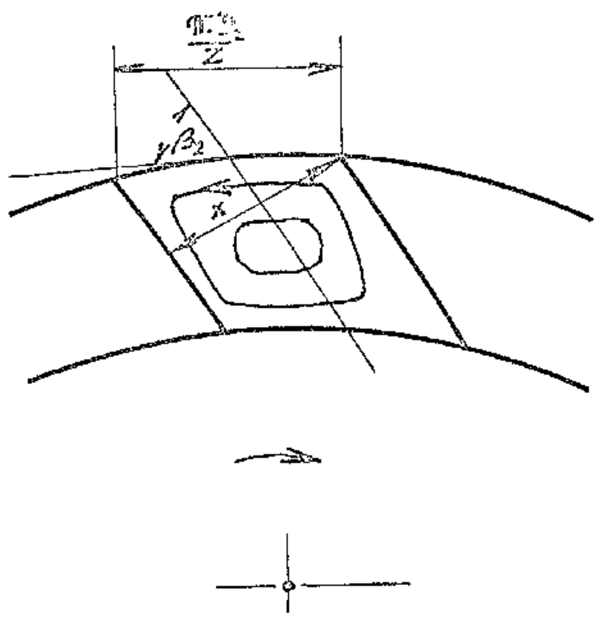

FIG. 8 STODOLA'S CORRECTION

velocities are changed. All these effects reduce the total head. Obviously, the deformation of Euler velocity triangles is smaller with a greater number of blades and vice versa. The deformation of the velocity triangle by the amount c_e is of great practical importance. Reduction of the velocity is usually defined by the expression c_{u_z} / c_{u_∞} and proper definition and deduction of this - called slip coefficient - has caused much argument and discussion.

A review of work already done on the above problem will be given below. Regardless of the approach of many authors, the entire work of estimating the value for c_{u_z} / c_{u_∞} can be split into two groups:

a) methods based on deriving the velocity correction from the rotation of the relative eddy by means of some simple approximation

b) methods based on the exact calculation of the absolute flow by means of the general theory and irrotational motion of frictionless fluid.

The first approach to determination of the slip coefficient c_{u_z} / c_{u_∞} was based on a proposal by Stodola (Ref.18) who suggested that the relative eddy velocity c_e is equal $\omega \frac{x}{2}$ where x

$x = \frac{\pi D_2}{z} \sin\beta_2$. See fig.8.

Then

$$c_e = \frac{\pi \mu_2}{z} \sin\beta_2 \qquad 2.4$$

and

$$\frac{c_{u_z}}{c_{u_\infty}} = \frac{c_{u_\infty} - c_e}{c_{u_\infty}} = 1 - \frac{\pi \mu_2 \sin\beta_2}{z\left(\mu_2 - \frac{Q}{\pi D_2 b_2} ctg\beta_2\right)} \qquad 2.5$$

The expression 2.5 does not involve energy loss but shows the amount of energy which the fluid can receive from the impeller.

Eck (Ref.23) improved Stodola's coefficient and gave the following equation:

$$\frac{C_{u_2}}{C_{u_\infty}} = \frac{1}{1 + \frac{\pi}{z}\left[\frac{\sin\beta_2}{1 - \frac{R_1}{R_2}}\right]^2} \qquad 2.6$$

This expression gives values of the slip coefficient considerably higher than those obtained by Stodola.

Pfleiderer (Ref.17) derived the slip coefficient by assuming that the pressure difference between leading and trailing face of the blade was constant along the channel and that linear velocity distribution exists across the channel.

The slip coefficient then becomes:

$$\frac{C_{u_2}}{C_{u_\infty}} = \frac{1}{1 + p} \qquad 2.7$$

where

$$p = \psi \frac{R_2}{z S} \qquad \psi = \tau \pi \sin\beta_2 \qquad S = \int_{R_1}^{R_2} R\,dx$$

and

τ is a factor obtained by experiment.

For centrifugal pumps and for radius ratio $R_1 / R_2 < 0.5$ the value of ψ thus given by Pfleiderer will be:

$$\psi = 0.6\ (\ 1 + \sin\beta_2\ )$$

To obtain the exact value for the slip coefficient Busemann (Ref.2) divided the absolute fluid motion in the impeller into two parts:

a) the through-flow describing the absolute fluid motion through the vane system at rest, and

b) the displacement flow describing the absolute fluid motion produced by the rotation of the vane system.

Later on, it will be seen that in addition to the flows mentioned above the circulation flow is introduced deflecting the resulting theoretical flow in such a manner that it leaves the trailing vane edge smoothly.

Prominent expounders of the theoretical development have used conformal mapping procedures to deduce the slip coefficient. Equation $C_{u_z} / C_{u_\infty} = f\,(z, \beta, R_1/R_2)$ represents the relationship among the variables involved.

The problem was solved for logarithmic shaped blades by Busemann (Ref.2), but his entire theory is too extensive to quote in detail, therefore only the final results will be given. Busemann modified the Euler equation and introduced two correction factors,

a) h_o - a head correction factor pertaining to the displacement flow and involving the approximation of one-dimensional theory according to two dimensional theory, and

b) h_v - a head correction factor pertaining to the through flow. Euler's equation corrected by Busemann becomes:

$$H_{th} = h_o \frac{u_2^2}{g} - h_v \frac{u_2\, C_{m_2}}{g} \, ctg\, \beta_2 \qquad 2.8$$

It is of great interest to note that Busemann's correction coefficient h_v is in complete agreement with Weinig's (Ref.4) results. Considering Weinig's results it is seen that the correction coefficient is constant and practically equal to unity when the vane length is greater than the vane spacing. Since the vanes of radial impellers are usually longer than the vane spacing factor h_o is a significant contribution to the Euler equation. In its final form the equation may be written:

$$\frac{H_{th}}{\frac{u_2^2}{g}} = h_o - \frac{C_{m2}}{u_2} ctg\beta_2 \qquad 2.9$$

Values of h_o have been calculated by Busemann.

Recently, a mathematical solution for the relative eddy effect was obtained by Reddy (Ref.1) who made the following assumptions in deriving the equations.

a) the fluid is incompressible and frictionless

b) channels are full of fluid

c) the planes of the fluid paths traverse the axis of rotation

d) the width of the impeller channel is constant.

Using Laplace equations and introducing the boundary conditions one of a set of simplified solutions for $\frac{C_e}{u}$ was obtained

$$\frac{C_e}{u} = 1 - \frac{tg\,\frac{2\pi}{z}}{\frac{2\pi}{z}} + \frac{32\,z}{\pi^2(z^2-16)} \qquad 2.10$$

Equation 2.10 is related to equation 2.5 by the expression:

$$\frac{C_u}{C_u} = 1 - \frac{C_e}{u} \qquad 2.11$$

Reddy made the interesting observation that the radius of relative rotation of the fluid decreases as the number of blades increases. Thus, the relative eddy velocity is the product of angular velocity ω and radius and would decrease as the number of blades increases.

2.3 Visual observation

In the general theory discussed above, the assumption was made that the impeller channels were running filled with the fluid. Experimental results and visual observation do not confirm that statement. The results obtained by Fischer (Ref. 3) show that dead-water zones form on the low-pressure sides of the blades for all discharge conditions. These zones increase in size as the discharge is decreased from above normal to subnormal or zero flow conditions.

The flow conditions at small discharges are different from those theoretically deduced and the active flow breaks away from the blade face.

In the previous discussion the intake conditions were not introduced, although they play an important part. The approach of the fluid to the impeller inlet and its distribution along the suction pipe is of great importance. These conditions vary with the discharge. To obtain a sufficiently accurate physical picture of fluid motion at low capacities extensive experimental studies and visual observation are required.

3. THEORY

3.1 Influence of number of blades and diameter ratio on the flow conditions

3.11 Theoretical analysis

Spannhake (Ref.19, 21) developed the mathematical theory using conformal mapping procedure. He simplified the idea of a centrifugal pump for his mathematical deductions. Impeller and casing were modified. Two parallel shrouds with a radial bladed impeller placed in the open space between represented the basic "theoretical shape" of the pump. See fig.12a.

For the above ideal arrangement the Kutta-Joukowski theorem was used to simplify the conformal mapping. By means of this transformation the impeller with straight radial blades could be transformed into a circle. Since this is the subject of the present investigation the theory is used and extended.

It is known that the Q - H (flow-head) characteristic is affected by varying the number of blades and the diameter ratio. The purpose of the present theory is to estimate the influence of both parameters on the flow conditions. In addition, the outlet velocities and outlet angles are obtained theoretically.

The deduction and explanation of the conformal transformation from the Z-plane into the W-plane (impeller plane) which leads to the final form of the impeller is shown in Appendix 3-I.

Thus the transformation which yields the final form of the impeller is:

$$W = \qquad 3.4$$

The geometry of the impeller in both planes (Z and W) has been solved by the Kutta-Joukowsky theorem and before explaining the velocity field, further simplification is introduced. Flow in the pump is periodic, the frequency depending on the number of blades and the speed, and these phenomena are neglected in the theoretical analysis.

As a result of the above simplification the flow relative to the impeller can be considered as steady and the velocity field for instantaneous absolute flow can be obtained.

The velocity field of the absolute flow can be split into two components:

a) flow through the system at rest

b) flow in the rotating channel at $Q = o$

These two points will be discussed separately.

a) flow through the system at rest

Assume that the fluid flows between two parallel walls which are perpendicular to the shaft as shown in figure 12.

The vicinity of the shaft is taken as a vortex source while a

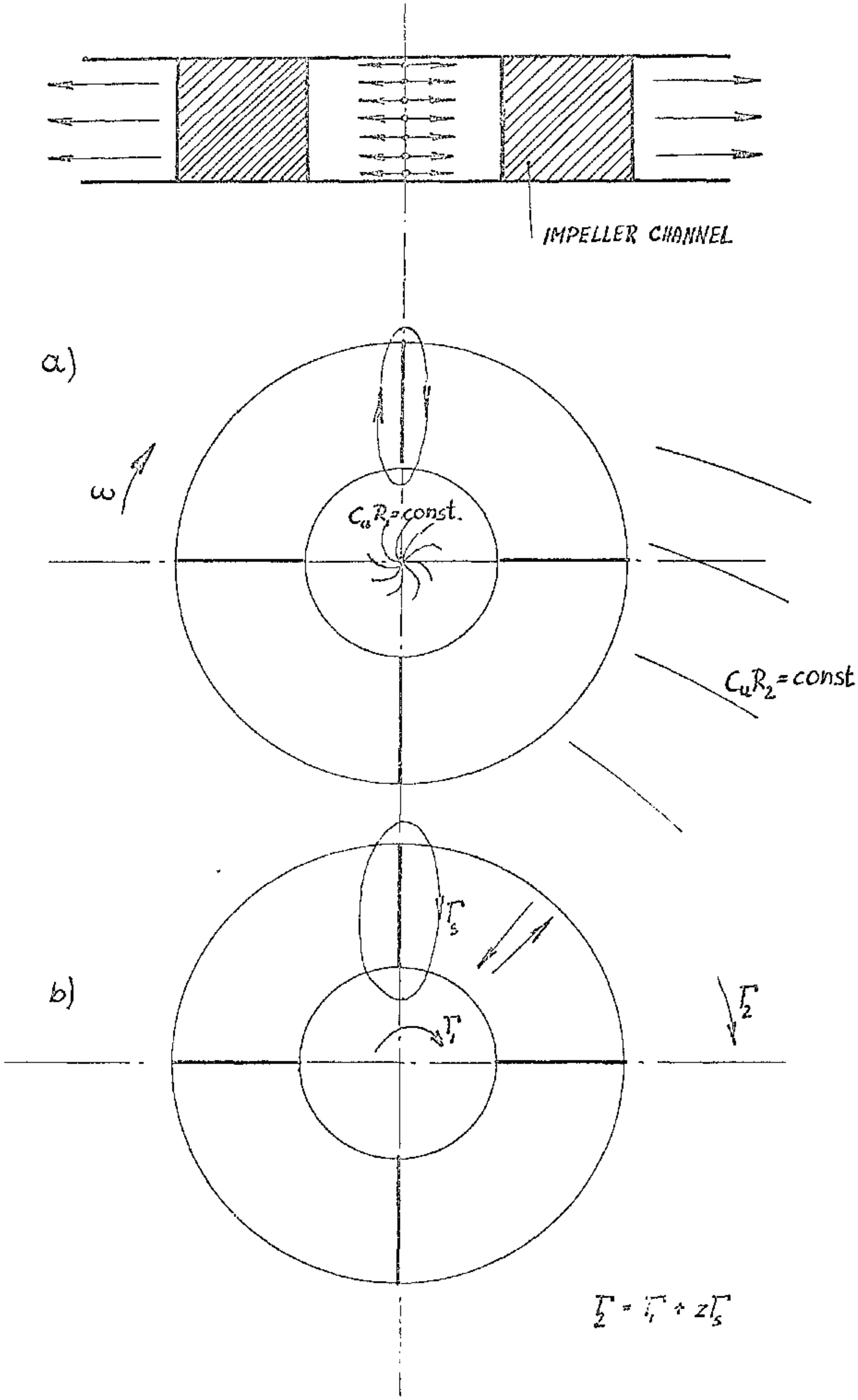

FIG. 12 THEORETICAL SHAPE OF THE IMPELLER

vortex sink is assumed to exist at infinity. A source of strength $\frac{Q}{2\pi} = C_r \cdot R$ and a circulation of strength $\frac{\Gamma_1}{2\pi} = (C_u R)_1$ are placed in the centre of the impeller. Finally, let the fluid flow out of the impeller with a circulation of strength $\frac{\Gamma_2}{2\pi} = (C_u R)_2$ and disappear into a sink of strength $\frac{Q}{2\pi}$ placed at infinity.

To study the velocity field a knowledge of the complex potential in the Z-plane is required. The complex potential can be determined from the velocity field and the geometry of the impeller. Detail deduction of the complex potential can be seen in Appendix 3-II.

Hence the complex potential is equal to:

$$F' = \sum_{i=1}^{7} F_i = \frac{Q - i\Gamma_1}{2\pi} \ln\left(Z + \lambda\tau\right) + \frac{Q + i\Gamma_1}{2\pi} \ln\left(Z + \frac{\tau}{\lambda}\right)$$

$$- \frac{Q + i\left(\Gamma_1 + \Gamma_s\right)}{2\pi} \ln Z \qquad 3.17$$

b) flow in the rotating channel at Q = o

The fluid rotating around the shaft in the impeller channel at zero flow experiences a pressure increase in front of each blade while that at the rear of the blade experiences a drop in pressure. This causes a turning motion in the fluid. The velocity distribution can be found by means of the potential function. Deduction of the potential function is given in Appendix 3-III.

The complex potential due to the flow in the rotating channel at $Q = o$ is:

$$F_8 = \frac{\omega\mu\tau^2}{\pi z}\int_0^{2\pi}\frac{\sin\vartheta . \ln(Z - \tau e^{i\vartheta})}{\left(1 + \frac{\cos\vartheta}{\mu}\right)^{1-\frac{2}{z}}}\,d\vartheta \qquad 3.28$$

Adding potentials F^1 and F_8 the total potential F is obtained.

$$F = \sum_{i=1}^{8} F_i = \frac{Q - i\Gamma_1}{2\pi}\ln(Z + \lambda\tau) + \frac{Q + i\Gamma_1}{2\pi}\ln\left(Z + \frac{\tau}{\lambda}\right) -$$

$$- \frac{Q + i(\Gamma_1 + \Gamma_s)}{2\pi}\ln Z +$$

$$+ \frac{\omega\mu\tau^2}{\pi z}\int_0^{2\pi}\frac{\sin\vartheta . \ln(Z - \tau e^{i\vartheta})}{\left(1 + \frac{\cos\vartheta}{\mu}\right)^{1-\frac{2}{z}}}\,d\vartheta \qquad 3.29$$

A further requirement is the estimation of the circulation which appears in equation 3.29. The explanation and deduction of the circulation is found in Appendix 3-IV which takes the following form:

$$\Gamma_{2_Z} = \Gamma_{1_Z}\left(\frac{\lambda - 1}{\lambda + 1}\right) + 2\,\frac{\omega\mu\tau^2}{z}\,I_1 \qquad 3.35$$

and

$$\Gamma_{2_W} = \Gamma_{1_W}\left(\frac{\lambda - 1}{\lambda + 1}\right) + 2\,\omega\mu\tau^2 I_1 \qquad 3.36$$

where

$$I_1 = \int_0^{2\pi} \frac{(1 + \cos\vartheta)}{\left(1 + \frac{\cos\vartheta}{\mu}\right)^{1-\frac{2}{z}}} \, d\vartheta \qquad 3.33$$

where Γ_{1Z} and Γ_{1W} are the circulations at the inlet in the Z and W-planes

and Γ_{2Z} and Γ_{2W} are the circulations at the outlet in the Z and W-planes

For the present there are no guide vanes and it may be stated that and are equal to zero, which simplified the equations 3.35, 3.36, 3.29.

Hence,

$$\Gamma_{2Z} = \frac{2\omega\mu\tau^2}{z} I_1 = \Gamma_s \qquad 3.37$$

$$\Gamma_{2W} = 2\omega\mu\tau^2 I_1 = z\Gamma_s \qquad 3.38$$

$$F = \frac{Q}{2\pi}\ln(Z+\lambda\tau) + \frac{Q}{2\pi}\ln\left(Z+\frac{\tau}{\lambda}\right) -$$

$$- \frac{Q + i\Gamma_s}{2\pi}\ln Z +$$

$$+ \frac{\omega\mu\tau^2}{\pi . z}\int_0^{2\pi} \frac{\sin\vartheta . \ln(Z - \tau e^{i\vartheta})}{\left(1+\frac{\cos\vartheta}{\mu}\right)^{1-\frac{2}{z}}} d\vartheta \qquad 3.39$$

The complex velocity in the Z-plane is given by the differential of the complex potential:

$$C_x - i\,C_y = \frac{dF}{dZ} \tag{3.40}$$

The complex velocity in the W-plane is given by:

$$c_x - i\,c_y = \frac{dF}{dZ}\;\frac{dZ}{dW} \tag{3.41}$$

Differentiation of equation 3.39 yields:

$$\frac{dF}{dZ} = \frac{Q}{2\pi}\,\frac{1}{Z+\lambda\tau} + \frac{Q}{2\pi}\,\frac{1}{Z+\frac{\tau}{\lambda}} - \frac{Q+i\Gamma_c}{2\pi}\cdot\frac{1}{Z} + \frac{\omega\mu\tau^2}{\pi z} I_2 \tag{3.42}$$

where

$$I_2 = \int_0^{2\pi} \frac{\sin\vartheta}{\left(1+\frac{\cos\vartheta}{\mu}\right)^{1-\frac{2}{z}}}\cdot\frac{d\vartheta}{Z-\tau e^{i\vartheta}} \tag{3.43}$$

The results obtained above are introduced into equation 3.41.

$$c_x - i c_y = \frac{Q}{2\pi}\left[\frac{1}{Z+\lambda\tau} + \frac{1}{Z+\frac{\tau}{\lambda}} - \frac{1}{Z}\right]\frac{1}{\frac{dW}{dZ}} + \left[-\frac{2\omega\mu\tau^2}{z}\cdot\frac{i}{2\pi Z} I_1\right]\frac{1}{\frac{dW}{dZ}} + \left[\frac{\omega\mu\tau^2}{\pi z} I_2\right]\frac{1}{\frac{dW}{dZ}} \tag{3.44}$$

In the present problem the flow-rate Q=o, and so the first term in the equation vanishes. The other two terms are constant for a given impeller and a constant angular velocity.

Hence,

$$\ell_x - i\ell_y = \left[- \frac{2\omega\mu\tau^2}{z} \frac{i}{2\pi Z} \right] \frac{1}{\frac{dW}{dZ}} +$$

$$+ \left[\frac{\omega\mu\tau^2}{\pi z} I_2 \right] \frac{1}{\frac{dW}{dZ}} \qquad 3.45$$

To solve the equation 3.45 it is still necessary to estimate the term I_1 and I_2.

Equation 3.43 is

$$I_2 = \int_0^{2\pi} \frac{\sin\vartheta}{\left(1 + \frac{\cos\vartheta}{\mu}\right)^{1-\frac{2}{z}} \left(Z - \tau e^{i\vartheta}\right)} d\vartheta$$

Integrating by parts and introducing the new unknowns

$$u = \frac{1}{Z - \tau e^{i\vartheta}} \qquad dv = \frac{\sin\vartheta}{\left(1 + \frac{\cos\vartheta}{\mu}\right)^{1-\frac{2}{z}}} d\vartheta \qquad 3.46$$

the following integral is obtained:

$$I_2 = \frac{z\tau\mu}{2} \int_0^{2\pi} \left(1 + \frac{\cos\vartheta}{\mu}\right)^{\frac{2}{z}} \frac{i e^{i\vartheta}}{\left(Z - \tau e^{i\vartheta}\right)^2} d\vartheta \qquad 3.47$$

By substitution it follows that,

$$W = e^{i\vartheta} \qquad dW = i e^{i\vartheta} d\vartheta$$

$$\cos\vartheta = \frac{1}{2}\left(W + \frac{1}{W}\right) \qquad 3.48$$

and the equation 3.47 becomes

$$I_2 = \frac{z\tau\mu}{2}\oint\left(1+\frac{W+\frac{1}{W}}{2\mu}\right)^{\frac{2}{z}}\frac{dW}{(Z-\tau W)^2} \tag{3.49}$$

It may be written that,

$$I_2 = \frac{z\tau\mu}{2}\oint F(W)\,dW \tag{3.50}$$

where

$$F(W) = \left(1+\frac{W+\frac{1}{W}}{2\mu}\right)^{\frac{2}{z}}\frac{1}{(Z-\tau W)^2} \tag{3.51}$$

The integral 3.50 can be solved by the residue theorem. The residue yields

$$\oint F(W)\,dW = 2\pi i A_{-1} \tag{3.52}$$

where A_{-1} is the residue of a Laurent series. Equation 3.51 can be solved by expanding both terms into two series.

The first term becomes,

$$\frac{1}{(Z-\tau W)^2} = \frac{1}{\tau^2}\left[\frac{1}{\left(\frac{Z}{\tau}-W\right)^2}\right] = \frac{1}{\tau^2}\left(\frac{\tau}{Z}\right)^2\left[1+2\left(\frac{\tau}{Z}W\right)+\right. \tag{3.53}$$

$$\left. +\,3\left(\frac{\tau}{Z}W\right)^2+\cdots+(n+1)\left(\frac{\tau}{Z}W\right)^n\right]$$

and the second term using Fourier's expansion becomes,

$$\left(1+\frac{\cos\vartheta}{\mu}\right)^{\frac{2}{Z}}=a_0+a_1\cos\vartheta+a_2\cos2\vartheta+\dots$$

$$\dots+a_n\cos n\vartheta \qquad 3.54$$

Forming the product of both series:

$$F(W)=\frac{1}{\tau^2}\left(\frac{\tau}{Z}\right)^2\left[1+2\left(\frac{\tau}{Z}W\right)+3\left(\frac{\tau}{Z}W\right)^3+\dots\right.$$

$$\left.\dots(n+1)\left(\frac{\tau}{Z}W\right)^n\right]\times$$

$$\times\left[a_0+\frac{a_1}{2}\left(W+\frac{1}{W}\right)+\frac{a_2}{2}\left(W^2+\frac{1}{W^2}\right)+\dots\right.$$

$$\left.\dots+\frac{a_n}{2}\left(W^n+\frac{1}{W^n}\right)\right] \qquad 3.55$$

enables us to find the residue.

$$A_{-1}=\frac{1}{\tau^2}\left(\frac{\tau}{Z}\right)^2\left[\frac{a_1}{2}+\frac{a_2}{2}.2\left(\frac{\tau}{Z}\right)+\frac{a_3}{2}3\left(\frac{\tau}{Z}\right)^2+\dots+\frac{a_n}{2}n\left(\frac{\tau}{Z}\right)^{n-1}\right]$$

By rearranging it is obtained finally that:

$$A_{-1}=\frac{1}{2}\;\frac{1}{\tau^2}\left(\frac{\tau}{Z}\right)^2\left[a_1+2a_2\left(\frac{\tau}{Z}\right)+3a_3\left(\frac{\tau}{Z}\right)^2+\dots+na_n\left(\frac{\tau}{Z}\right)^{n-1}\right]$$

$$3.56$$

These values are introduced into equation 3.50 which becomes:

$$I_2 = \frac{z\mu\tau}{2}\, 2\pi i A_{-1} =$$

$$= \frac{z\mu\pi}{2\tau}\, i\left(\frac{\tau}{Z}\right)^2\left[a_1 + 2a_2\left(\frac{\tau}{Z}\right) + 3a_3\left(\frac{\tau}{Z}\right)^2 + \right.$$

$$\left. + \cdots\cdots + n\,a_n\left(\frac{\tau}{Z}\right)^{n-1}\right] \qquad 3.57$$

To solve equation 3.44 the integral I_1 has to be evaluated. The integral I_1 is complete eleiptic integral, but by taking, in the Z-plane, the value of Z equal to the radius of circle "K" see fig.9, it can be shown that the integral I_2 is part of the integral I_1.

By making use of the above supposition equation 3.43 may be cast in the following form:

$$I_2 = \frac{1}{\tau}\int_0^{2\pi}\frac{\sin\vartheta}{\left(1+\frac{\cos\vartheta}{\mu}\right)^{1-\frac{2}{Z}}}\;\frac{1}{\left(1-e^{i\vartheta}\right)}\,d\vartheta =$$

$$= \frac{1}{\tau}\int_0^{2\pi}\frac{\sin\vartheta}{\left(1+\frac{\cos\vartheta}{\mu}\right)^{1-\frac{2}{Z}}}\;\frac{1+e^{-i\vartheta}}{\left(1-e^{-i\vartheta}\right)\left(1+e^{i\vartheta}\right)}\,d\vartheta =$$

$$= \frac{i}{2\tau}\left[\int_0^{2\pi}\frac{(1+\cos\vartheta)}{\left(1+\frac{\cos\vartheta}{\mu}\right)^{1-\frac{2}{Z}}} - i\int_0^{2\pi}\frac{\sin\vartheta}{\left(1+\frac{\cos\vartheta}{\mu}\right)^{1-\frac{2}{Z}}}\right]d\vartheta =$$

$$= \frac{i}{2\tau}\int_0^{2\pi}\frac{(1+\cos\vartheta)\,d\vartheta}{\left(1+\frac{\cos\vartheta}{\mu}\right)^{1-\frac{2}{Z}}} = \frac{i}{\tau}\int_0^{\pi}\frac{(1+\cos\vartheta)\,d\vartheta}{\left(1+\frac{\cos\vartheta}{\mu}\right)^{1-\frac{2}{Z}}}$$

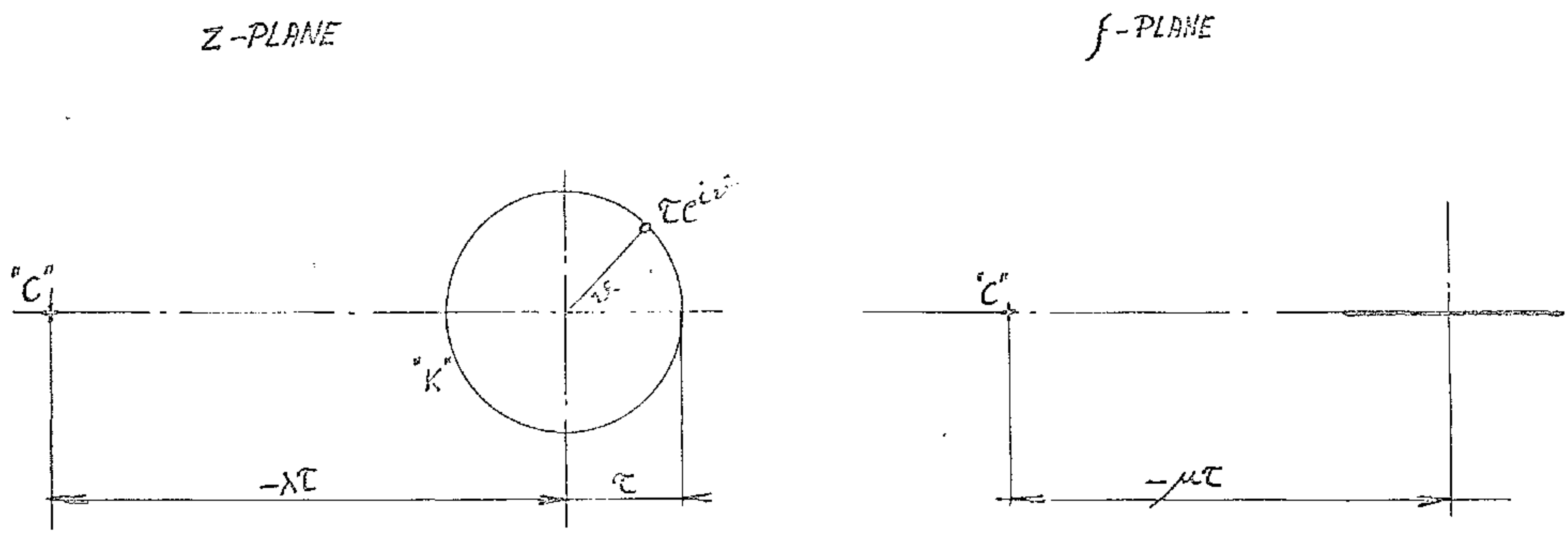

FIG.9 CONFORMAL TRANSFORMATION Z-ζ PLANE

Thus,

$$I_2 = \frac{i}{\tau} I_1 \qquad 3.58$$

and so the value of integral I_1 becomes:

$$I_1 = \frac{\pi . z . \mu}{2} (a_1 + 2a_2 + 3a_3 + \cdots) \qquad 3.59$$

Further, the terms a_1; a_2; ...a_n have to be found. Accordingly, the value of the first few terms of the Fourier series are obtained.

$$\left(1 + \frac{\cos\vartheta}{\mu}\right)^{\frac{2}{z}} = a_0 + a_1 \cos\vartheta + a_2 \cos 2\vartheta + \cdots$$

Thus

at $\vartheta = 0°$ $\left(1 + \frac{\cos\vartheta}{\mu}\right)^{\frac{2}{z}} = \left(1 + \frac{1}{\mu}\right)^{\frac{2}{z}} = b_1$

at $\vartheta = 45°$ $\left(1 + \frac{\cos\vartheta}{\mu}\right)^{\frac{2}{z}} = \left(1 + \frac{0.707}{\mu}\right)^{\frac{2}{z}} = b_2$

at $\vartheta = 90°$ $\left(1 + \frac{\cos\vartheta}{\mu}\right)^{\frac{2}{z}} = 1 = b_3$

at $\vartheta = 135°$ $\left(1 + \frac{\cos\vartheta}{\mu}\right)^{\frac{2}{z}} = \left(1 - \frac{0.707}{\mu}\right)^{\frac{2}{z}} = b_4$

at $\vartheta = 180°$ $\left(1 + \frac{\cos\vartheta}{\mu}\right)^{\frac{2}{z}} = \left(1 - \frac{1}{\mu}\right) = b_5$

Substituting the above values into Fourier's series the set of five equations is found.

$$b_1 = a_0 + a_1 + a_2 + a_3 + a_4$$

$$b_2 = a_0 + \frac{a_1}{\sqrt{2}} - \frac{a_3}{\sqrt{2}} - a_4$$

$$b_3 = a_0 - a_2 + a_4$$

$$b_4 = a_0 - \frac{a_1}{\sqrt{2}} + \frac{a_2}{\sqrt{2}} - a_4$$

$$b_5 = a_0 - a_1 + a_2 - a_3 + a_4 \qquad 3.61$$

The solutions for the individual a - coefficients are as follows:

$$a_1 = \frac{1}{4}(b_1 + \sqrt{2}\, b_2 - \sqrt{2}\, b_4 - b_5)$$

$$a_2 = \frac{1}{4}(b_1 - 2\, b_3 + b_5)$$

$$a_3 = \frac{1}{4}(b_1 - 2\, b_2 + \sqrt{2}\, b_4 - b_5)$$

$$a_4 = \frac{1}{8}(b_1 - 2\, b_2 + 2\, b_3 - 2\, b_4 + b_5) \qquad 3.62$$

Since all the terms in equation 3.45 are known the complex velocity in the W-plane can be worked out.

The final expression for the complex velocity is:

$$\ell_x - i\ell_y = -(\mu\tau)^{3-z} \cdot z \cdot \omega \frac{i}{Z} \frac{W^{z-1}}{1-\frac{\tau^2}{Z^2}} \left(a_1 + 2a_2 + 3a_3 + \dots\right) +$$

$$+(\mu\tau)^{2-z} \mu \tau^2 \cdot z \cdot \omega \frac{i}{Z^2} \frac{W^{z-1}}{1-\frac{\tau^2}{Z^2}} \left[a_1 + 2a_2\left(\frac{\tau}{Z}\right) + \dots + n a_n \left(\frac{\tau}{Z}\right)^{n-1}\right] \qquad 3.63$$

3.12 Numerical example

A numerical example will be worked out for the following conditions:

$\psi = 0$ $\quad R_1 = 7''$ $\quad z = 4$

$n = 2520$ R.P.M. $\quad R_2 = 20''$

The necessary coefficients are as follows:

$$\frac{1}{\gamma} = \frac{R_2}{R_1} = \frac{20}{7} = 2.857$$

$$\mu = \frac{\left(\frac{1}{\gamma}\right)^z + 1}{\left(\frac{1}{\gamma}\right)^z - 1} = 1.03$$

$$\tau = \frac{R_2}{\mu\sqrt{\frac{\mu+1}{\mu}}} = 0.82\, R_2$$

b - coefficients are calculated from equation 3.60

$$b_1 = \left(1 + \frac{1}{1.03}\right)^{\frac{2}{4}} = 1.403$$

$$b_2 = \left(1 + \frac{0.707}{1.03}\right)^{\frac{2}{4}} = 1.30$$

$$b_3 = 1$$

$$b_4 = \left(1 - \frac{0.707}{1.03}\right)^{\frac{2}{4}} = 0.56$$

$$b_5 = \left(1 - \frac{1}{1.03}\right)^{\frac{2}{4}} = 0.173$$

a - coefficients are calculated from equation 3.62

$$a_1 = \frac{1}{4}\ (1.403 + 1.83 - 0.792 - 0.173) = 0.569$$

$$a_2 = \frac{1}{4}\ (1.403 - 2.0 + 0.173) = -0.106$$

$$a_3 = \frac{1}{4}\ (1.403 - 1.84 + 0.792 - 0.173) = 0.0452$$

$$a_4 = \frac{1}{8}\ (1.403 - 2.6 + 2 - 1.12 + 0.173) = -0.018$$

The integral I_1 is obtained from equation 3.53

$$I_1 = \frac{\pi \cdot 4 \cdot 1.03}{2}\ (0.569 - 0.212 + 0.1356 - 0.072)$$

$$I_1 = 2.720$$

To estimate the velocity at any one point on the rim of the impeller an arbitrary angle between radius vector from the centre to a chosen point and the x - axis is used. Let this angle be $\pi/4$, then:

$$W = R e^{\frac{\pi}{4} i}$$

From equation 3.4 we deduce:

$$\zeta = \frac{W^4}{(\mu\tau)^3} - \mu\tau$$

$$\left(e^{\frac{\pi}{4} i}\right)^4 = e^{\pi i} = \cos\pi + i \sin\pi = -1$$

Hence,

$$\zeta = -\frac{R_2^4}{0.602\ R_2^3} - 0.845\ R_2 = -2.507\ R_2$$

$$Z = 2\zeta + \frac{\tau^2}{2\zeta} = -5.148\ R_2$$

To solve equation 3.57 it is advisable to calculate the following values:

$$\frac{1}{Z} = -\frac{0.1942}{R_2}$$

$$\frac{1}{Z^2} = \frac{0.0377}{R_2^2}$$

$$\frac{1}{Z^3} = -\frac{0.00733}{R_2^3}$$

The integral I_2 becomes:

$$I_2 = 5.3\,i\,\frac{R_2}{Z^2}\left[0.569 - 0.174\left(\frac{R_2}{Z}\right) + 0.0911\left(\frac{R_2}{Z}\right)^2 - 0.0398\left(\frac{R_2}{Z}\right)^3\right]$$

$$I_2 = 0.1212\ \frac{i}{R_2}$$

To simplify the computation it is better to use the reciprocal of equation 3.24.

$$\frac{1}{\frac{dW}{dZ}} = \frac{13.3\ \frac{W^3}{R_2^3}}{1 - 0.672\left(\frac{R_2}{Z}\right)^2}$$

$$\left(e^{\frac{\pi}{4}i}\right)^3 = -0.707 + 0.707\,i$$

$$\frac{1}{\frac{dW}{dZ}} = 9.66\,(-1 + i)$$

The complex velocity in the Z-plane is calculated from equation 3.40.

$$C_x - i\,C_y = \frac{\mu\,\tau^2}{\pi \cdot z}\left[I_2 - \frac{I_1 \cdot i}{4}\right]\omega$$

$$C_x - i\,C_y = 0.0551\left[0.1212\,i - 2.72\,i\,(-0.1942)\right]\cdot \omega\,R_2$$

$$C_x - i\,C_y = 0.0358\,i\,\omega\,R_2$$

The complex velocity in the W-plane is given by equation 3.41.

$$c_x - i\,c_y = 0.0358\,i\,\omega\,R_2\left[9.66\,(-1+i)\right]$$

$$c_x - i\,c_y = (-0.346 - 0.346\,i)\,\omega\,R_2$$

And the resulting velocity which is equal to absolute discharge velocity is:

$$c = 0.49\,\omega\,R_2$$

Similarly, for all other points the resulting velocity can be found.

Analysing the complete problem, it can be seen that by keeping the same conditions but increasing only the number of blades the resulting velocity will be increased. Similarly, by keeping the number of blades constant and increasing the area ratio, the resulting velocity will be decreased.

Furthermore, the angle between the resultant velocity and the peripheral velocity component β_2 can be estimated from the known components of the complex velocity.

Hence,

$$c_x - i\,c_y = (-0.346 - 0.346\,i)\,\omega\,R_2$$

$$c_x = -0.346\,\omega\,R_2$$

$$c_y = 0.346\,\omega\,R_2$$

In our case the chosen angle is $\frac{\pi}{4}$ so the angle β_2 can be calculated. See fig.13.

The tangential component of absolute velocity is:

$$c_{u_2} = (- c_x \sin\vartheta + c_y \cos\vartheta)\, \omega R_2$$

$$\vartheta = \pi/4$$

$c_{u_2} = 0.49\, \omega\, R_2$ and the radial component of absolute velocity is:

$$c_{m_2} = (- c_x \cos\vartheta - c_y \sin\vartheta)\, \omega R_2$$

$$C_{m_2} = 0$$

The angle thus obtained is:

$$tg\,\beta_2 = \frac{C_{m_2}}{C_{u_2}} = 0$$

and $\beta_2 = 0$

The negative radial velocity shows that the velocity is directed towards the centre of the impeller and vice versa.

Hence the head becomes:

$$\frac{U_2\, c_{u_2}}{g} = \frac{1}{g}\,\omega\, R_2 \cdot 0.49\, \omega\, R_2 = \frac{0.49\, (\omega\, R_2)^2}{g}$$

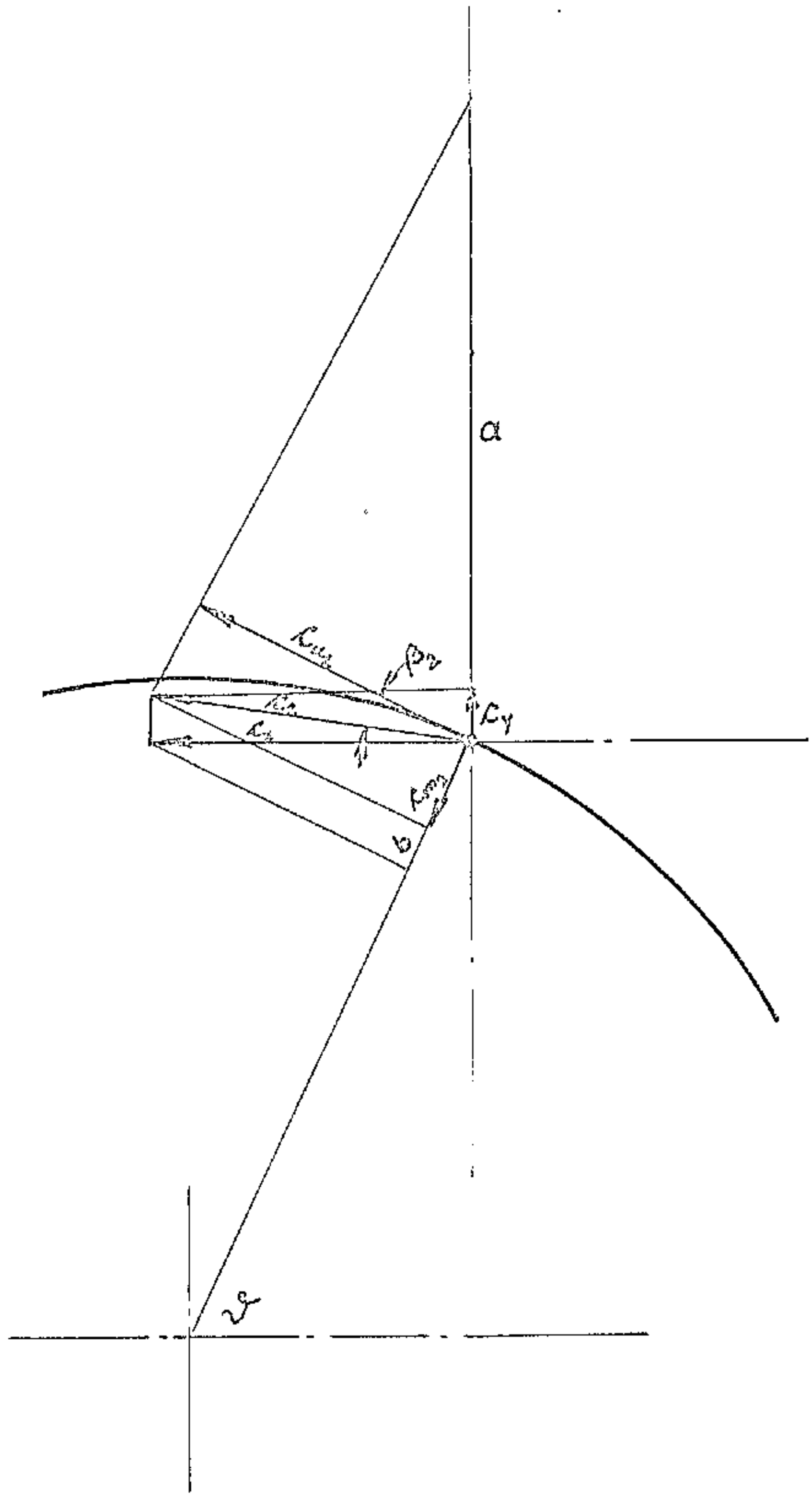

FIG. 13 VELOCITY COMPONENTS AT THE DISCHARGE

Appendix 3-I

Making use of the Kutta-Joukowski transformation

$$\zeta = \frac{1}{2}\left(Z + \frac{\tau^2}{Z}\right) \qquad 3.1$$

a circle is transformed into a line.

For this purpose the circle "k" with radius and the point "C" at the distance $-\lambda\tau$ outside of the circle were chosen, see fig.9. Later it is shown that the circle "K" corresponds to the impeller blade and the point "C" to the centre of the impeller.

The first transformation gives the following values:

Point "C" in the Z-plane corresponds to

$$\zeta_c = \frac{1}{2}\left(-\lambda\tau - \frac{\tau^2}{\lambda\tau}\right) = -\mu\tau$$

in the ζ-plane,

where $\mu = \frac{1}{2}\left(\lambda + \frac{1}{\lambda}\right)$

Thus, the circle "K" is transformed into a line.

Further transformations are required to obtain the proper geometrical shape of the impeller, and so the second transformation is - see fig.10

$$\zeta' = \zeta + \mu\tau$$

Since

$$\zeta_c = \mu\tau$$

point "C" in the ζ - plane corresponds to $\zeta' = 0$ in the ζ'-plane.

In addition to the co-ordinates of point "C", the following interesting values are found in the ζ'-plane.

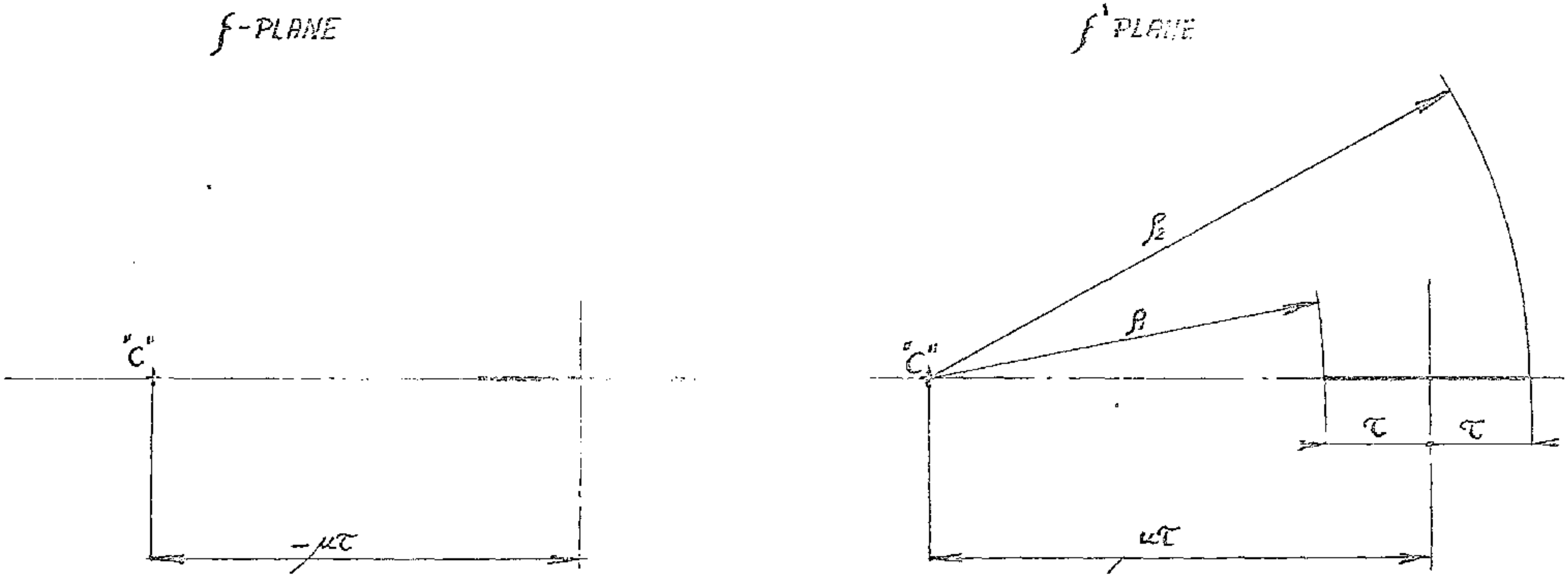

FIG. 10 CONFORMAL TRANSFORMATION ζ-ζ' PLANE

Inlet radius

$$\rho_1 = \mu\tau - \tau$$

and outlet radius

$$\rho_2 = \mu\tau + \tau$$

The third transformation leads to the final form of the impeller. See fig.11.

$$W = \mu\tau \sqrt[z]{\frac{\zeta'}{\mu\tau}} \tag{3.4}$$

or

$$\zeta' = \left(\frac{W}{\mu\tau}\right)^z \mu\tau$$

The relationship between the W-plane and the ζ'-plane is better seen if polar co-ordinates are introduced.

$$W = Re^{i\vartheta} \qquad \zeta' = \rho e^{i\psi}$$

$$Re^{i\vartheta} = (\mu\tau)^{1-\frac{1}{z}} \cdot \rho^{\frac{1}{z}} \cdot e^{i\frac{\psi}{z}}$$

The last transformation shows that the complete ζ'-plane is transformed into only $\frac{2\pi}{z}$ of the W-plane, i.e. the segment of the W-plane bounded by the rays $\vartheta = 0$ and $\vartheta = \frac{2\pi}{z}$ transforms into the entire ζ'-plane. Thus, one point in the W-plane corresponds to z-points in the ζ'-plane. To study the problem, it is necessary to know the fluid conditions in only one plane.

The inlet radius in the W-plane is given by:

$$R_1 = \mu\tau \sqrt[z]{\frac{\mu\tau - \tau}{\mu\tau}} = \mu\tau \sqrt[z]{\frac{\mu - 1}{\mu}}$$

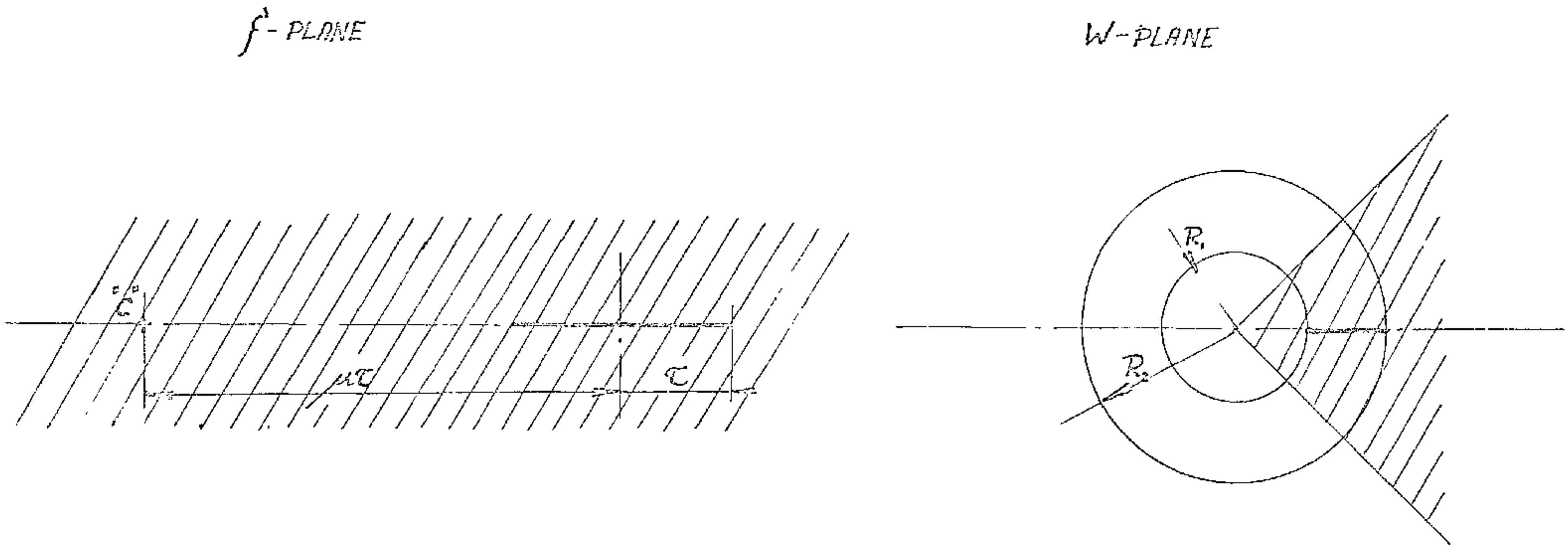

FIG. II CONFORMAL TRANSFORMATION ζ'-W PLANE and the outlet radius by:

$$R_2 = \mu\tau \sqrt[z]{\frac{\mu\tau + \tau}{\mu\tau}} = \mu\tau \sqrt[z]{\frac{\mu + 1}{\mu}} \qquad 3.5$$

Radius ratio is then

$$\frac{1}{r} = \frac{R_2}{R_1} = \sqrt[z]{\frac{\mu + 1}{\mu - 1}} \qquad 3.6$$

Hence,

$$\mu = \frac{\left(\frac{1}{r}\right)^z + 1}{\left(\frac{1}{r}\right)^z - 1} \qquad 3.7$$

From equation 3.5,

$$\tau = \frac{R_2}{\mu \sqrt[z]{\frac{\mu + 1}{\mu}}} \qquad 3.8$$

From equation 3.2,

$$\lambda = \mu + \sqrt{\mu^2 + 1} \qquad 3.9$$

Appendix 3-II

From the explanation listed in the text and taking into account the fact that the centre of the impeller in the z-plane (see fig.9) corresponds to the point "C", the two components of the potential function are found:

$$F_1 = \frac{Q}{2\pi} \ln (z + \lambda\tau) \qquad 3.10$$

$$F_2 = - \frac{\Gamma_1}{2\pi} \ln (z + \lambda\tau) \qquad 3.11$$

To avoid any separation of the stream lines the flow should move around the circle "K", so that any tangential components will be obtained. This condition will be satisfied by finding an image source with circulation of the same strength with respect to the circle "K". The image system consists of a source at the inverse point $-\left(\frac{\lambda}{\tau}\right)^{-1}$ and a circulation of opposite sense. Therefore, the complex potentials for the stated conditions are:

$$F_3 = \frac{Q}{2\pi} \ln (z + \frac{\tau}{\lambda}) \qquad 3.12$$

$$F_4 = \frac{i\Gamma_1}{2} \ln (z + \frac{\tau}{\lambda}) \qquad 3.13$$

As already mentioned, the sink at infinity was chosen to satisfy the equation of continuity and the image of the sink with respect to the circle "K" must be found. The inverse point of the sink at infinity is obtained at the centre of the circle "K".

Thus, the complex functions are:

$$F_5 = -\frac{Q}{2\pi} \ln z \qquad 3.14$$

$$F_6 = -\frac{Q}{2\pi} \ln z \qquad 3.15$$

To avoid the infinite velocity at outlet and inlot of the impeller the circulation round the circle (blade) is stated and the potential is found.

$$F_7 = -\frac{i\Gamma_s}{2\pi} \ln z \qquad 3.16$$

Hence the sum of potentials is equal to:

$$F' = \sum_{i=1}^{7} F_i = \frac{Q - i\Gamma_1}{2\pi} \ln\left(Z + \lambda\tau\right) + \frac{Q + i\Gamma_1}{2\pi} \ln\left(Z + \frac{\tau}{\lambda}\right) - \frac{Q + i\left(\Gamma_1 + \Gamma_s\right)}{2\pi} \ln Z \qquad 3.17$$

Appendix 3-III

Flow in the rotating channel at Q=o. By distributing the elementary sources of strength $2\rho_n ds$ over the circumference of the circle the elementary potential is obtained,

$$dF_8 = \frac{2\rho_n \, ds}{2\pi} \ln\left(Z - \tau e^{i\vartheta}\right) \tag{3.18}$$

where ρ_n - normal velocity component in the Z-plane

and s - circumference of the circle.

Normal component of the velocity in the w-plane is

$$\rho_n^1 = /W/\omega \tag{3.19}$$

where /W/ is the absolute value.

From equation 3.4,

$$W = \mu\tau\left(1 + \frac{\cos\vartheta}{\mu}\right)^{\frac{1}{2}} \tag{3.20}$$

Thus,

$$\rho_n^1 = \mu\tau\left(1 + \frac{\cos\vartheta}{\mu}\right)^{\frac{1}{2}} \cdot \omega \tag{3.21}$$

Normal velocity component in the Z-plane is

$$\rho_n = \rho_n^1 \quad / \frac{dW}{dZ} / \tag{3.22}$$

The term $/\frac{dW}{dZ}/$ has to be obtained.

Differentiation of equation 3.4 yields,

$$\frac{dW}{dZ} = \frac{dW}{df^1} \cdot \frac{df^1}{df} \cdot \frac{df}{dZ} \tag{3.23}$$

Now

$$\frac{df'}{dW} = (\mu\tau)^{1-z} \cdot z \cdot W^{z-1},$$

$$\frac{df'}{df} = 1$$

and $$\frac{df}{dZ} = \frac{1}{2}\left(1 - \frac{\tau^2}{Z^2}\right)$$

These values are introduced in equation 3.23.

Thus

$$\frac{dW}{dZ} = \frac{1}{(\mu\tau)^{1-z} \cdot z \cdot W^{z-1}} \cdot \frac{1}{2}\left(1 - \frac{\tau^2}{Z^2}\right) \qquad 3.24$$

The last term in this equation is shown to be

$$\left(1 - \frac{\tau^2}{Z^2}\right) = 1 - \frac{\tau^2}{\tau^2 e^{2i\vartheta}} = 1 - e^{-2i\vartheta}$$

The absolute value of the above expression is:

$$\sqrt{(1 - \cos 2\vartheta)^2 + \sin^2 2\vartheta} = 2 \sin \vartheta$$

Thus,

$$\left|\frac{dW}{dZ}\right| = \frac{2 \sin \vartheta}{2 (\mu\tau)^{1-z} \cdot z \cdot W^{z-1}} \qquad 3.25$$

By substituting equation 3.20 in equation 3.25 we obtain,

$$\left|\frac{dW}{dZ}\right| = \frac{\sin \vartheta}{z \left(1 + \frac{\cos \vartheta}{\mu}\right)^{1 - \frac{1}{z}}} \qquad 3.26$$

From equation 3.26 and 3.22 the normal velocity component in the Z-plane is obtained,

$$c_n = \frac{\omega \mu \tau}{Z} \quad \frac{\sin \vartheta}{\left(1 + \frac{\cos \vartheta}{\mu}\right)^{1-\frac{2}{Z}}} \tag{3.27}$$

Introducing equation 3.27 into equation 3.18 and integrating, we obtain:

$$F_8 = \frac{\omega \mu \tau^2}{\pi . Z} \int_0^{2\pi} \frac{\sin \vartheta \ \ln \left(Z - \tau e^{i\vartheta}\right) d\vartheta}{\left(1 + \frac{\cos \vartheta}{\mu}\right)^{1-\frac{2}{Z}}} \tag{3.28}$$

The total potential thus becomes:

$$F = \sum_{i=1}^{8} F_i =$$

$$= \frac{Q - i\Gamma_1}{2\pi} \ln\left(Z + \lambda\tau\right) + \frac{Q + i\Gamma_1}{2\pi} \ln\left(Z + \frac{\tau}{\lambda}\right) -$$

$$- \frac{Q + i\left(\Gamma_1 + \Gamma_5\right) \ \ln Z}{2\pi} +$$

$$+ \frac{\omega \mu \tau^2}{\pi Z} \int_0^{2\pi} \frac{\sin \vartheta \ \ln \left(Z - \tau e^{i\vartheta}\right) d\vartheta}{\left(1 + \frac{\cos \vartheta}{\mu}\right)^{1-\frac{2}{Z}}} \tag{3.29}$$

Appendix 3-IV

Estimation of the circulation which appears in equation 3.29. For that purpose differentiation of equation 3.29 is needed.

$$\frac{dF}{dZ} = \frac{Q - i\Gamma_1}{2\pi(Z + \lambda\tau)} + \frac{Q + i\Gamma_1}{2\pi\left(Z + \frac{\tau}{\lambda}\right)} - \frac{Q + i\left(\Gamma_1 + \Gamma_s\right)}{2\pi Z} +$$

$$+ \frac{\omega\mu\tau^2}{\pi z}\int_0^{2\pi}\frac{\sin\vartheta .\, d\vartheta}{\left(1 + \frac{\cos\vartheta}{\mu}\right)^{1-\frac{2}{z}}\left(Z - \tau e^{i\vartheta}\right)} \qquad 3.30$$

and

$$\frac{dF}{dW} = \frac{dF}{dZ} \cdot \frac{dZ}{dW} \qquad 3.31$$

For the value $Z = +\tau$ equation 3.24 becomes zero. Consequently, the velocity would become infinite if at the same time term $\frac{dF}{dZ}$ did not approach to zero. Thus, all quantities $Q, \Gamma_1, \Gamma_s, \omega$ should be so determined that $\frac{dF}{dZ}$ for $Z = \pm\tau$ would become zero in equation 3.30. If that condition is fulfilled, the velocity will remain finite and tangential along the blade.

The flow-rate Q plays no role in this relationship. Q causes only pure radial flow with finite velocity directed tangentially along the blade.

Making use of the foregoing conditions (i.e. $\frac{dF}{dZ} = 0$ for $Z \pm \tau$) Q may be omitted.

Equation 3.30 now becomes:

$$\frac{-i\Gamma_1}{2\pi\tau(1+\lambda)} + \frac{i\Gamma_1}{2\pi\tau\left(1+\frac{1}{\lambda}\right)} - \frac{i(\Gamma_1+\Gamma_s)}{2\pi\tau} +$$

$$+\frac{\omega\mu\tau}{\pi z}\int_0^{2\pi}\frac{\sin\vartheta\, d\vartheta}{\left(1+\frac{\cos\vartheta}{\mu}\right)^{1-\frac{2}{z}}\left(1-e^{i\vartheta}\right)} = 0 \qquad 3.32$$

The following term in equation 3.32 will be estimated:

$$\frac{\omega\mu\tau}{\pi z}\int_0^{2\pi}\frac{\sin\vartheta\, d\vartheta}{\left(1+\frac{\cos\vartheta}{\mu}\right)^{1-\frac{2}{z}}\left(1-e^{i\vartheta}\right)}$$

Thus,

$$\frac{1}{1-e^{i\vartheta}}\ \frac{1-e^{-i\vartheta}}{1-e^{-i\vartheta}} = \frac{1}{2}\left(\frac{1-e^{-i\vartheta}}{1-\cos\vartheta}\right) =$$

$$=\frac{1}{2}\left[1+i\left(\frac{1+\cos\vartheta}{\sin\vartheta}\right)\right]$$

giving

$$\frac{1}{2}\ \frac{\omega\mu\tau}{\pi z}\left[\int_0^{2\pi}\frac{\sin\vartheta\, d\vartheta}{\left(1+\frac{\cos\vartheta}{\mu}\right)^{1-\frac{2}{z}}} + \frac{i(1+\cos\vartheta)\, d\vartheta}{\left(1+\frac{\cos\vartheta}{\mu}\right)^{1-\frac{2}{z}}}\right.$$

The value of the first term is equal to zero (odd function with period 2π) and so we obtain:

$$\frac{1}{2}\omega\mu\tau i\int_0^{2\pi}\frac{(1+\cos\vartheta)\, d\vartheta}{\left(1+\frac{\cos\vartheta}{\mu}\right)^{1-\frac{2}{z}}} = \frac{1}{2}\ \frac{\omega\mu\tau i\, I_1'}{\pi z}$$

where

$$I_1' = \int_0^{2\pi}\frac{(1+\cos\vartheta)\, d\vartheta}{\left(1+\frac{\cos\vartheta}{\mu}\right)^{1-\frac{2}{z}}} = 2I_1$$

and

$$I_1 = \int_0^{2\pi} \frac{(1 + \cos\vartheta)}{\left(1 + \frac{\cos\vartheta}{\mu}\right)^{1-\frac{2}{z}}} \, d\vartheta \qquad 3.33$$

Using the fact that

$$\Gamma_2 = \Gamma_1 + \Gamma_s \qquad 3.34$$

the equation 3.32 for the Z-plane becomes

$$\Gamma_{2_Z} = \Gamma_{1_Z}\left(\frac{\lambda - 1}{\lambda + 1}\right) + \frac{2\omega\mu\tau^2}{z} I_1 \qquad 3.35$$

In the W-plane Γ_{2_Z} is now increased by factor z.

$$\Gamma_{2_Z} = \Gamma_{1_W} \frac{\lambda - 1}{\lambda + 1} + 2\omega\mu\tau^2 I_1 \qquad 3.36$$

where

Γ_{1_Z} and Γ_{1_W} are circulation at the inlet in the Z and the W-plane

and, Γ_{2_Z} and Γ_{2_W} are circulation at the outlet in the Z and the W-plane

4. PRESENTATION OF RESULTS

4.1 Theory of similarity

Throughout the history of hydraulic research it is evident that the question of when and how model tests could be transferred to full-scale performance played a considerable role. The above problem is important for everybody engaged in research work. It was seen to be more complex when the same model was tested, for example, in different wind-tunnels, when apparently different results were obtained. However, nowadays it is possible to explain most of these differences. It was discovered that different air turbulence in tunnels affected the aerodynamical properties of models on test. For particular values of Reynolds number it is not sufficient to define each individually; multiplication by a turbulence factor is necessary.

The first step in the discussion is to define the conditions under which the model must operate by using Navier-Stokes equations for incompressible fluids.

For further discussion only the x-component of the Navier-Stokes equation will be used since the same rules can be applied for the other components. The deduction and transformation of the Navier-Stokes equation is given in Appendix 4-I.

The simplest way to compare model and full-scale results is to change the basic equations into a dimensionless form. For that purpose at an undisturbed point in the flow, the velocity C_o, the specific density ρ_o viscosity μ_o linear dimension L_o time t_o and acceleration due to gravity g_o are chosen. Accordingly, each term of the equation 4.1, see Appendix 4-I, is multiplied and divided by the physical and geometrical properties which are constant at this particular point.

To obtain similar differential equations for both flows (round the model and the object) and at the same time similar solutions for the unknowns C_x/C_o C_y/C_o C_z/C_o it is necessary that the equation 4.3 - see Appendix 4.I - should be valid for both the model and the prototype. Therefore for the similarity of general motions the dimensionless numbers must be equal.

The dimensionless numbers which satisfy equation 4.3 are as follows:

Strauhal's number: $st = \dfrac{C_o t_o}{L} = \dfrac{C_o}{Lf_o}$

Reynolds' number: $R_e = \dfrac{C_o L}{\frac{\mu_o}{\rho_o}} = \dfrac{C_o L}{\nu_o}$

Froude's number: $F = \dfrac{C_o^2}{g_o L}$

Euler's number: $E_u = \dfrac{P_o}{\rho_o C_o^2}$ 4.4

Mach number can be obtained from the equation:

$$\frac{\rho_o C_o^2}{P_o} = \frac{C_o^2}{a^2} k = k.M^2$$

where $M = \frac{C_o}{a}$

Euler and Mach numbers are physically identical.

Introduction of the new symbols into equation 4.3 - see Appendix 4-I - leads to:

$$\frac{1}{S_t}\frac{\partial\left(\frac{c_x}{c_o}\right)}{\partial\left(\frac{t}{t_o}\right)} + \frac{\partial\left(\frac{c_x}{c_o}\right)}{\partial\left(\frac{x}{L}\right)}\frac{c_x}{c_o} + \frac{\partial\left(\frac{c_x}{c_o}\right)}{\partial\left(\frac{y}{L}\right)}\frac{c_y}{c_o} + \frac{\partial\left(\frac{c_x}{c_o}\right)}{\partial\left(\frac{z}{L}\right)}\frac{c_z}{c_o} -$$

$$-\frac{1}{R_e}\frac{\frac{\mu}{\mu_o}}{\frac{\rho}{\rho_o}}\left[\frac{\partial^2\left(\frac{c_x}{c_o}\right)}{\partial\left(\frac{x}{L}\right)^2} + \frac{\partial^2\left(\frac{c_x}{c_o}\right)}{\partial\left(\frac{y}{L}\right)^2} + \frac{\partial^2\left(\frac{c_x}{c_o}\right)}{\partial\left(\frac{z}{L}\right)^2}\right] =$$

$$= \frac{1}{F_r}\frac{g_x}{g_o} - E_u\frac{\partial\left(\frac{p}{p_o}\right)}{\partial\left(\frac{x}{L}\right)} \qquad 4.5$$

The conditions shown in equation 4.5 are not sufficient since there are still some terms which have to satisfy the conditions of similarity.

Equality of the ratio g_x/g_o can be obtained easily by placing the model in the same gravity field as the prototype. It seems to be more difficult to obtain equality of the terms ρ/ρ_o and μ/μ_o as both quantities can be changed by the effect of temperature.

However, since the effect of temperature is not particularly great in the low speed tests, it may be disregarded.

Analysing the dimensionless numbers it is shown that the condition of complete similarity cannot be obtained. Comparison of

Reynolds' and Froude's numbers indicates that certain quantities in both numbers have an opposite effect.

The nature of testing indicates when and which dimensionless numbers are the most important and which of them may be neglected.

4.2 Dimensionless coefficients

The study of the effects of particular hydraulic parameters and their mutual comparison is facilitated by means of dimensionless coefficients. Dimensionless coefficients are independent of velocity, pressure, number of revolutions, dimensions etc. This fact is of great advantage in the study of experimental results. To enable us to analyse the results obtained from experiment the dimensionless coefficients are derived for our particular case.

Parameters which characterise the flow conditions in our problem are as follows:

$H\ [L]$ – head

$Q\ [L^3/T]$ – flow rate

$n\ [1/T]$ – number of revolutions

$D\ [L]$ – diameter of the impeller

$g\ [L/T^2]$ – acceleration due to gravity

$\rho\ [FT^2/L^4]$ – specific density

$\mu\ [FT/L^2]$ – dynamic viscosity

$E\ [L^2/T^2]$ – specific energy

$\nu = \frac{\mu}{\rho}$ Kinematic viscosity.

Units:

L - length   T - time   F - force

The following functional equation expresses the general relation among the quantities:

$$f\,(Q,\ E,\ n,\ D,\ \rho\ ,\mu\ ) = 0 \qquad 4.6$$

According to the theory of dimensionless products the complete set of variables is reduced to the rank which is expressed as follows:

$$Y = x - s \qquad 4.7$$

where

x - is the number of variables which occurs in our case.

and

s - is the rank of determinant formed from dimensionless matrix.

In our case:

$Y = 3$

Consequently, our parameters are reduced to the three dimensionless coefficients:

$$\Pi_1 = \frac{Q \cdot \rho}{D \cdot \mu}$$

$$\Pi_2 = \frac{E^2 D^2 \rho^2}{\mu^2}$$

and

$$\Pi_3 = \frac{n D^2 \rho}{\mu} \qquad 4.8$$

Obviously, various complete sets of dimensionless products can be formed again from the above coefficients. By making use of them, various dimensionless coefficients which are already known, are chosen for our problem:

Reynolds' number

$$\pi_1 = \frac{Q}{D \cdot \nu} = \frac{Q}{\nu} \frac{D}{D^2} = \frac{D}{\nu} \cdot c \qquad 4.9$$

Flow coefficient:

$$\pi_4 = \frac{\pi_1}{\pi_3} = \frac{Q}{n D^3} \qquad 4.10$$

Head coefficient:

$$\pi_6 = \frac{\pi_2}{\pi_3^2} = \frac{gH}{n^2 D^2} \qquad 4.11$$

Specific speed;

$$\pi_5 = \frac{\pi_3}{\sqrt{\pi_2}} = \frac{n \cdot Q^{1/2}}{(gH)^{3/4}} \qquad 4.12$$

Power coefficient:

$$\pi_7 = \frac{\pi_1 \cdot \pi_2}{\pi_3^2} = \frac{gHQ}{n^3 D^5} \qquad 4.13$$

Diameter coefficient:

$$\pi_8 = \sqrt{\frac{\sqrt{\pi_2}}{\pi_1}} = \frac{E^{1/4} \cdot D}{Q^{1/2}} \qquad 4.14$$

With the usual symbols the dimensionless coefficients have the following notation: $\varphi = \pi_4$ $\sigma = \pi_5$ $\Delta = \pi_8$

$\psi = \pi_6$ $\lambda = \pi_7$

If measurements are made in the following units:

H	[m]	D	[m]	N	[kgm/s]
Q	[m^3/s]	g	[m/s^2]		
n	[1/min]	γ	[kg/m^3]		

the dimensionless coefficients become:

$$\varphi = \frac{Q}{n D^3} \; \frac{4}{\pi^2} = 24{\cdot}4 \; \frac{Q}{n D^3} \tag{4.15}$$

$$\psi = \frac{2g H}{n^2 D^2} \; \frac{1}{\pi^2} = 7160 \cdot \frac{H}{n^2 D^2} \tag{4.16}$$

$$\sigma = \frac{\varphi^{1/2}}{\psi^{3/4}} = \frac{n \, Q^{1/2}}{(2g H)^{3/4}} \cdot 2\sqrt{\pi} = 0{\cdot}00633 \, n \, Q^{1/2} H^{3/4} \tag{4.17}$$

$$\Delta = \frac{\psi^{1/4}}{\varphi^{1/2}} = \frac{D \, (2gH)^{1/4}}{Q^{1/2}} \sqrt{\frac{\pi}{4}} = 1{\cdot}865 \, D \, H^{1/4} Q^{1/2} \tag{4.18}$$

$$\lambda = \frac{\varphi \psi}{2\eta} = \frac{N}{\frac{\gamma}{2g}} \; \frac{1}{n^3 D^5} \; \frac{4}{\pi^4} = 174500 \, \frac{N}{2\gamma} \, \frac{1}{n^3 D^5} \tag{4.19}$$

From the foregoing procedure it is obvious that only three basic coefficients describe our problem from the hydraulic point of view.

Thus, the fundamental coefficients are

Reynolds' number

Flow coefficient

Head coefficient

The physical meaning of Reynolds' number used in our case may be entirely different from the fundamental definition for a straight pipe. However, anything which disturbs the velocity of fluid changes the pattern of flow through a passage. Consequently the definition of Reynolds' number based on the average velocity is changed. Therefore, similarity of Reynolds' number does not ensure similarity of flow, since the change from laminar to turbulent flow may take place at different Reynolds' numbers when the pipe is not straight.

The following points are the main difficulties and differences;

a) the definition of the length of the channel

b) normally 20 to 40 pipe diameters are required to obtain the final velocity distribution. No such length is available in centrifugal pumps. Besides, the channels are rotating.

c) sections of the channels are mostly irregular.

From the above points it can be seen that many values of Reynolds' number can be assigned to the flow as it passes through a pump. Regardless of how Reynolds' number is defined, the points mentioned above will be reflected in it.

In addition to the specified definitions of Reynolds' number for the straight pipe and impeller channel, the question of kinematic viscosity arises.

In the present review of tests, using air instead of water for the working fluid this question is of great importance.

The kinematic viscosities for air and water at 20°C and 760 mmHg are respectively:

water : 0.01 $[cm^2/s]$

air : 0.149 $[cm^2/s]$

To obtain the same Reynolds' number in a water and air test it appears that the product C.D (C - velocity, D - diameter) requires to be approximately 15 times higher in the air test.

By changigg the speed and dimensions of the impeller the required conditions can be satisfied to a certain extent.

Appendix 4-I

The x - components of the Navier-Stokes equation are

$$\frac{\partial c_x}{\partial t} + \frac{\partial c_x}{\partial x} c_x + \frac{\partial c_x}{\partial y} c_y + \frac{\partial c_x}{\partial z} c_z - \frac{\mu}{\rho}\left(\frac{\partial^2 c_x}{\partial x^2} + \frac{\partial^2 c_x}{\partial y^2} + \frac{\partial^2 c_x}{\partial z^2}\right) = g_x - \frac{1}{\rho}\frac{\partial P}{\partial x} \tag{4.1}$$

Transforming the above equation into a dimensionless form we obtain:

$$\frac{c_o}{t_o}\frac{\partial\left(\frac{c_x}{c_o}\right)}{\partial\left(\frac{t}{t_o}\right)} + \frac{c_o^2}{L}\left[\frac{\partial\left(\frac{c_x}{c_o}\right)}{\partial\left(\frac{x}{L}\right)}\frac{c_x}{c_o} + \frac{\partial\left(\frac{c_x}{c_o}\right)}{\partial\left(\frac{y}{L}\right)}\frac{c_y}{c_o} + \frac{\partial\left(\frac{c_x}{c_o}\right)}{\partial\left(\frac{z}{L}\right)}\frac{c_z}{c_o}\right] -$$

$$- \frac{\mu_o}{\rho}\frac{c_o}{L^2}\frac{\frac{\mu}{\mu_o}}{\frac{\rho}{\rho_o}}\left[\frac{\partial^2\left(\frac{c_x}{c_o}\right)}{\partial\left(\frac{x}{L}\right)^2} + \frac{\partial^2\left(\frac{c_x}{c_o}\right)}{\partial\left(\frac{y}{L}\right)^2} + \frac{\partial^2\left(\frac{c_x}{c_o}\right)}{\partial\left(\frac{z}{L}\right)^2}\right] =$$

$$= g_o\frac{g_x}{g_o} - \frac{P_o}{\rho_o L}\cdot\frac{1}{\frac{\rho}{\rho_o}}\frac{\partial\left(\frac{P}{P_o}\right)}{\partial\left(\frac{x}{L}\right)} \tag{4.2}$$

Dividing the equation 4.2 by Co^2/L leads to the following:

$$\frac{L}{c_o t_o}\frac{\partial\left(\frac{c_x}{c_o}\right)}{\partial\left(\frac{t}{t_o}\right)} + \frac{\partial\left(\frac{c_x}{c_o}\right)}{\partial\left(\frac{x}{L}\right)}\frac{c_x}{c_o} + \frac{\partial\left(\frac{c_x}{c_o}\right)}{\partial\left(\frac{y}{L}\right)}\frac{c_y}{c_o} + \frac{\partial\left(\frac{c_x}{c_o}\right)}{\partial\left(\frac{z}{L}\right)}\frac{c_z}{c_o} -$$

$$- \frac{\mu_o}{\rho_o c_o L}\frac{\frac{\mu}{\mu_o}}{\frac{\rho}{\rho_o}}\left[\frac{\partial^2\left(\frac{c_x}{c_o}\right)}{\partial\left(\frac{x}{L}\right)^2} + \frac{\partial^2\left(\frac{c_x}{c_o}\right)}{\partial\left(\frac{y}{L}\right)^2} + \frac{\partial^2\left(\frac{c_x}{c_o}\right)}{\partial\left(\frac{z}{L}\right)^2}\right] =$$

$$= \frac{g_o L}{C_o^2} \frac{g_x}{g_o} - \frac{P_o}{\rho_o C_o^2} \frac{1}{\frac{\rho}{\rho_o}} \frac{\partial\left(\frac{P}{P_o}\right)}{\partial\left(\frac{x}{L}\right)} \qquad 4.3$$

Introduction of the symbols from the equation 4.4 into equation 4.3 result in equation 4.5. See chapter 4.1

5. EXPERIMENTAL WORK.

5.1 Design

The theoretical conditions predicted in chapter 3 require a simplified shape of impeller and casing with a suction nozzle and pipe attached.

Since the energy and flow phenomena have to be observed at the flow rate $Q=0$ only, it was felt that this simplification of the design was permissible. The question of efficiency does not arise and may be omitted. On the other hand, by simplifying the design certain geometrical influences are excluded and only important geometrical variables are explored.

The simplified rig was designed to fulfil the theoretical requirements as closely as possible. See figure 14 and plate No. 1 and 2.

An impeller of specific speed $\sigma = 0.16$ $n = 2520$ R.P.M. outlet diameter $D_2 = 20"$ and width of impeller 2" was chosen.

To correspond with the specific speed $\sigma = 0.16$ we must have for duty point, flow coefficient $\varphi = 0.03$ and head coefficient $\psi = 1.1$.

Since the increase and decrease of recirculation caused by the impeller geometry has to be studied, certain variations of impeller shape have been used.

Firstly, an impeller with parallel shrouds and straight radial

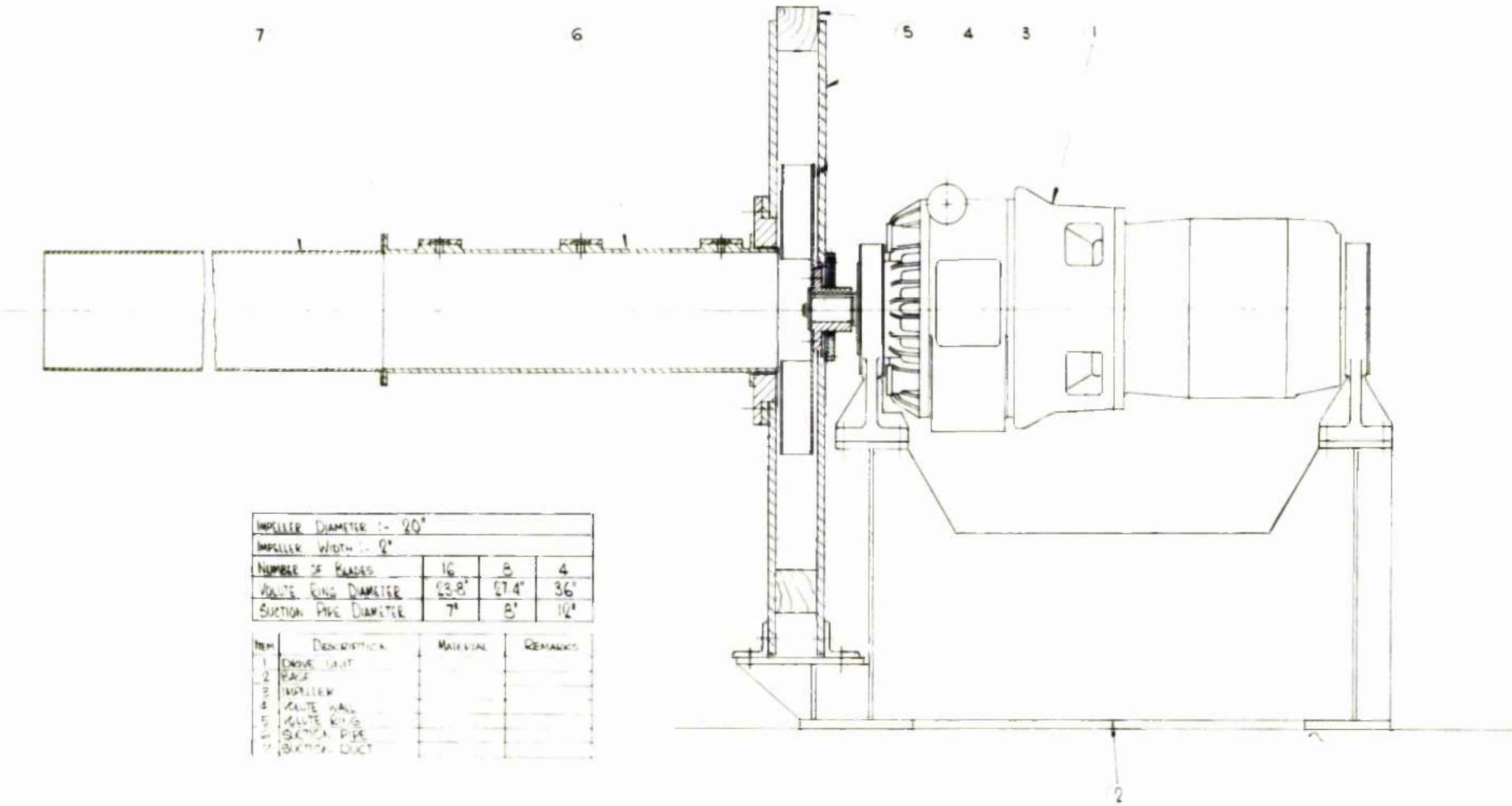

IMPELLER DIAMETER :- 20"			
IMPELLER WIDTH :- 2"			
NUMBER OF BLADES	16	8	4
VOLUTE RING DIAMETER	23.8"	27.4"	36"
SUCTION PIPE DIAMETER	7"	8"	10"

ITEM	DESCRIPTION	MATERIAL	REMARKS
1	DRIVE UNIT		
2	BASE		
3	IMPELLER		
4	VOLUTE WALL		
5	VOLUTE RING		
6	SUCTION PIPE		
7	SUCTION DUCT		

Fig.14 General lay-out.

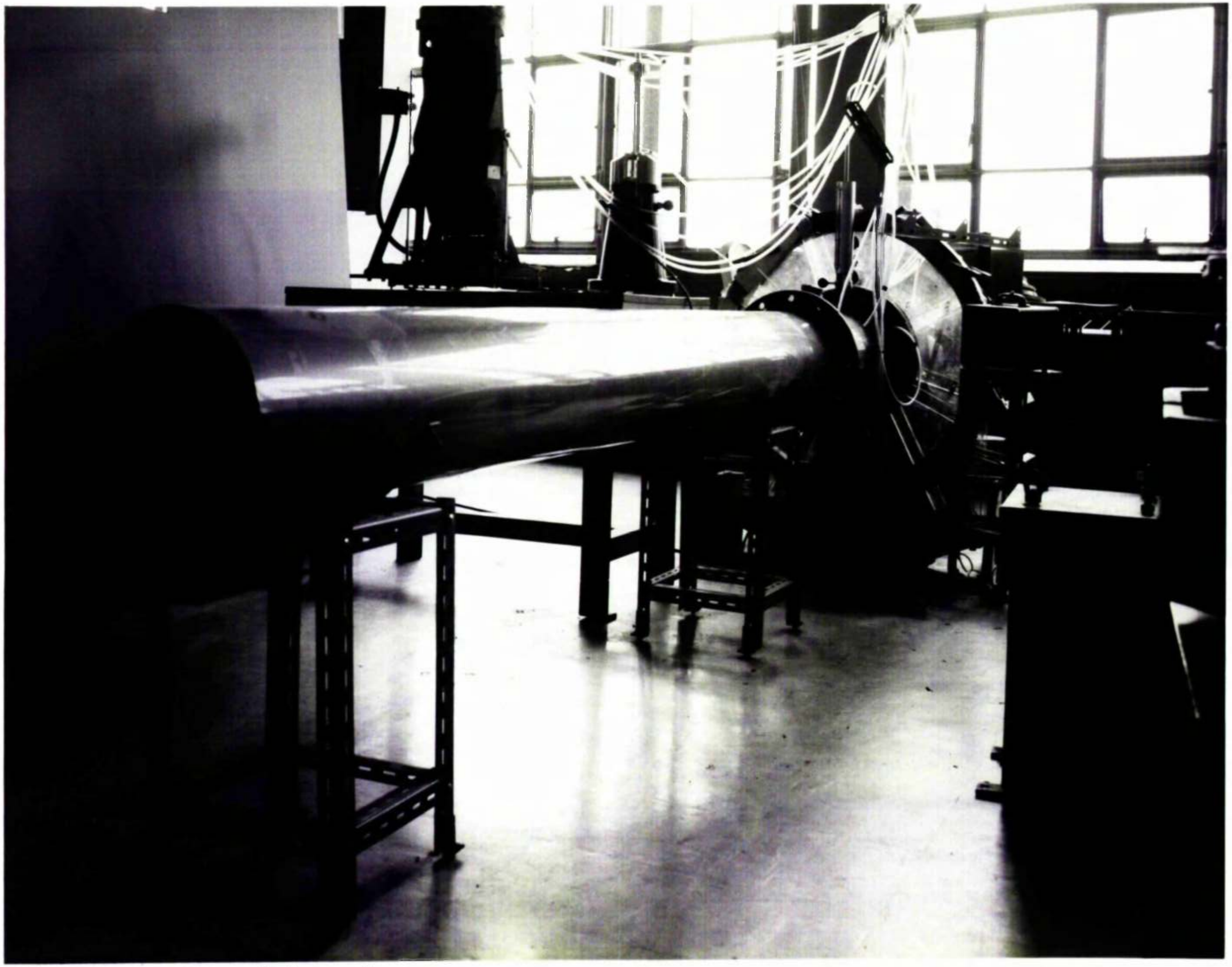

Plate No 1. General lay-out

blades was chosen. The general lay-out is shown in figure 14. Secondly, the number of blades was varied from:

$z = 4; \quad 8; \quad 16$

Thirdly, the inlet diameters chosen are listed below:

$D_1 = 7"$ $\qquad D_1 = 8"$ $\qquad D_1 = 12"$

With a view to approaching the theoretical fluid motion the casing was designed in cylindrical form with parallel side walls.

The influence of the casing on inlet conditions, recirculation and outlet conditions has been observed for three different diameters of casing $D_3 = 23.8"$ $\qquad D_3 = 27.4"$ $\qquad D_3 = 36"$ and 3" wide.

5.2 Description of the rig

5.21 General

A rig had to be designed for the purpose of this investigation. Due to specific requirements considerable simplification was made so that every element of the apparatus could be changed in a short time.

For the reason stated above the shrouds of the impeller and blades were screwed together. This enabled the number of blades to be changed if desired.

In addition, three variations of suction nozzle and suction pipe were made each of which could be simply screwed to the casing. See plate No.2.

The cylindrical casing consisted of two parallel walls with

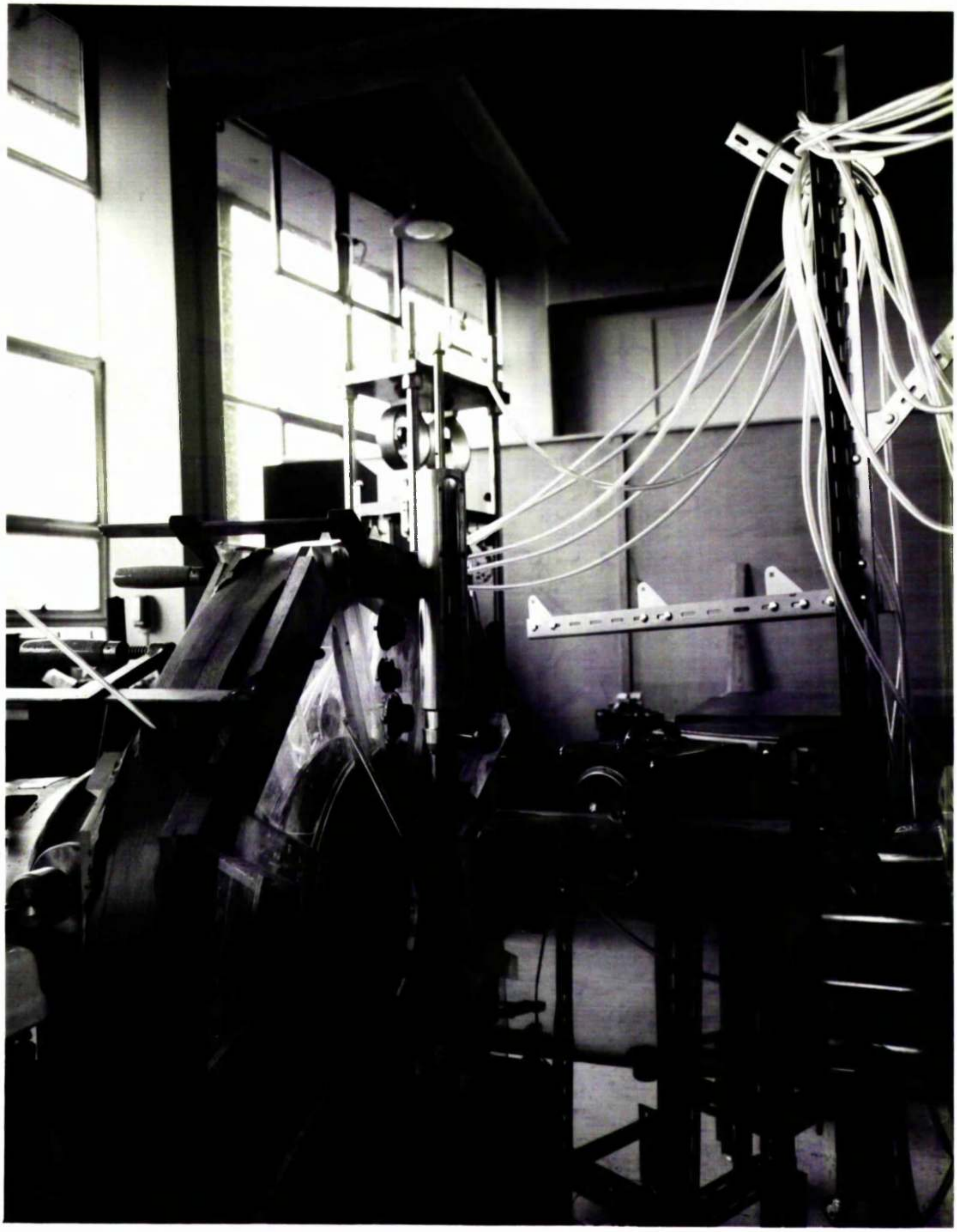

Plate No 2. Probe fitted at suction side an outer wooden ring whose diameter could be changed. The side walls and wooden rings were secured by means of clamps and sealed with plasticine. See plate No.3.

On the suction side arrangements were made to fit the cylindrical probe at three different sections. See figure 15 and plate 2 and 3. At each section four traverses could be made by rotating the suction nozzle by 45°.

Transparent gauge connecting lines were used to link the cylindrical probe with the manometer. Pressure readings were read on a Schiltknect-Zurich manometer of accuracy 1/10mm.

Temperature measurement was facilitated by means of a thermometer fitted in the special "pocket" at each section.

A similar arrangement was provided at the discharge side where the same cylindrical probe was used. The probe was connected to a multi-tube manometer with plastic tubes. A scale divided in tenths of an inch was used for pressure readings. See plate No.4.

The impeller was driven by a swinging field motor made by KOPP and rated at 10 H.P. A mechanical device was used to change the speed of the output shaft. In addition, the impeller speed was observed by stroboscope.

The reaction torque was measured by applying loads to the tray suspended from an arm attached to the frame. See plate No. 1 and 5.

The other arm was used as a control arm which was fitted to an Avery balance.

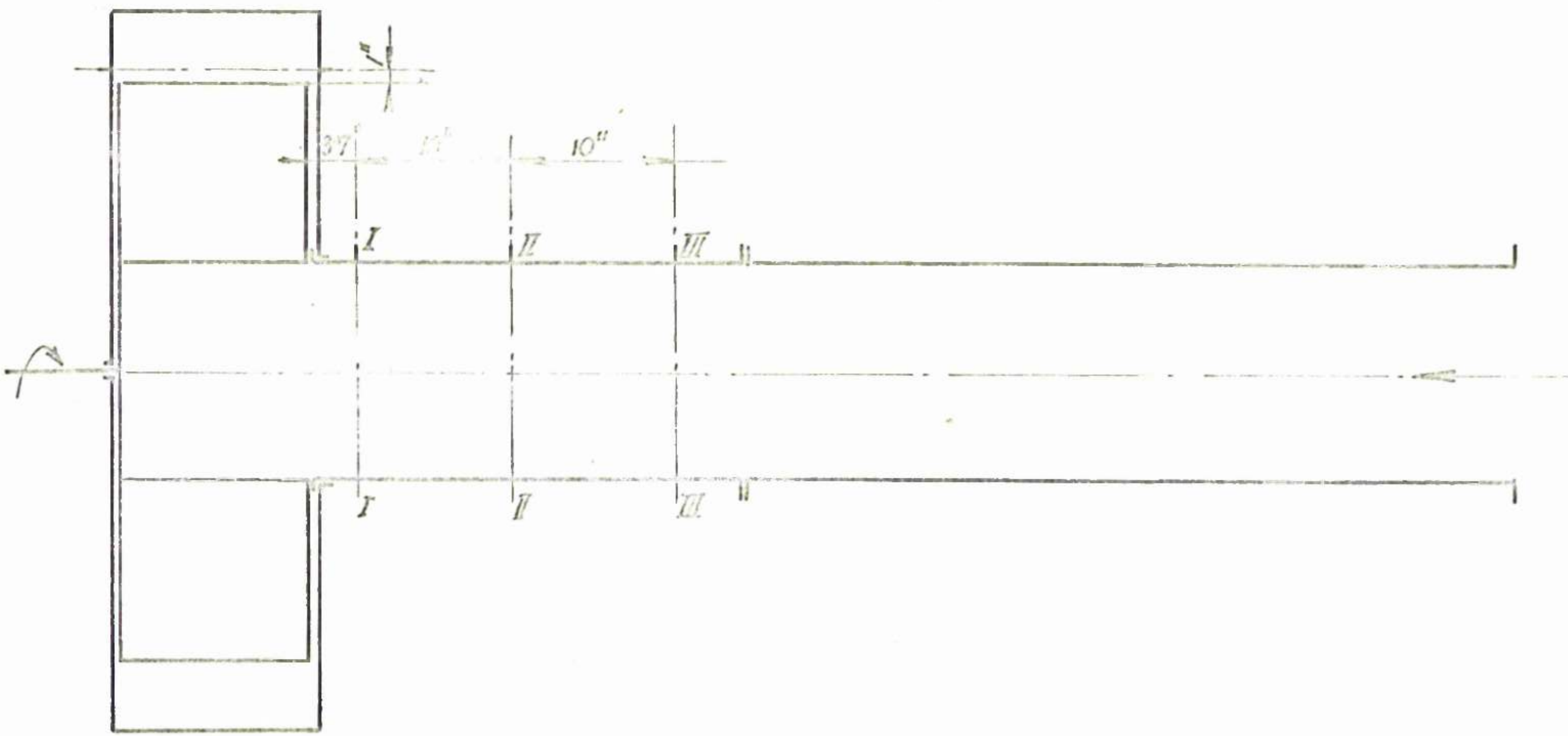

FIG. 15 MEASUREMENT POSITIONS

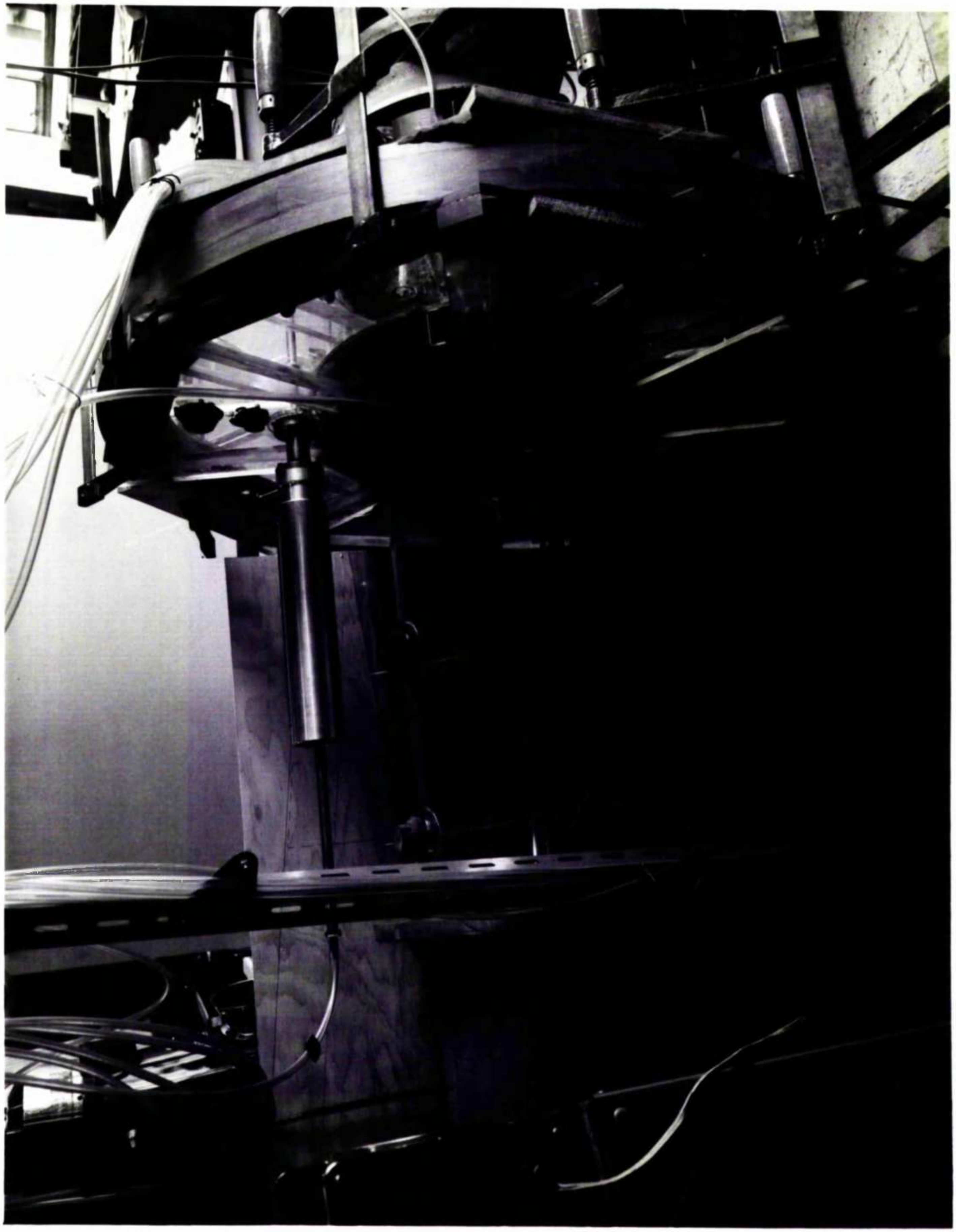

Plate No.3 Probe fitted at discharge side

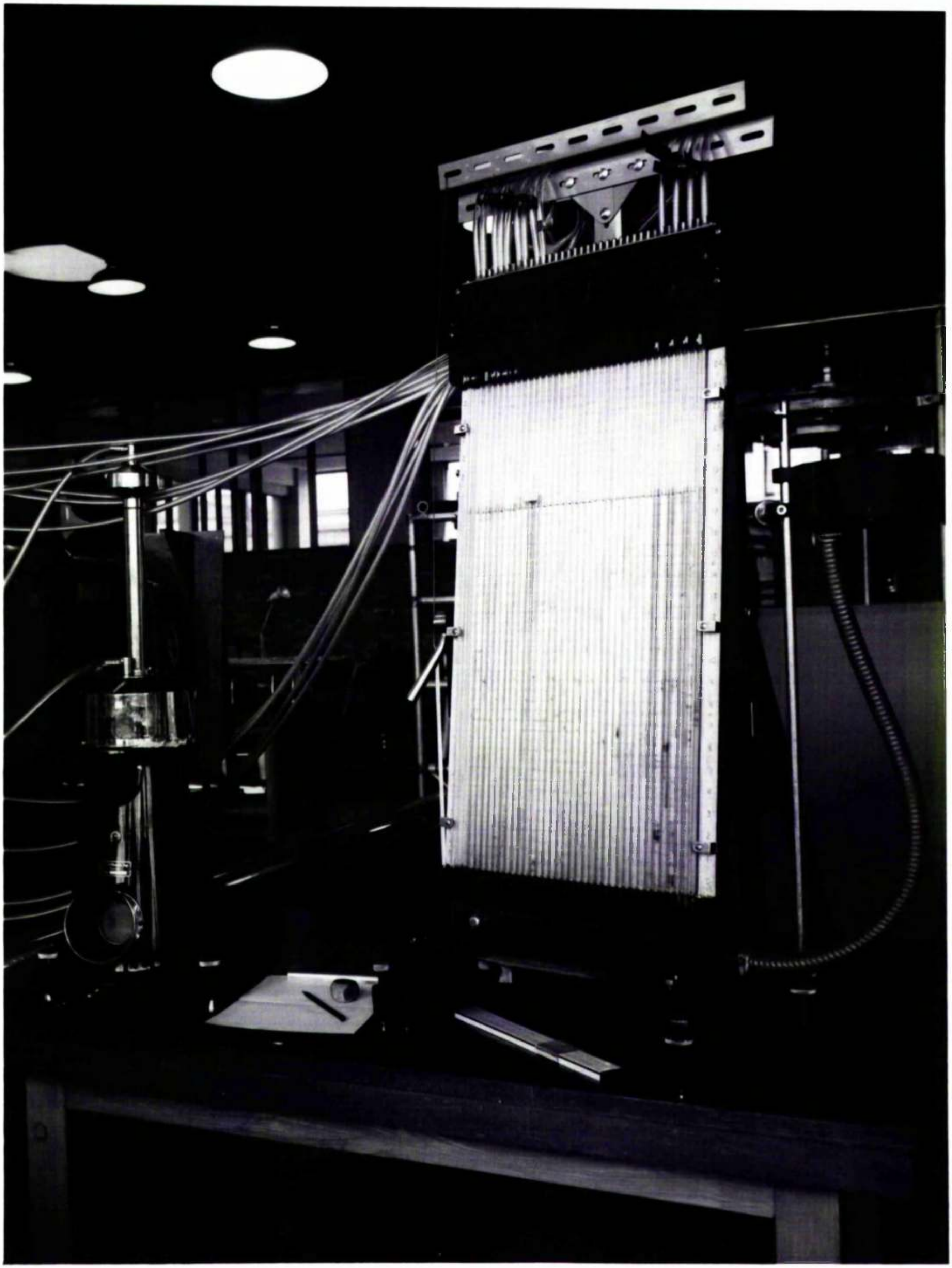

Plate No.4 Pressure instruments

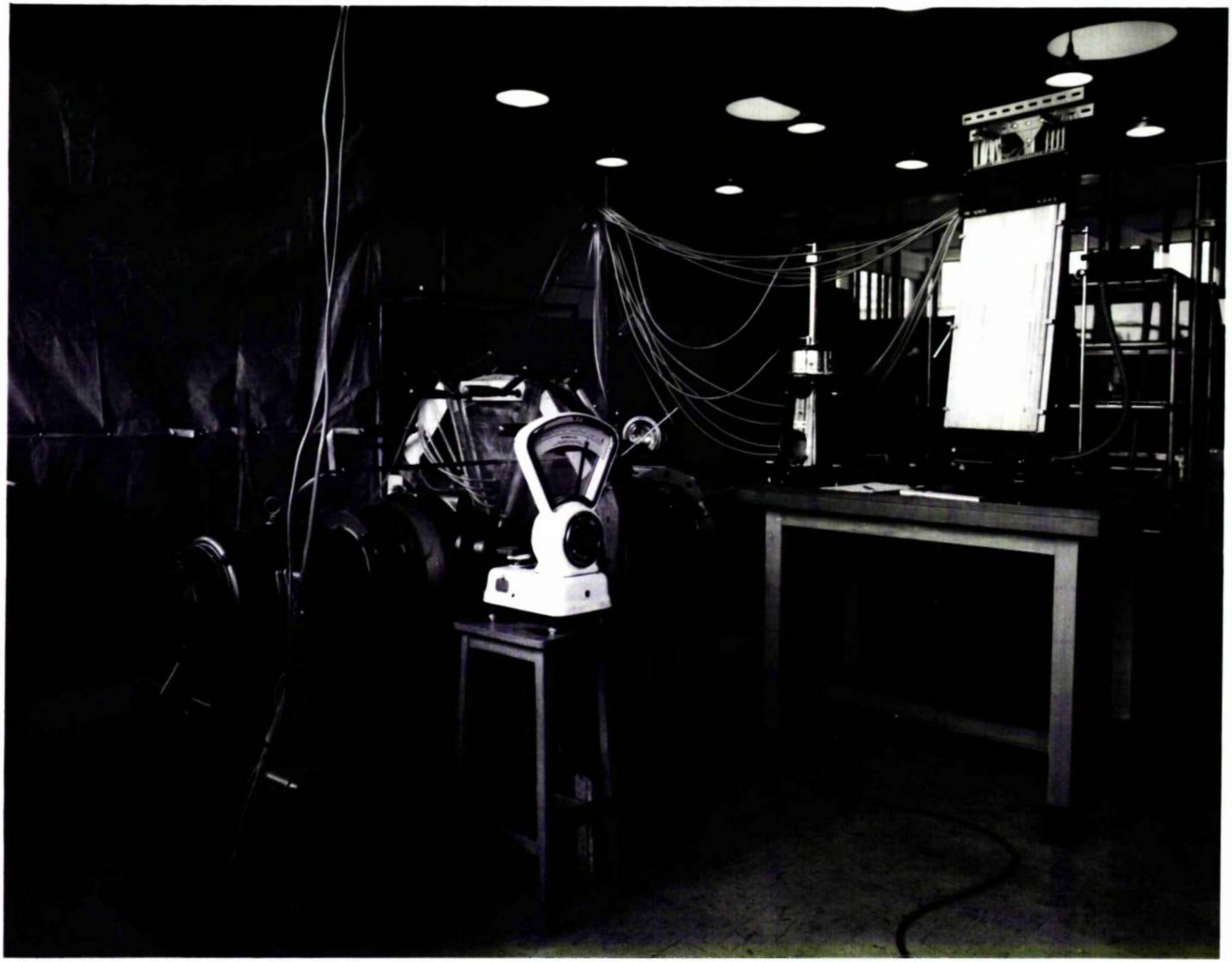

Plate No.5 Power measurement

When the swinging motor with both arms and the balance were in equilibrium no torque was applied to the shaft and the pointer of the balance pointed to zero.

To eliminate as many losses as possible the motor with speed variator was balanced at n = 2520 R.P.M before the impeller was fitted on the shaft. In this way only the mechanical loss between hub and sealing (felt) was left and put on impeller account.

5.22 Flow visualisation

To make a comprehensive study of velocity and pressure distribution throughout the suction nozzle and also at the impeller outlet, it was desirable to have visual observation.

The suction nozzle and volute walls were made of perspex to allow observation of the flow distribution at the inlet and outlet of the impeller. See plates Nos. 6, 7, 8, 9 & 10.

To obtain more information about the flow pattern and recirculation, arrangements were made to fit a network of cotton tufts at various positions in the suction pipe. See plates 6, 7, 8 and 9.

Special care was taken to fit tufts properly, to avoid introducing any initial direction. A thick brass wire was drilled at 1/2" distance and in each hole a tuft was placed having a knot on one side and being loose on the other side.

Facilities were made to fix tufts at three different sections in the suction pipe and at one position at the discharge of the

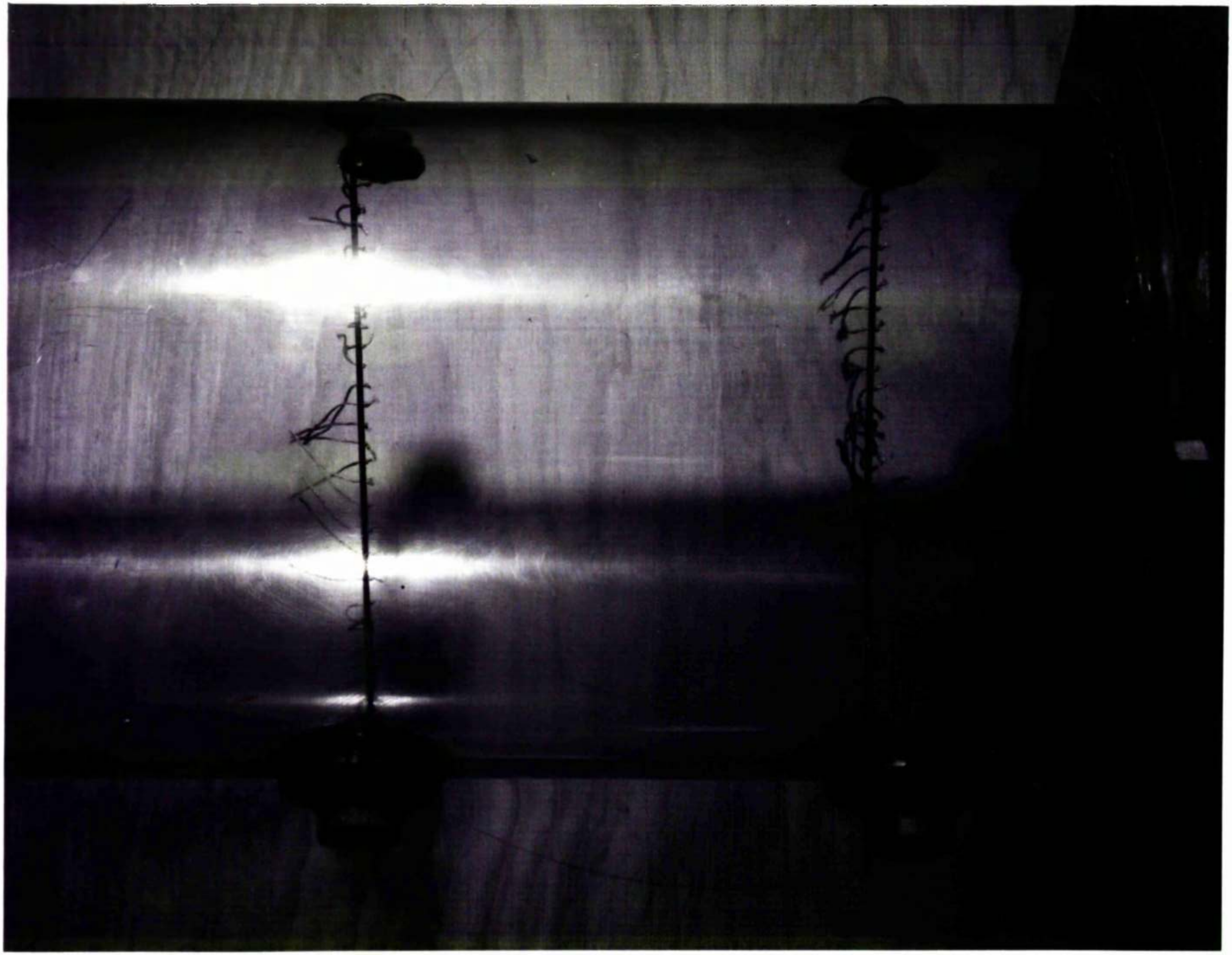

Plate No.6 Observation of flow by means of tufts at suction side

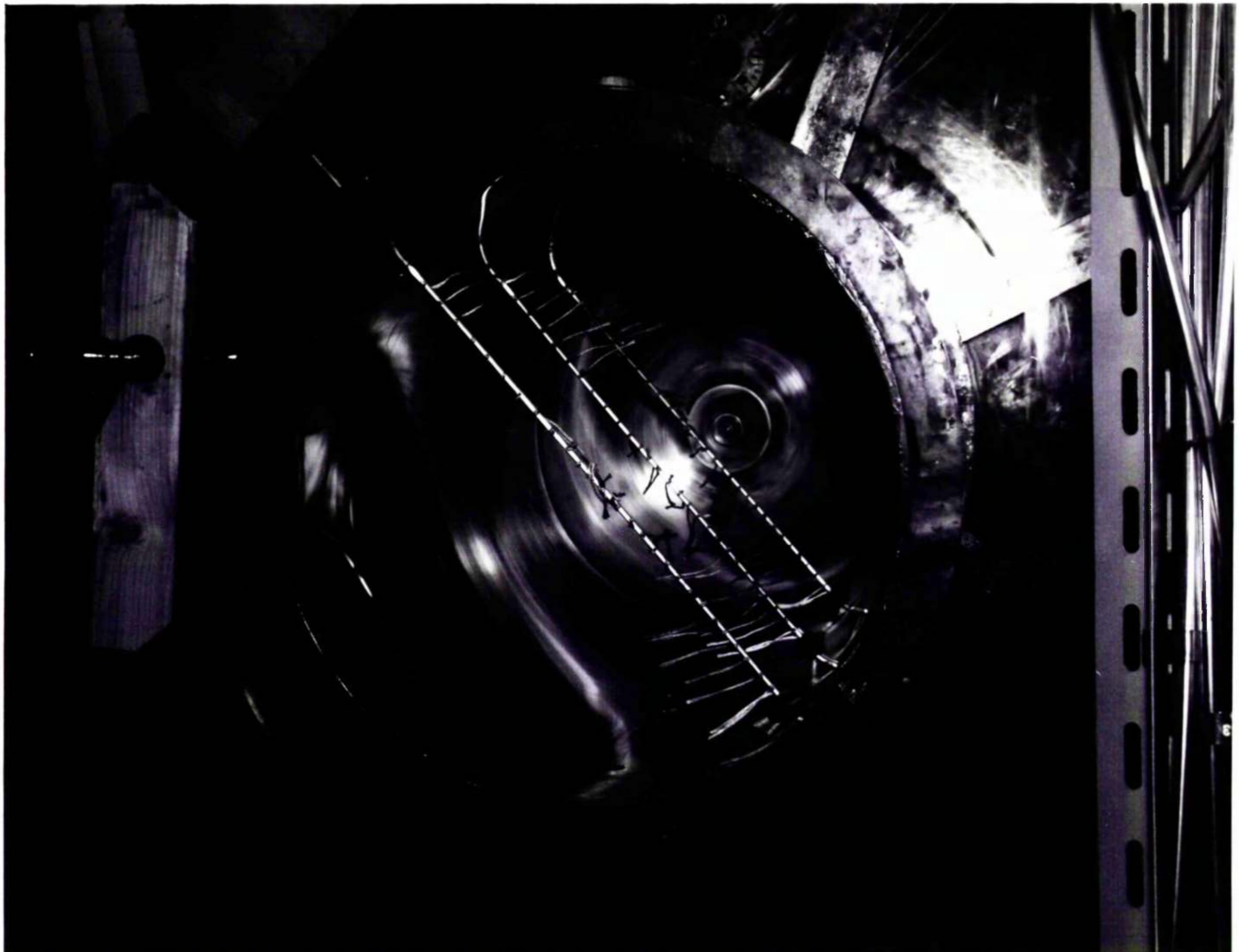

Plate No.7 Observation of flow at suction side (suction pipe removed)

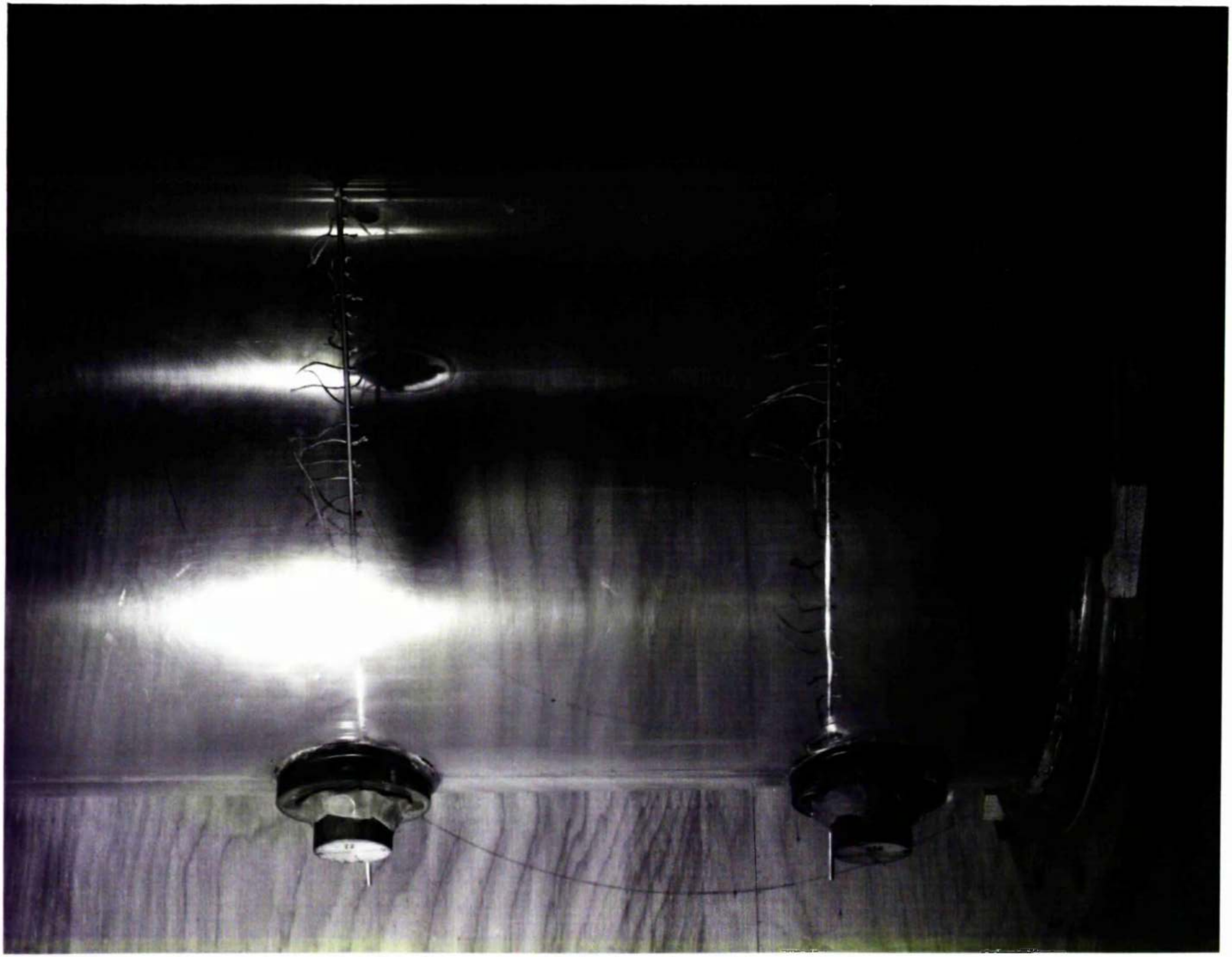

Plate No 8. Observation of flow by means of tufts at suction side

Plate No.9. Observation of flow at suction side (suction pipe removed)

Plate No.10 Observation of flow by means of tufts at discharge side impeller. This enabled the author to get a good visual picture of the flow conditions along the suction pipe and at the exit. The behaviour of the flow across the entire section was seen by rotating a suction nozzle with detached tufts. Disposition of the tufts and its picture can be seen in figure 15 and plates 6, 7, 8 and 9.

5.3 Estimation of flow properties

5.31 General

Hydraulic and flow properties will now be discussed in detail:

a) Velocity

b) Specific weight

c) Flow rate

d) Pressure

e) Power

f) Speed

5.32 Velocity

As very little information was available regarding the flow conditions at Q=o the author wished to get first of all a good general idea of flow distribution.

For that purpose the visual method was used. The first network of cotton tufts was placed at the distance of 3.7" from the impeller. The other two network were fitted along the suction nozzle

10" apart. By turning the suction nozzle 4 times through 45° the whole section was visualised and a good picture of the flow distribution was obtained.

The velocity field in the middle of the pipe was seen to be neutral, with no indication of flow whatever, and it might be said that dead-space existed in the core of the pipe.

Outside this core the velocity field rotated impellerwise with indication of a strong forced vortex. The velocity field between core and pipe wall could be divided into two annuli where the inner part of this annulus moved towards the pump and the outer part near the pipe wall moved away from the pump. The recirculation decayed rapidly along the suction pipe and entirely died out before it reached the entrance of the suction pipe. No flow movement was observed at the entrance of the pipe.

These first observations indicated that the radial pressure gradient changed its value from positive to negative.

Similarly, fitted tufts were used to investigate the discharge from the impeller. The velocity distribution was fairly constant. The resultant velocity near the side walls was directed toward the impeller but outward from the impeller near the middle of the issuing velocity field. Pressure gradient parallel to the axis of rotation was found to be constant except near the side walls.

The type of instrument selected for the measurement of velocity depended on the geometrical conditions of the test and the accuracy required. Further features to be looked for were those desirable in all probes for flow surveys.

a) Sufficiently small to avoid significant alterations in the flow

b) Measurement as nearly as possible at a point

c) Suitable for use in restricted spaces, easy to introduce and seal

d) Sufficiently easy to handle

For the preliminary test the pitot cylinder of the cantilever type with four orifices was used. The probe of 1/2" diameter was equipped with one orifice at the probe tip and the other three orifices in one section at a distance of 1" from the tip.

First measurements were taken in the suction pipe. Careful analysis was made as it was seen that the radial static pressure gradient changed its direction very rapidly. This rapid change of static pressure indicated that the distance of the fourth orifice (i.e.1") was too big to give reliable results. The worst situation happened when the probe was placed in the flow field where the first three orifices were in the positive pressure region and the fourth one in the negative pressure region.

The same probe was used at the discharge side. The main disadvantages of this probe were found to be:

a) Flow was asymmetrically squeezed and disturbed

b) Technical conditions required two accesses to fit a probe

Since the probe described above was not suitable for the velocity measurement no further comments will be made.

First observations of the flow conditions at the discharge indicated that the velocity field was almost two-dimensional. The flow conditions at the suction side were more complicated and it was expected that only moderate accuracy of velocity measurement could be obtained.

A simple 1/2" cylindrical probe with two orifices and the attached device for angle measurement was used. See plates Nos. 2 and 3.

It is known that the pressure on the front of the cylinder is equal to the sum of the pressure head and the velocity head of the fluid. The pressure falls away on either side of this point and at approximately 40 degrees the wall pressure is equal to the static pressure of the fluid. By taking measurement of the pressure on the wall of a cylinder it is therefore possible to calculate the total and static head of fluid in which it is inserted. Since the distribution is symmetrical about the diameter parallel to the line of flow, it is also possible to deduce the direction of flow by finding two points on the same circumference at which the pressure is equal.

Great care was taken in alignment of the probe with the rig. The line drawn between the two orifices on the probe represented the reference line to which all the other geometrical lines were aligned. The apparatus was considered to be aligned properly when the centre line of the suction pipe and the centre line of impeller matched in a horizontal line and formed an angle of

90 degrees with the reference line of the probe. In addition, the reference line between the two orifices had to be perpendicular so that the datum was well fixed.

Similar alignment was made at the discharge side where the reference line of the probe and side wall of the casing formed an angle of 90 degrees. The reference line between orifices had to be orientated vertically and orifices faced away from the impeller, thus the datum was fixed. See figure 16a.

The two-hole probe required certain manipulation at each measuring point. Firstly the pressure at each hole was balanced on a differential manometer and the static head measured directly. The total head was then obtained by rotating the probe through the angle θ so that one hole faced directly into the flow. Simultaneously, the angle of the flow direction was taken. See figure 16.

Later it will be shown how the velocity at any point could be found. The relation between total, static and dynamic pressures is usually expressed by the following equation:

$$P_t = P_{st} + P_d \qquad 5.1$$

and the dynamic pressure could be expressed by the equation,

$$P_d = \frac{\gamma c^2}{2g} \qquad 5.2$$

giving for the velocity,

$$c = \sqrt{\frac{2g}{\gamma} . Pd} \qquad 5.3$$

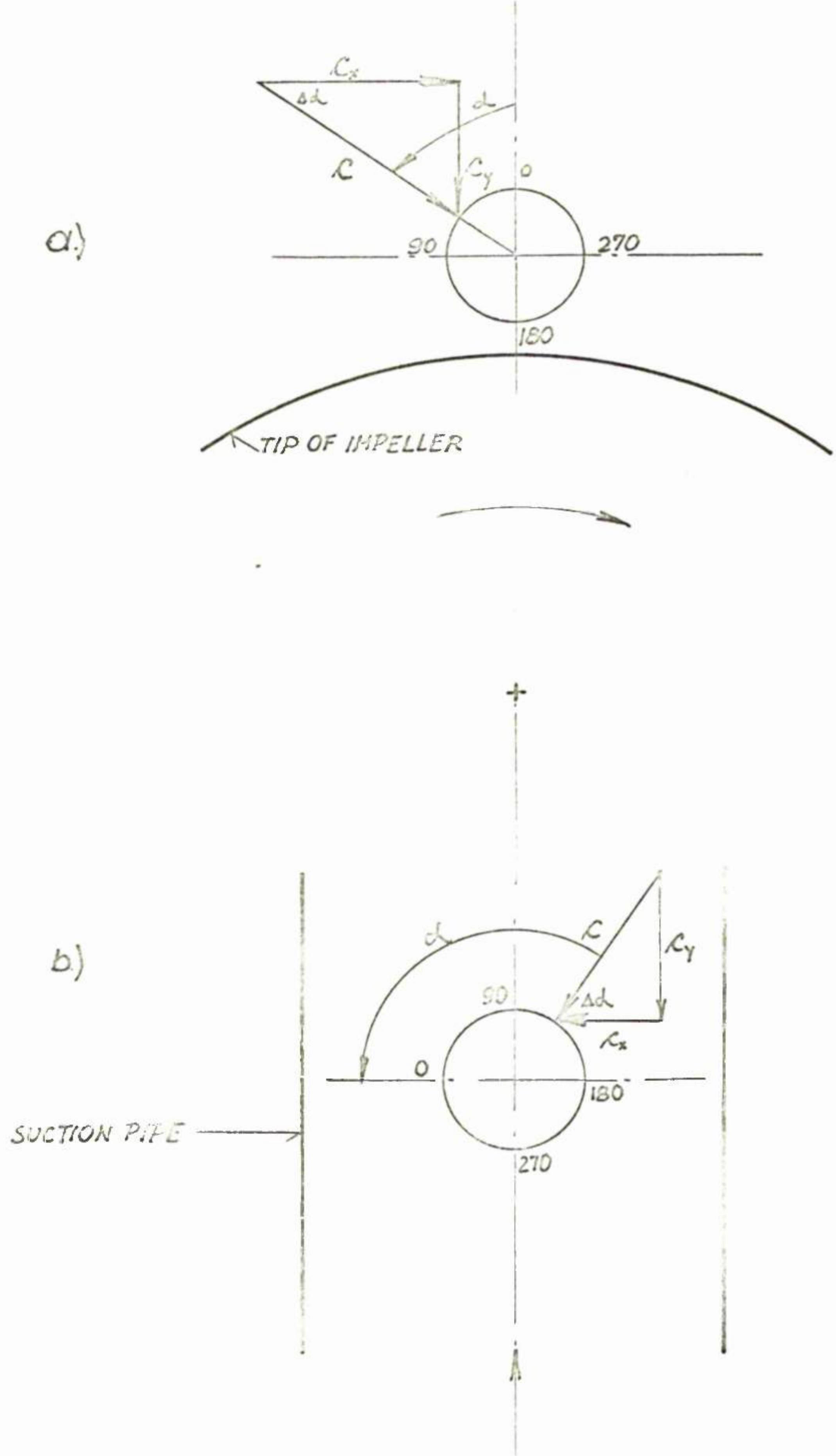

FIG. 16 ORIENTATION OF THE PROBE AT THE SUCTION AND DISCHARGE SIDE

Two velocity components at the suction side of the pump were found, see figure 16.

$$C_y = C \sin \Delta\alpha$$

and

$$C_x = C \cos \Delta\alpha \qquad 5.4$$

where

C_y - axial velocity

C_x - circumferential velocity

If C_y was directed towards the pump its direction was taken as positive and vice versa.

The velocity components at the discharge side were as shown below, see figure 16

$$C_y = C \sin \Delta\alpha$$

and

$$C_x = C \cos \Delta\alpha \qquad 5.5$$

where

C_y - radial velocity

C_x - circumferential velocity

If C_y was pointed away from impeller the velocity was considered as positive and vice versa.

It is understood that in equation 5.3 specific weight of the measuring fluid γ has to be known before velocity can be worked out.

5.33 Specific weight

Specific weight (weight/volume) γ of the air depends on atmospheric pressure P_{at} and on the relative humidity. The relative humidity is the ratio of the actual amount of water present to that required to saturate it at the same temperature and at the same volume.

A "wet and dry bulb" hygrometer was used to measure humidity. It consists of two thermometers of which one bulb is always wet (tw) and the other is dry (td). The difference in temperature between both thermometers depends on the relative humidity of the air.

The following relationship defines γ:

$$\gamma = f(P_{at},\ td,\ tw) \qquad 5.6$$

Since in our rig the pressure and temperature conditions were different to those in the ambient atmosphere the correction for that discrepancy was made.

The following equation for specific weight of the air was used,

$$\gamma = 116.2\ P_{st}\ 10^{-6}\ \frac{24}{273.15 + te} \left[0.49\ P_{at} - 0.378\ P_{sat} + 0.00359\ (td - tw) \right] \qquad 5.7$$

which takes into account increase in temperature te and the change in pressure P_{st} in the rig at the measuring point

γ - specific weight $[Kg/m^3]$

P_{at} - barometric pressure $[in\ Hg]$

P_{st} - static pressure relative to atmosphere $[mm\ W.G.]$

P_{sat} - saturated pressure of steam at te $[lb/in^2]$

te - line temperature $[^\circ C]$

td - dry bulb temperature $[^\circ C]$

Although the change in specific weight of air at the suction side was not very significant, considerable change was noticed at the discharge side.

5.34 Flow rate

The circulatory flow rate was determined at the suction side and at the discharge side of the pump. By visual observation it was noticed that strong decay of recirculatory flow existed along the suction pipe. To obtain exact data of the velocity and flow distribution along the suction pipe measurements were made across three different sections. See figure 15. Due to considerable velocity variation across each section complete traverses were made in order to get full profiles of velocity distribution and to minimize errors in flow measurements. It was found that the velocity profile at the suction side was fairly symmetrical so that only one traverse was necessary. For convenience the vertical traverse was always taken. The disposition of the flow measurement planes is shown in figure 15.

The direction of the flow is the same as that chosen for the velocity component Cy.

The flow entering the pump at the suction side and the flow discharging into the casing were both taken as positive.

The flow rate across any section is determined from the known velocity distribution and the area of the section. By integrating the velocity/radius graph, the flow rate can be obtained.

Estimation of flow rate at suction side:

Two simple principles already known were used for flow rate determination.

The flow rate is expressed mathematically:

$$Q = 2\pi \int_0^r C_y r\,dr = \pi \int_0^r C_y \, d\,(r^2) \qquad 5.8$$

In practice the equation 5.8 is solved graphically. The velocity at each point of the traverse is multiplied by the corresponding radius and plotted along the radius. It can be seen that the same results are obtained by plotting velocity against r^2 See figure 17. The graph is finally integrated by planimeter and the area obtained is directly proportional to the flow rate.

When the traverse is made across the whole diameter of the pipe the flow rate becomes:

$$Q^1 = 2\pi \int_{-r}^{r} C_y\, r\,dr = 2\pi \int_{-r}^{0} C_y\, r\,dr + 2\pi \int_{0}^{r} C_y\, r\,dr$$

$$= \pi \int_{-r}^{0} C_y\, d(r^2) + \pi \int_{0}^{r} C_y\, d(r^2) \qquad 5.9$$

where

$$Q = \frac{Q^1}{2} \qquad 5.10$$

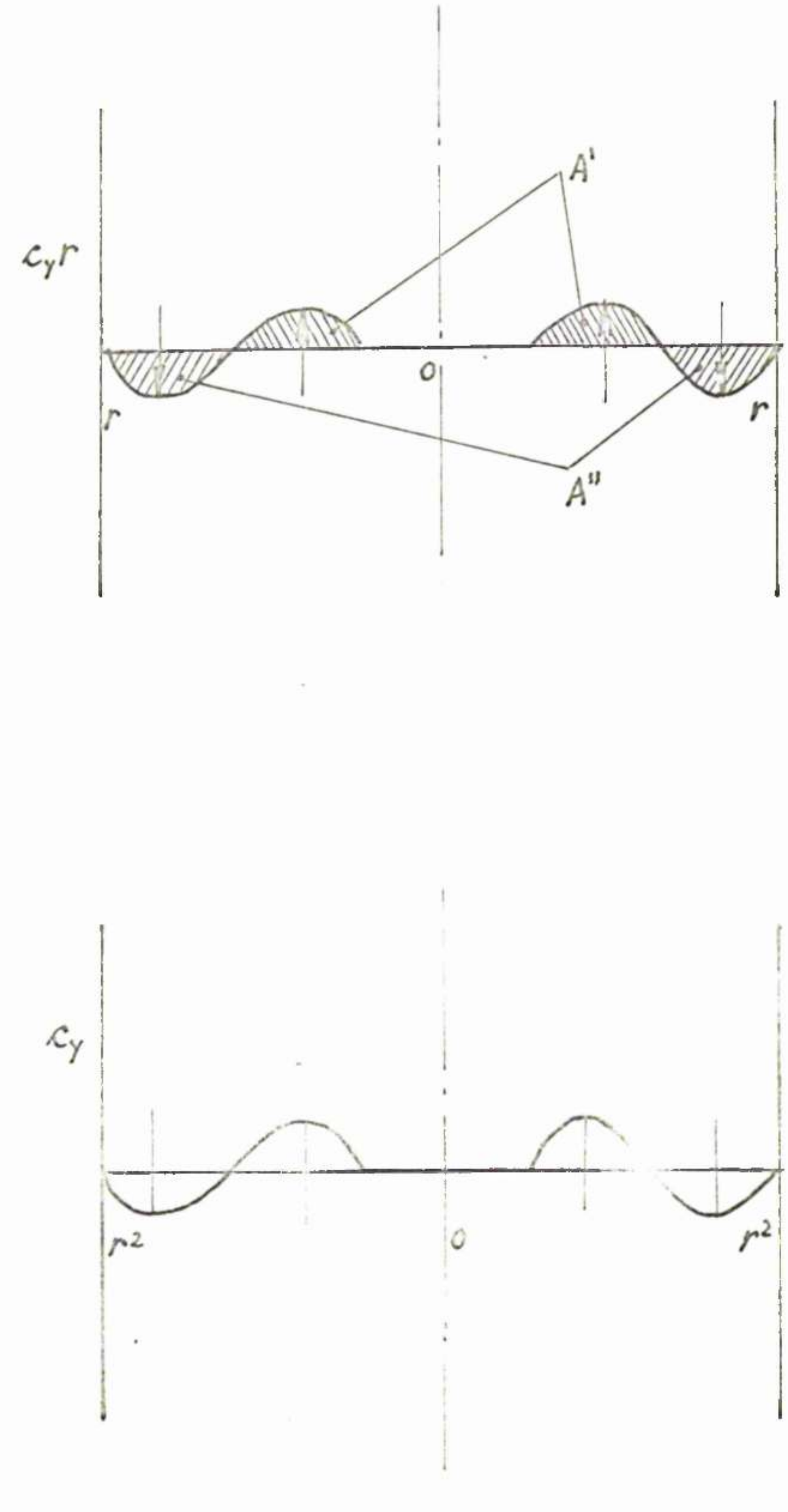

FIG. 17 ESTIMATION OF FLOW RATE AT THE SUCTION

Generally, if traverses across the whole section are made the flow rate is:

$$Q^{1} = \frac{2\pi}{n}\int_{-r}^{r} c_y r\,dr = \frac{2\pi}{n}\int_{-r}^{0} c_y r\,dr + \frac{2\pi}{n}\int_{0}^{r} c_y r\,dr = \frac{2\pi}{n} A \qquad 5.11$$

where

$$Q = \frac{Q^{1}}{2n} = \frac{\pi}{n^2} A \qquad 5.12$$

and

$$A = \int_{-r}^{0} c_y r\,dr + \int_{0}^{r} c_y r\,dr \quad \text{integrated area} \qquad 5.13$$

In our case one or two traverses were usually made. When only one traverse was made equation 5.9 was used, but when two traverses were made the following equation was deduced:

$n = 2$

$Q^{1} = \pi A$

Actual flow rate is then

$$Q = \frac{\pi}{4} A \qquad 5.14$$

The equation 5.14 represents flow rate across one quarter of the section.

For "positive flow" the flow rate across each quarter of the section is:

$$Q_1^{1} = \frac{\pi}{4} A_1^{1} \qquad Q_3^{1} = \frac{\pi}{4} A_3^{1}$$

$$Q_2^{1} = \frac{\pi}{4} A_2^{1} \qquad Q_4^{1} = \frac{\pi}{4} A_4^{1} \qquad 5.15$$

and the total average flow rate becomes:

$$Q = \frac{\pi}{4} (A_1' + A_2' + A_3' + A_4') \qquad 5.16$$

Similarly "negative flow" across each quarter of the section is:

$$Q_1'' = \frac{\pi}{4} A_1'' \qquad Q_3'' = \frac{\pi}{4} A_3''$$

$$Q_2'' = \frac{\pi}{4} A_1'' \qquad Q_4'' = \frac{\pi}{4} A_4'' \qquad 5.17$$

and the total average flow rate becomes:

$$Q = \frac{\pi}{4} (A_1'' + A_2'' + A_3'' + A_4'') \qquad 5.18$$

For continuity, positive flow and negative flow should be equal.

Estimation of flow rate at the discharge:

The average "positive flow" rate was obtained by the following equation see figure 18.

$$Q^1 = 2\pi R \int_0^b C_y \, db = 2\pi R B^1 \qquad 5.19$$

where

$$B^1 = \int_0^b C_y \, db \quad \text{- integrated area}$$

and

b - width of the casing

R - radius where readings were taken,

and for "negative flow"

$$Q'' = 2\pi R \int_0^b C_y \, db = 2\pi R B'' \qquad 5.20$$

where

$$B'' = \int_0^b C_y \, db \quad \text{- integrated area.}$$

For continuity, both flows should be equal.

$$Q^1 = Q''$$

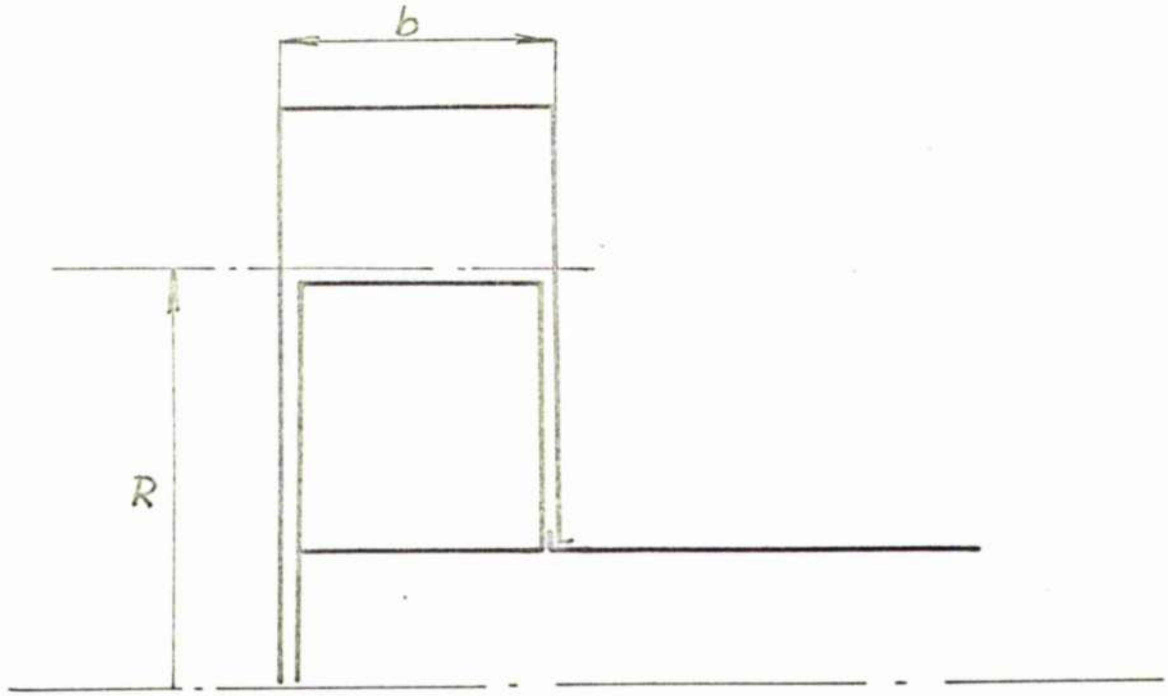

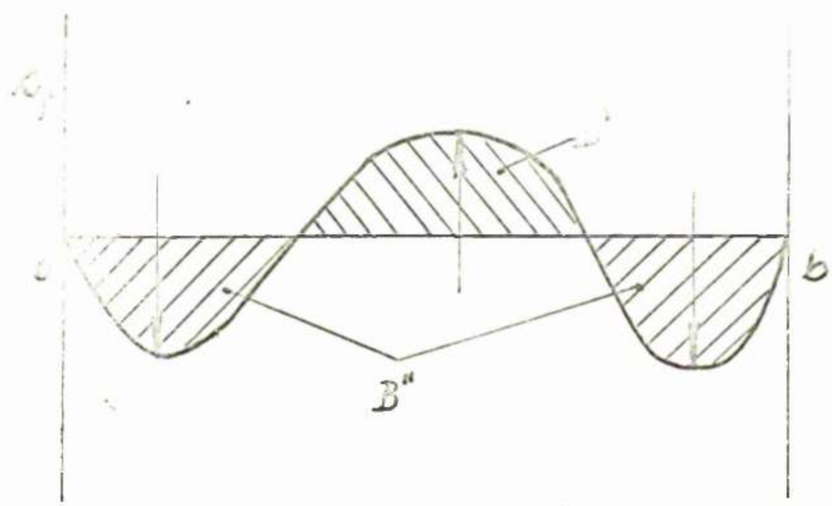

FIG.18 ESTIMATION OF [illegible] RATE AT THE DISCHARGE

5.35 Total pressure

Total pressure at any point is defined by equation:

$$P_t = P_{st} + Pd = P_{st} + \frac{1}{2}\rho C^2$$

Due to considerable variation of total and static pressure at the inlet the average total pressure across the measuring section was required.

The average total pressure across one diameter is expressed by:

$$P_{t_s} = \frac{\pi \int_{-r}^{r} P_t' C_y r\,dr}{Q} = \pi \frac{A}{Q} \qquad 5.21$$

where

$$A = \int_{-r}^{0} P_t' C_y r\,dr + \int_{0}^{r} P_t' C_y r\,dr \quad \text{- integrated area} \qquad 5.22$$

and

P_t' total pressure at measured point

The quantity ($P_t' C_y r$) was plotted for several points along the diameter as shown in figure 19. Obviously, the area of the above graph was equal to the integral defined by term A. When the term A was divided by flow rate Q, the average total pressure was obtained.

In a situation where variation of total pressure was not very significant (at the discharge) the average total pressure was directly obtained by integrating the total pressure plot.

The total head definitions as defined above were used for positive and negative flow with corresponding variables introduced

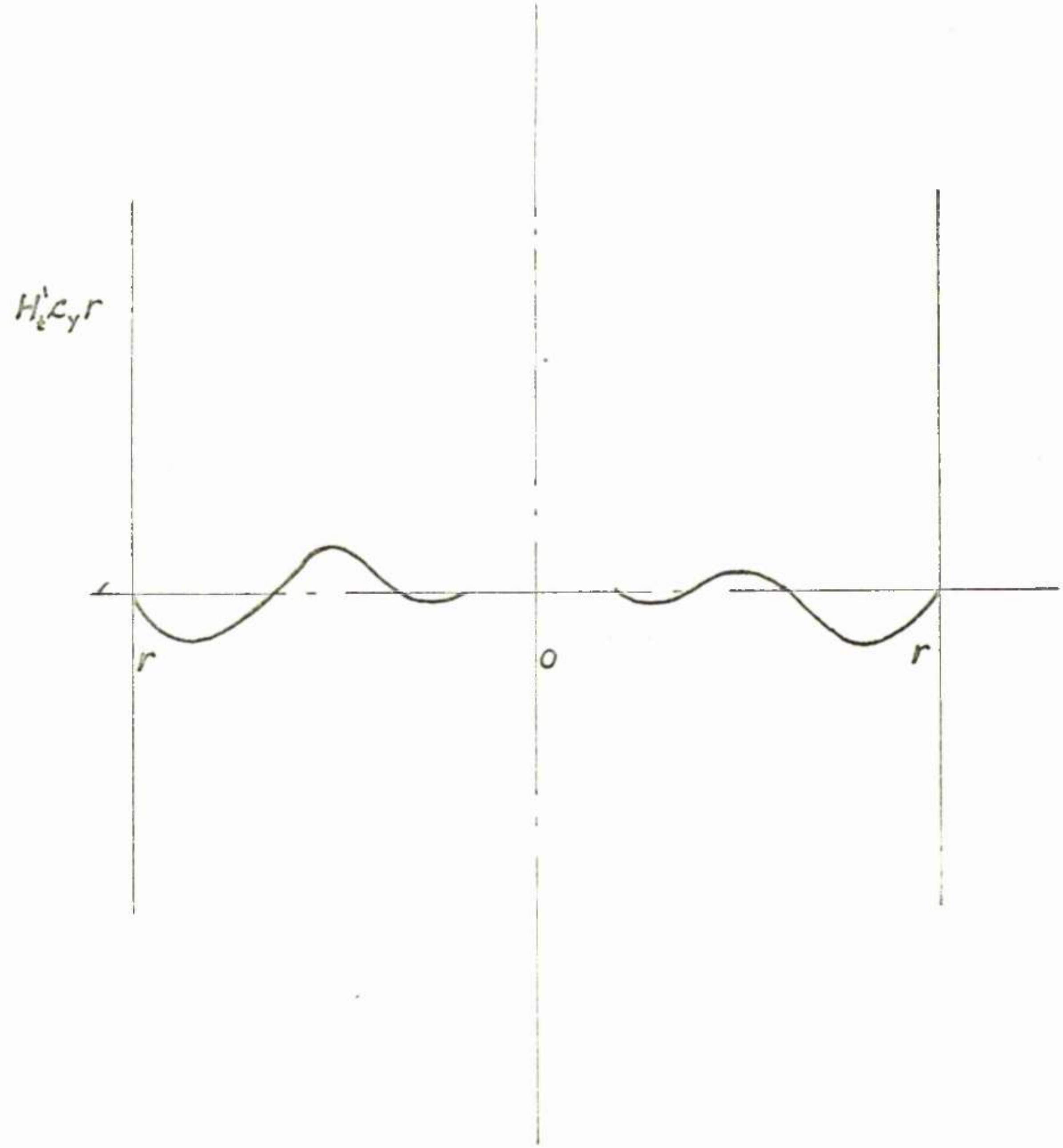

FIG. 19 ESTIMATION OF TOTAL HEAD

into equation.

Knowing the average total head at the discharge and at the suction side the average total differential head was easily worked out.

The average total differential head for positive flow is:

$$\Delta H_{t1} = H_{td} - H_{ts} \qquad 5.23$$

$$\Delta H_{t1} = H_{td} - \frac{\pi \int_{r}^{r} H_t' c_y r\,dr}{Q} \qquad 5.24$$

and the average total differential head for negative flow

$$\Delta H_{t2} = H_{td} - H_{ts} \qquad 5.25$$

$$\Delta H_{t2} = H_{td} - \frac{\pi \int_{r}^{r} H_t'' c_y r\,dr}{Q}$$

where

$H_{td} = \frac{P_{td}}{\gamma_d}$ - average total head at the discharge

$H_{ts} = \frac{P_{ts}}{\gamma_s}$ - average total head at the suction

$H_t' = \frac{P_t'}{\gamma}$ - total head at suction at any point in the region of positive flow

$H_t'' = \frac{P_t''}{\gamma}$ - total head at suction at any point in the region of negative flow.

Beside the above head a static wall pressure tapping was made at the suction and at the discharge side of the pump where static pressure readings were taken. The pressure tappings were placed one in each plane of the pressure traverses.

In addition wall static pressure tappings were made in the back wall of the casing, along the vertical line so that the static pressure gradient could be observed.

5.36 Power

Power was measured by a swinging field motor. Weighing the reaction torque and measuring the speed allowed the power consumption to be worked out:

$$N = G.\ell\ \omega = M.\omega \quad [\text{Kgm/s}] \tag{5.26}$$

where

$$\omega = \frac{\pi . n}{30}$$

G – weight $[\text{Kg}]$

$l = 0.374$ $[\text{m}]$ length of the arm

$M = G.\ell$ – torque $[\text{Kgm}]$

Putting ω in equation 5.26 and changing the units, equation 5.26 becomes:

$$N = \frac{M.n}{716} \quad [\text{H.P.}] \tag{5.27}$$

which represents the power fed into the pump shaft.

The power imported to the liquid is expressed by:

$$\frac{\gamma . Q . \Delta H_t}{75} \quad [\text{H.P.}] \tag{5.28}$$

The equation 5.27 and 5.28 can be linked if the efficiency η is introduced.

$$N = \frac{M.n}{716} = \eta^{-1} \frac{\gamma . Q . \Delta H_t}{75} \qquad 5.29$$

and it follows that

$$\frac{N}{\gamma} = \eta^{-1} \frac{Q \Delta H_t}{75} \qquad 5.30$$

The last equation was used to express the power consumption and by eliminating the specific weight different results could be compared.

The same equation 5.27 was used when the outlet of the impeller was blocked up with tape and the friction losses N_{fr} were measured.

The output horse power at the suction side was determined by the equation below:

$$N_{h_s} = \frac{\gamma_s \pi \int_{-r}^{r} H_{t_r}' c_y r dr}{75} \qquad 5.31$$

where the same technique to solve the above integral was applied as in case of the total head.

To define the output horse power at the discharge the following equation was used:

$$N_{h_d} = \frac{\gamma_d Q . H_{td}}{75} \qquad 5.32$$

Equations 5.31 and 5.32 were applied separately to positive and negative flow.

5.37 Speed

The impeller was kept running at a constant speed of n = 2520 R.P.M. The speed was controlled and measured by straboscope. With the aid of the speed variator any required speed could be achieved. In addition, a tachometer was used to calibrate and check the strabo-scope but only at a certain speed. When the system was set no variations in speed were observed during tests.

6. EXPERIMENTAL RESULTS

6.1 Introduction

Since the conditions at flow rate Q=o are fairly complicated it is wise to analyse the flow pattern of the suction side and flow pattern at the discharge side separately.

Due to the considerable number of variables which affect the flow patterns, only some of the geometrical variables will be outlined.

The following geometrical variables can affect the performance of flow-head characteristic:

a) the number of blades in the impeller

b) the inlet and outlet diameter

c) the volute shape

d) the inlet and outlet blade angle

e) the blade shape and length

f) the convergence of the impeller shrouds

g) the eye design (i.e. shape of the suction nozzle, position of the inlet edge etc.)

h) the clearance space between the fixed volute and rotating impeller

Besides the foregoing geometrical variables, the performance of the flow head characteristics can be affected by certain hydraulic parameters. More about these phenomena will be discussed later.

Only some of the quoted geometrical variables were taken into account, see chapters 3 and 5. The others were simplified in order to enable the author to understand the complicated nature of the flow at shut-off conditions.

First indications about flow phenomena were obtained by using tufts as a visual method. When sufficient information was obtained the more precise method was applied by means of a cylindrical probe.

6.2 The suction side

Numerous traverses at the inlet and along the suction pipe show an interesting flow pattern. See figures 20 (1) to 20 (18). By analysing the flow pattern across each section of the suction pipe the flow field can be divided into three separate regions.

a) the core

b) the inner annulus

c) the outer annulus

and the following conclusions can be drawn:

a) There is no indication of a flow pattern in the core therefore a dead space exists in the middle of the pipe.

b) In the inner annulus, the velocity field rotates impellerwise and moves towards the pump.

c) In the outer annulus, the velocity field rotates also

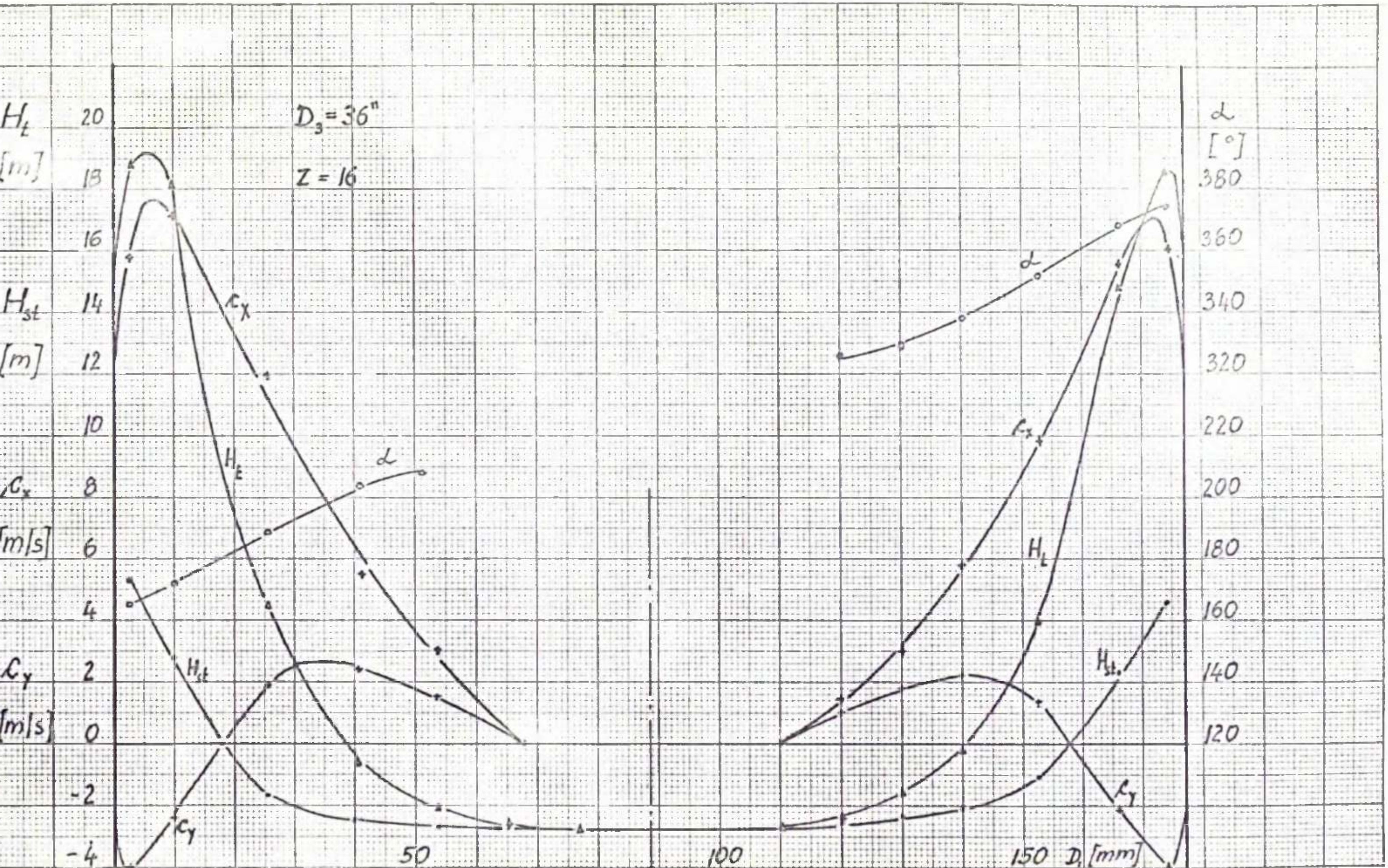

FIG 20-1 SUCTION

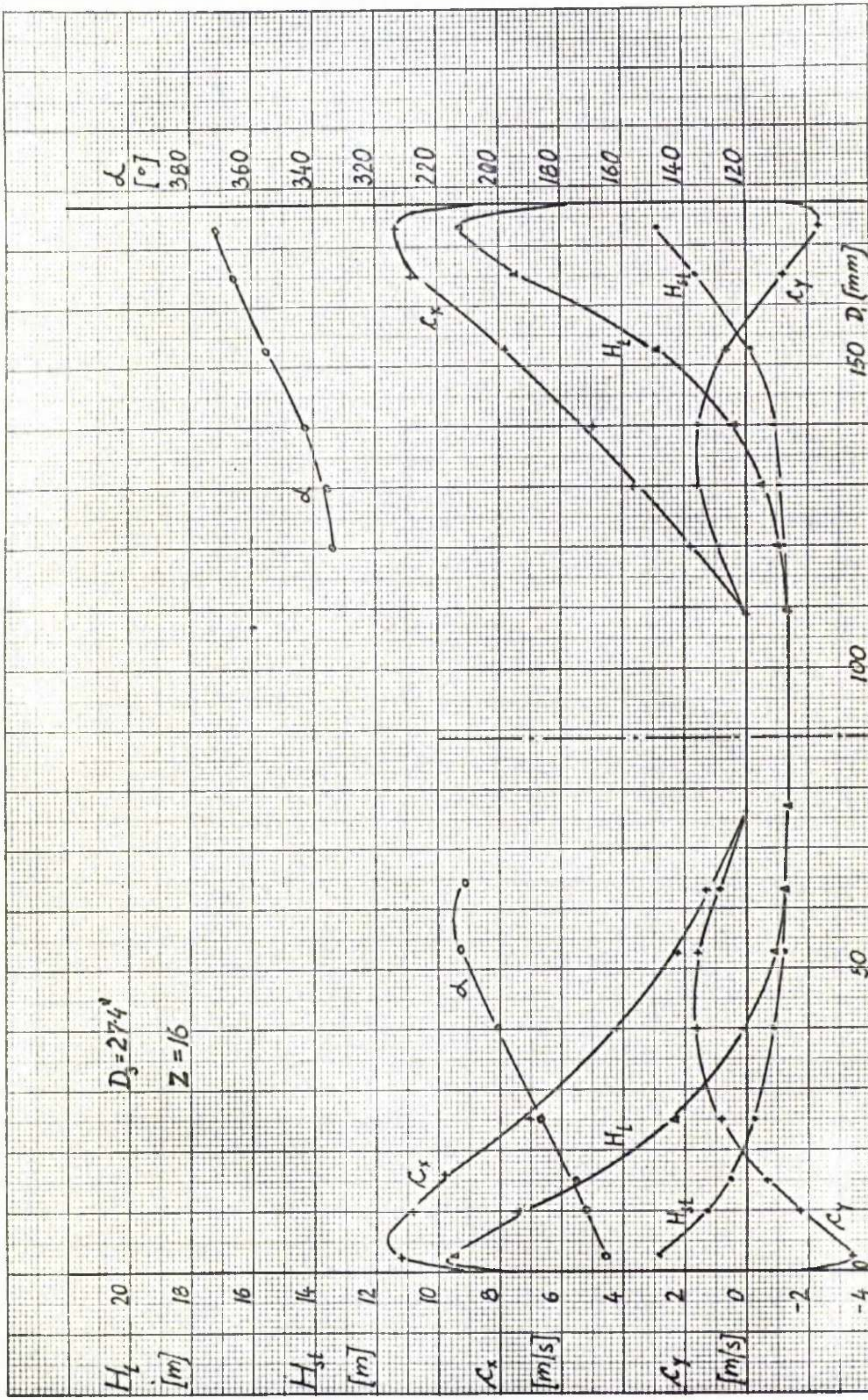

FIG 20-2 SUCTION

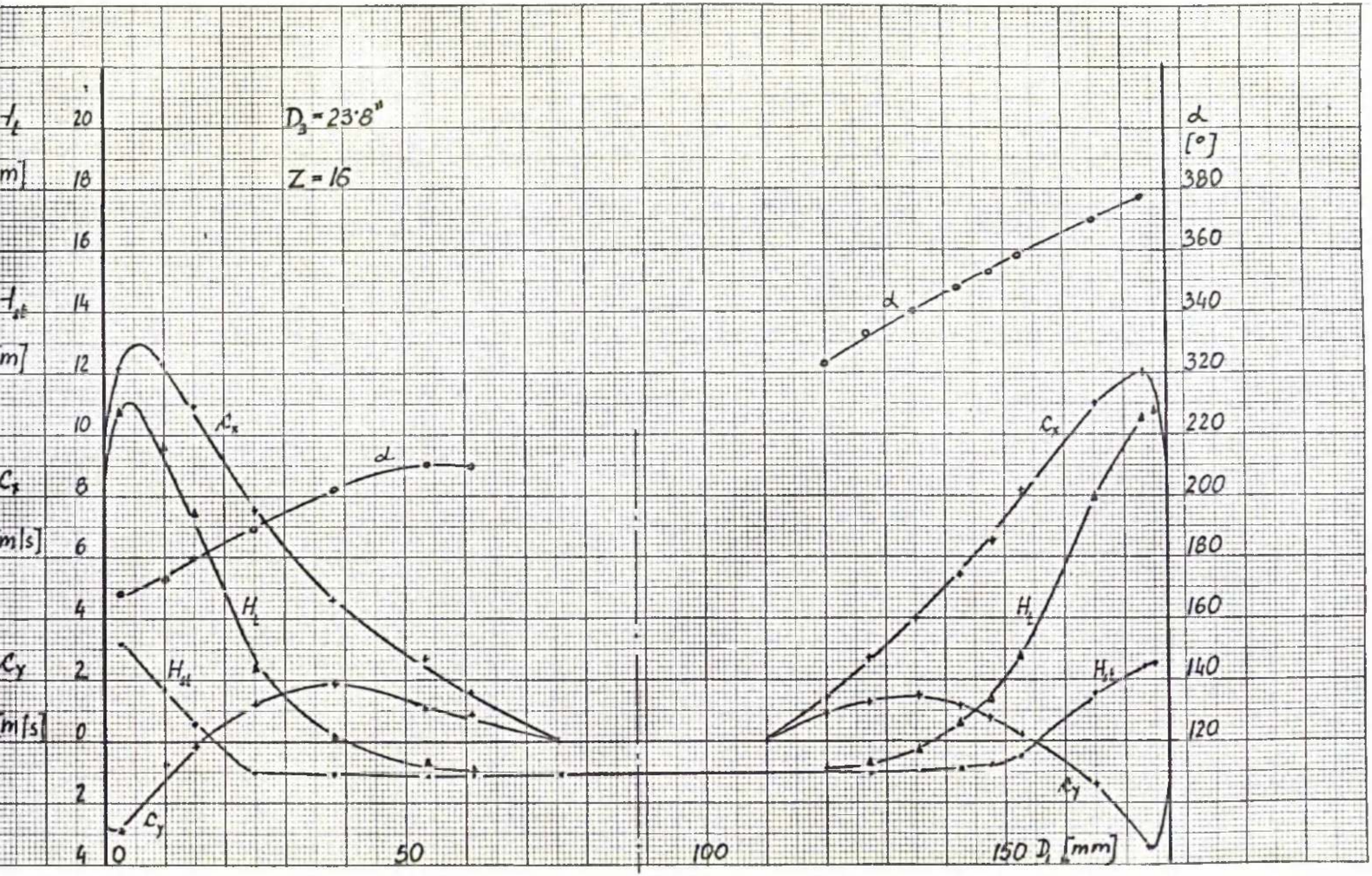

FIG. 20-3 SUCTION

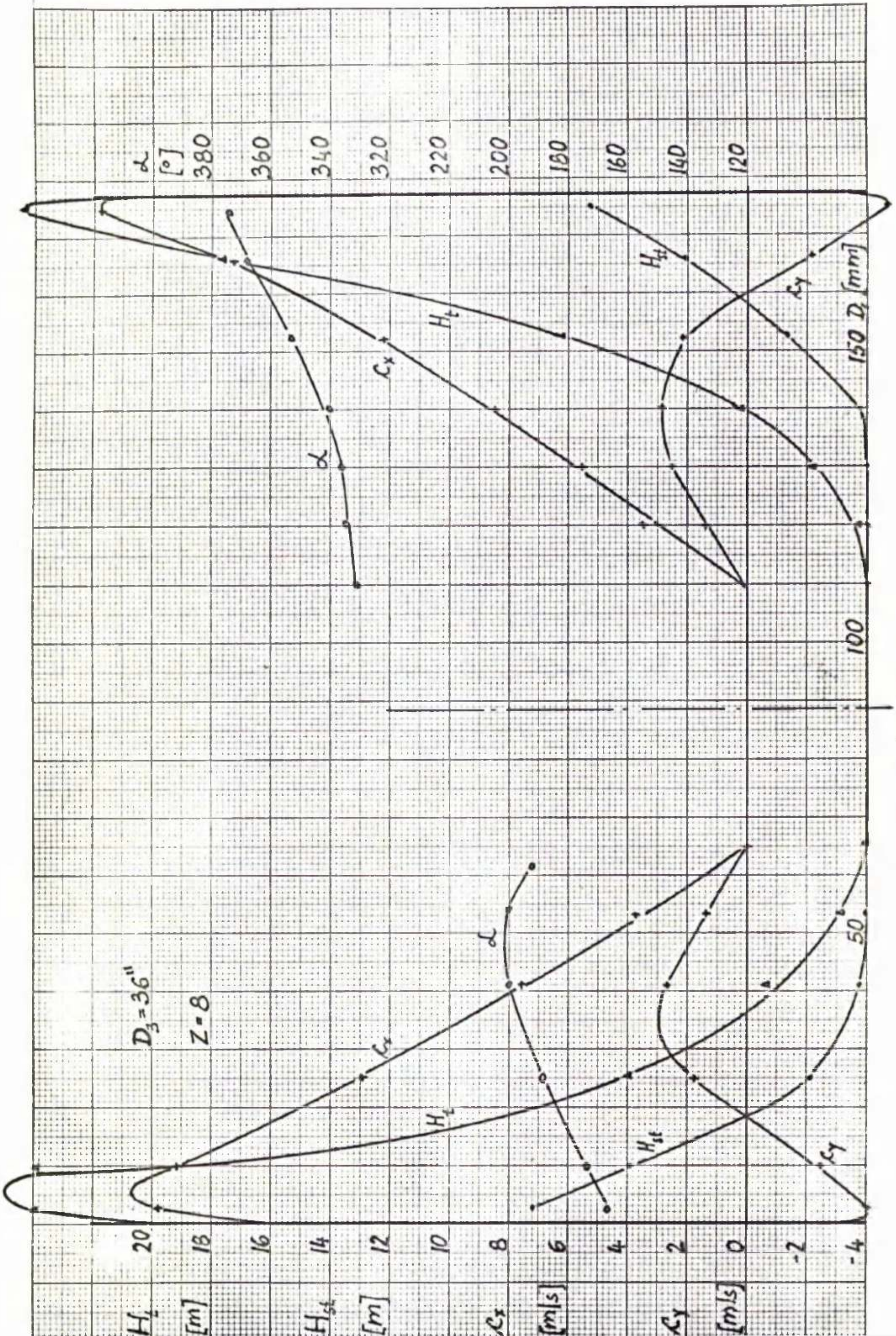

FIG. 20-4 SUCTION

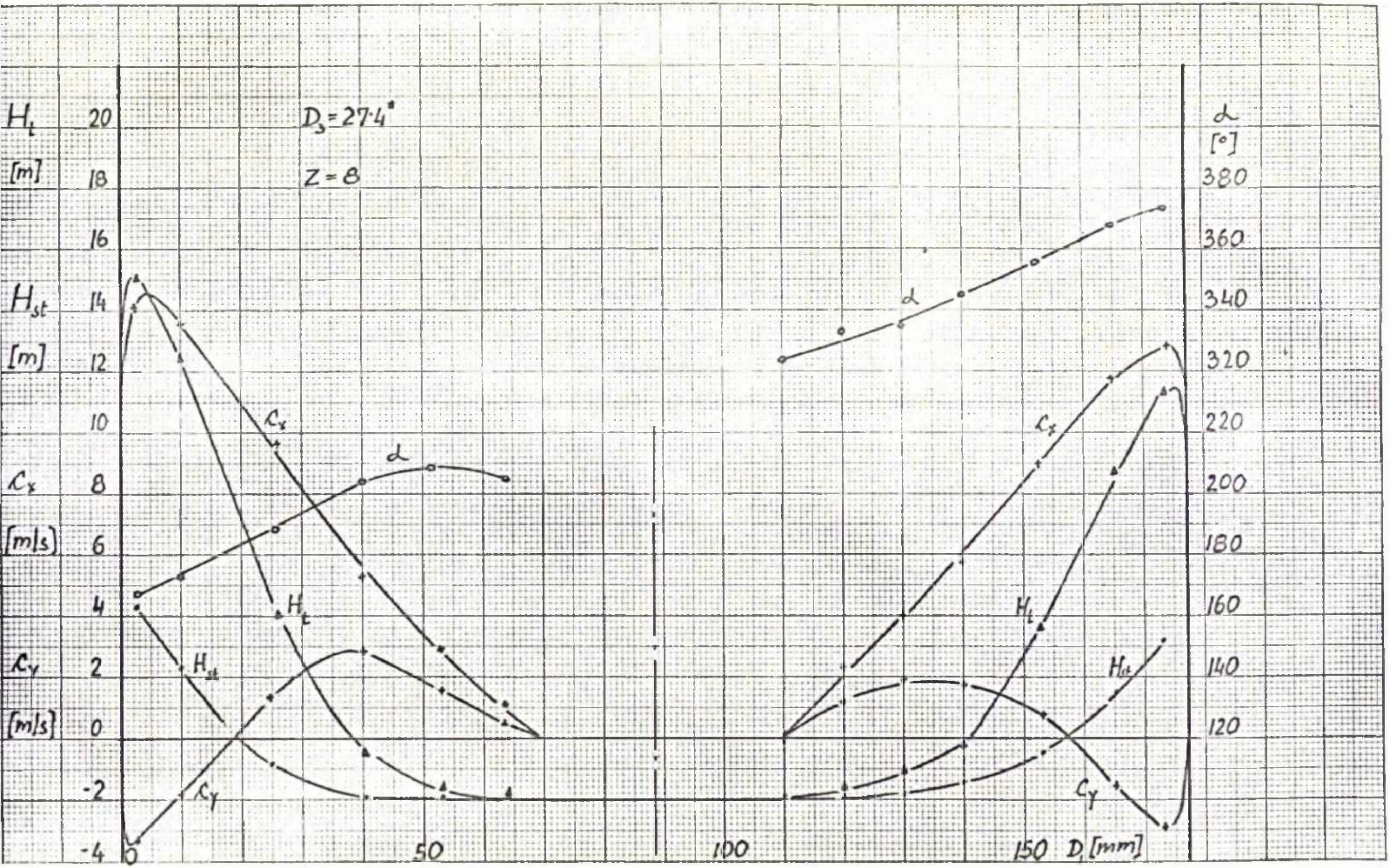

FIG. 20-5 SUCTION

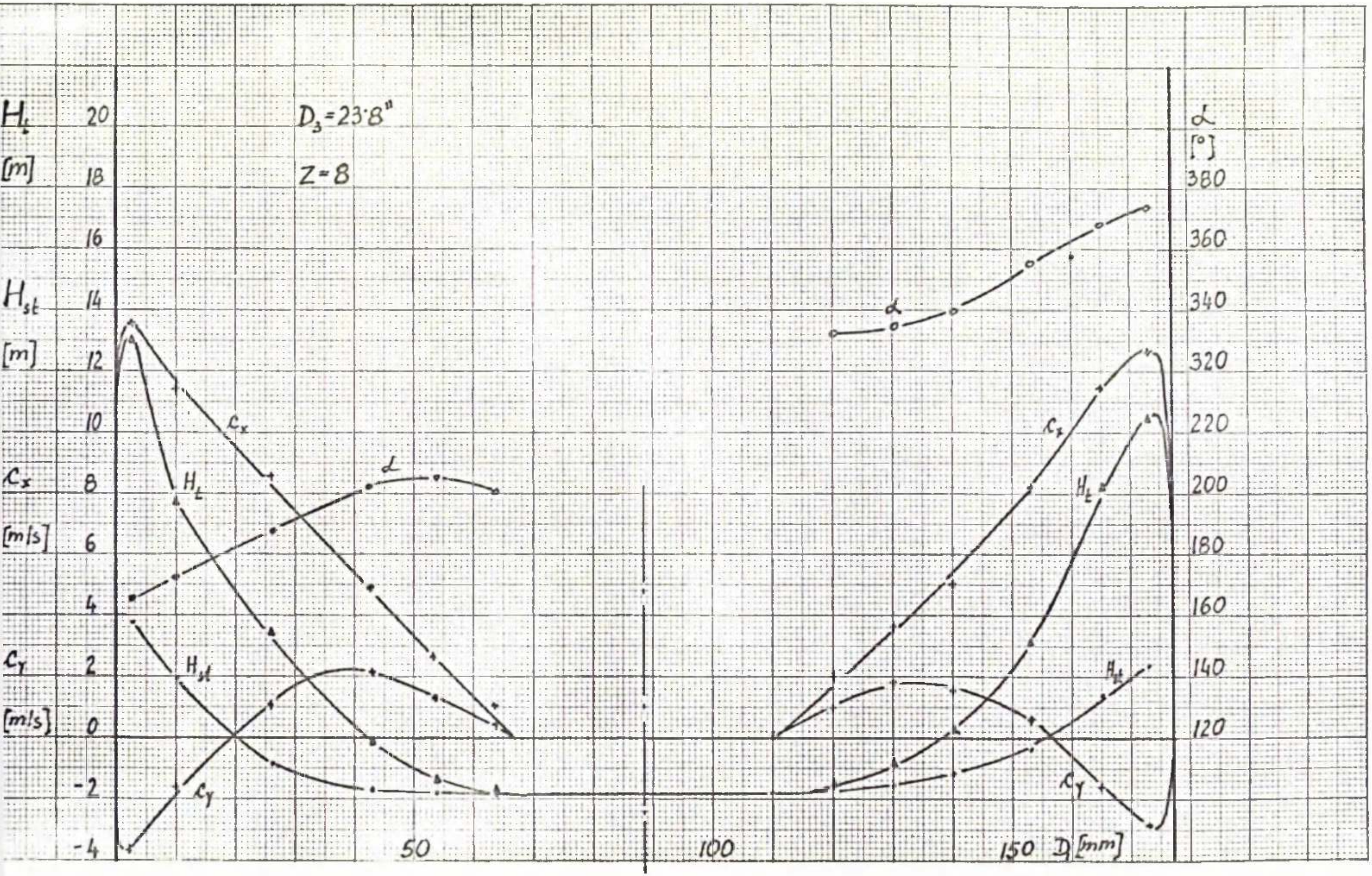

FIG 20-6 SUCTION

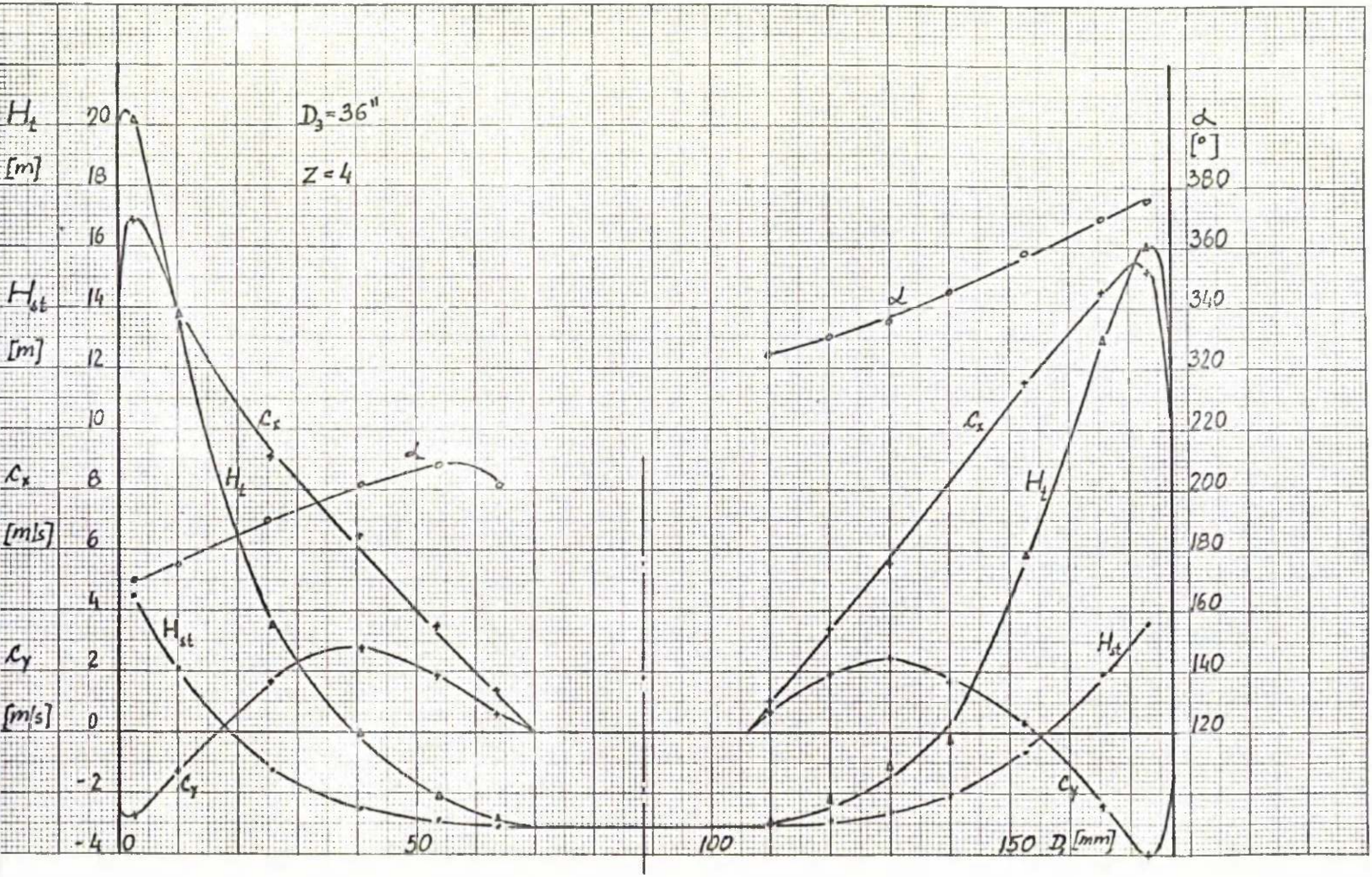

FIG 20-7 SUCTION

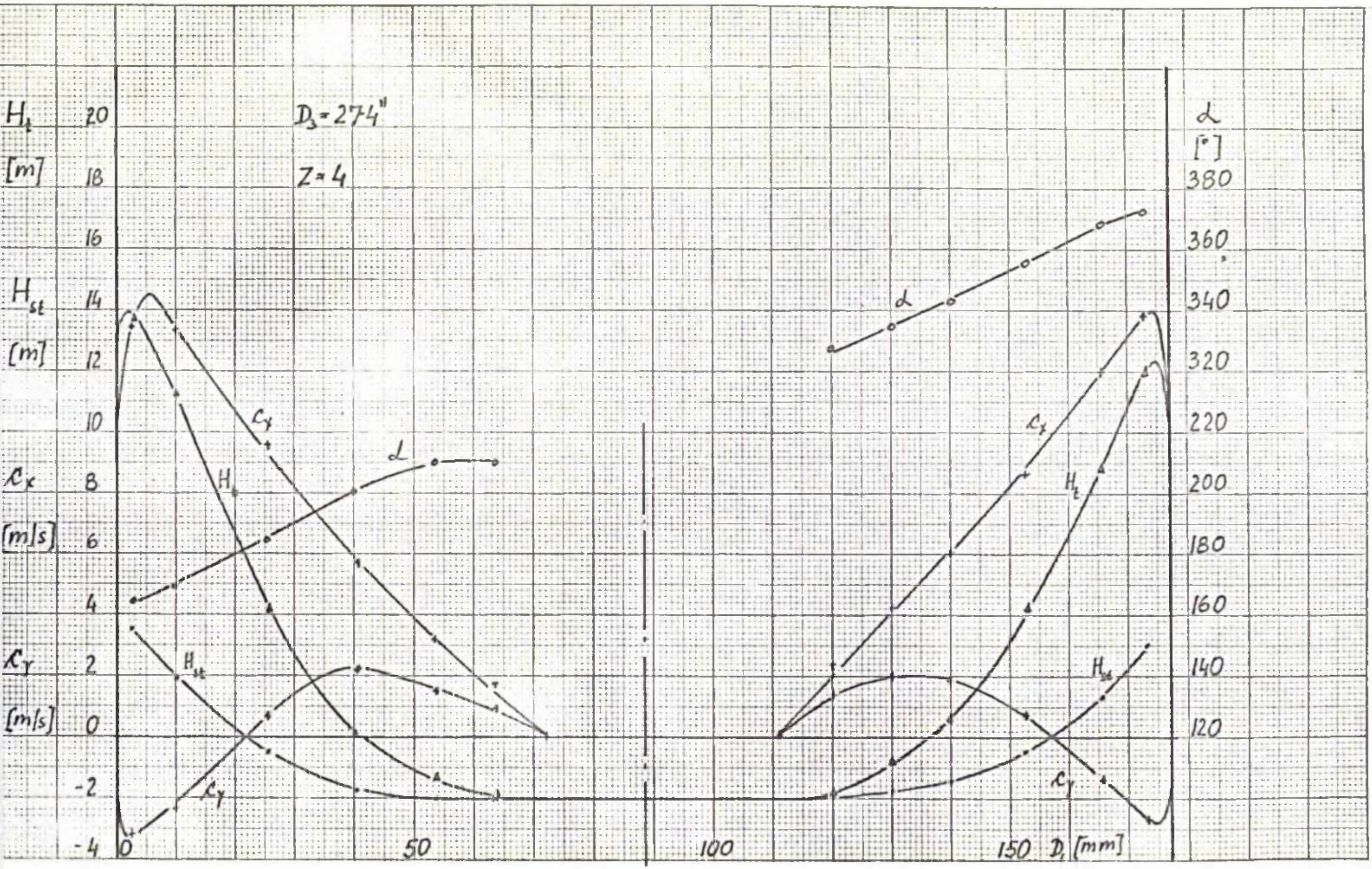

FIG. 20-8 SUCTION

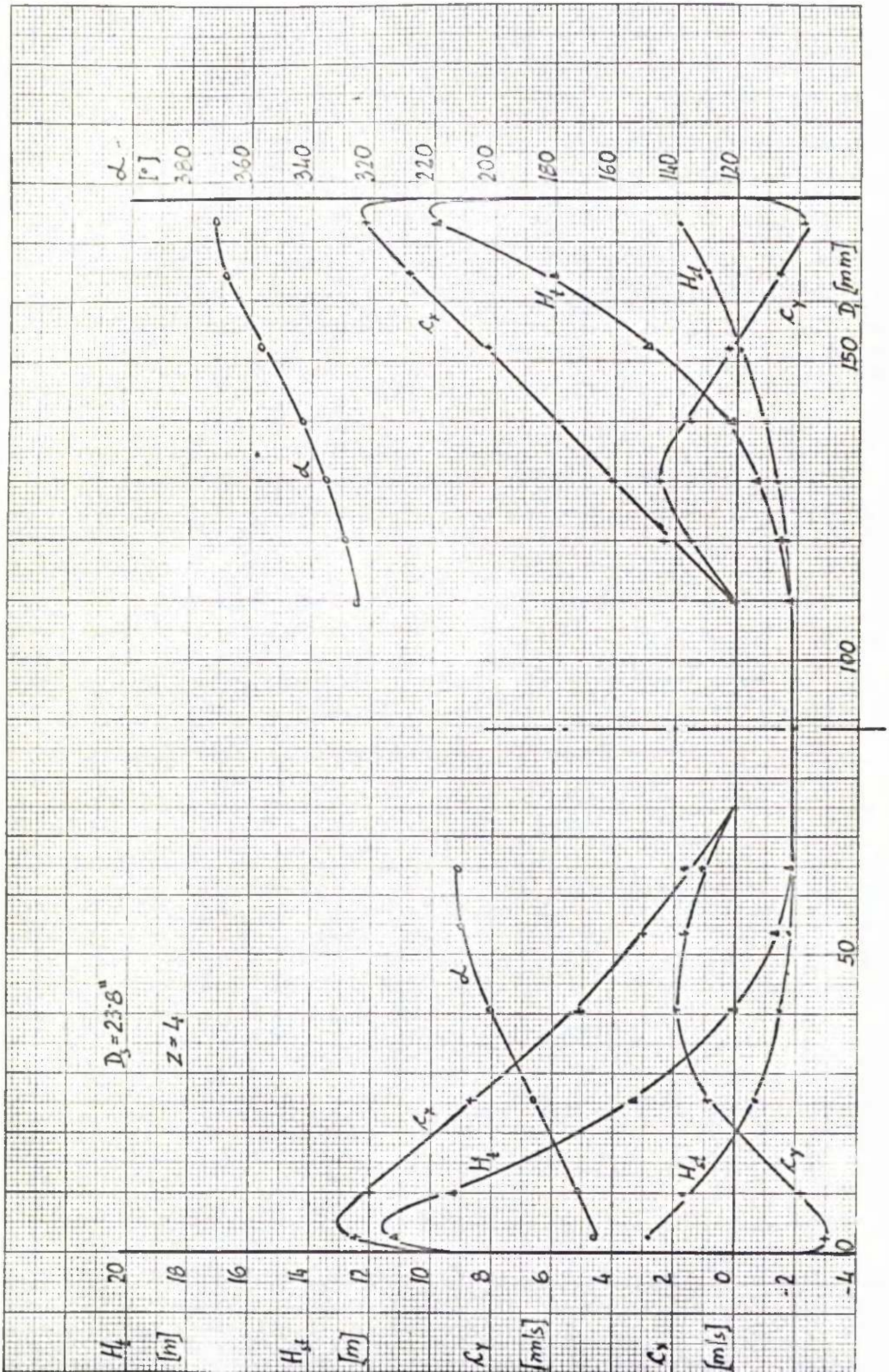

FIG 20-9 SUCTION

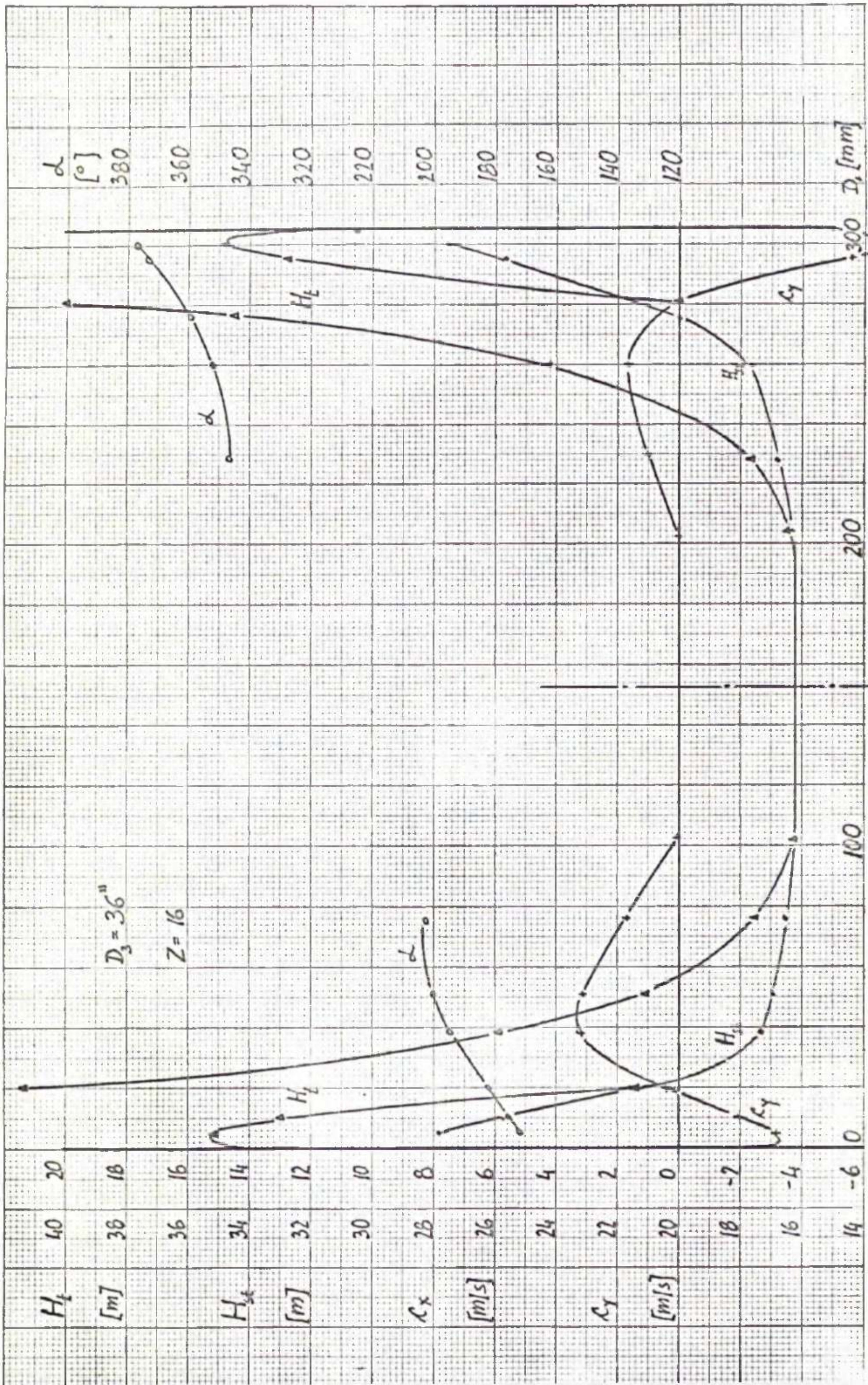

FIG. 20-10 SUCTION

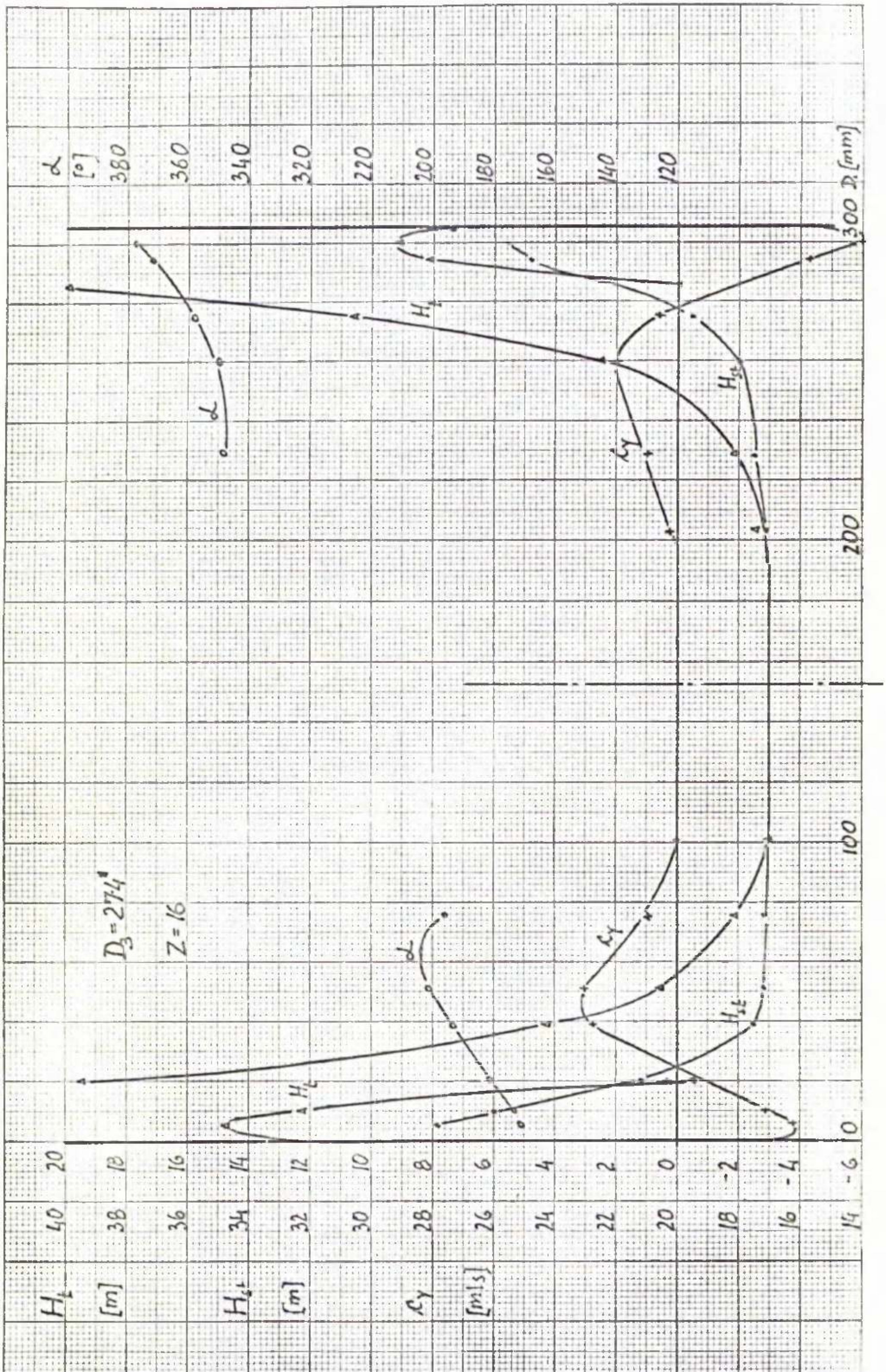

FIG 20-11 SUCTION

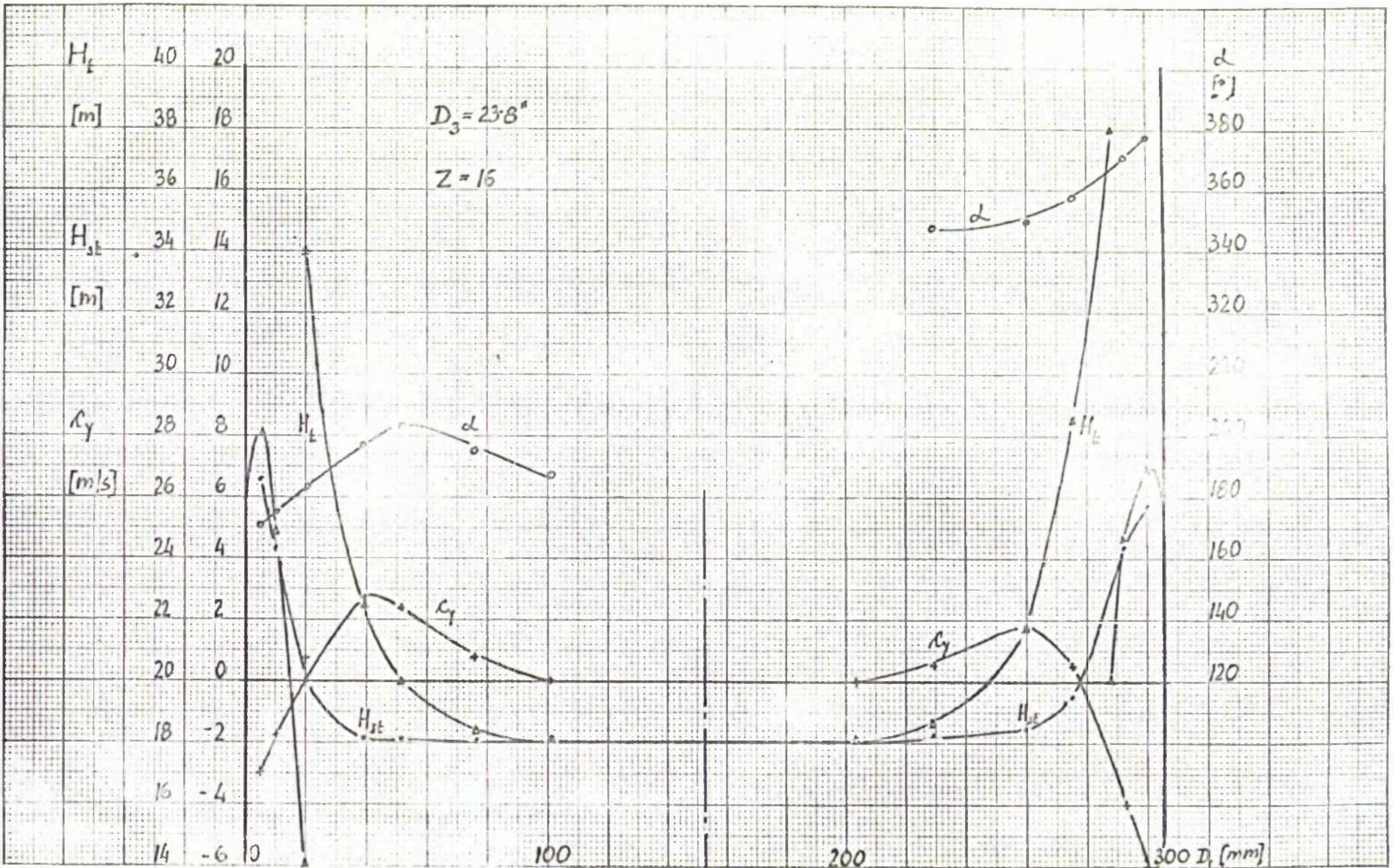

FIG.20-12 SUCTION

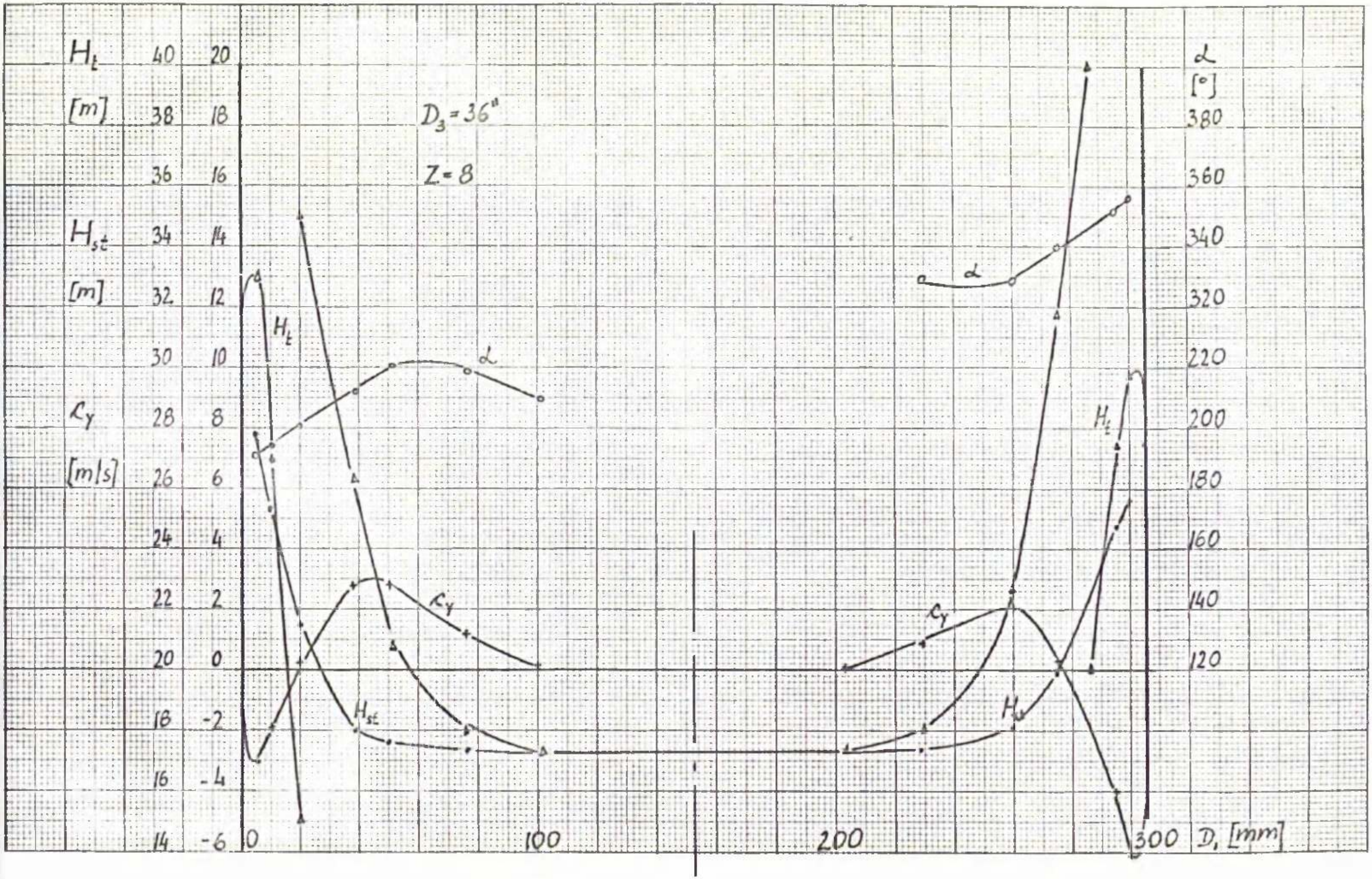

FIG. 20-13 SUCTION

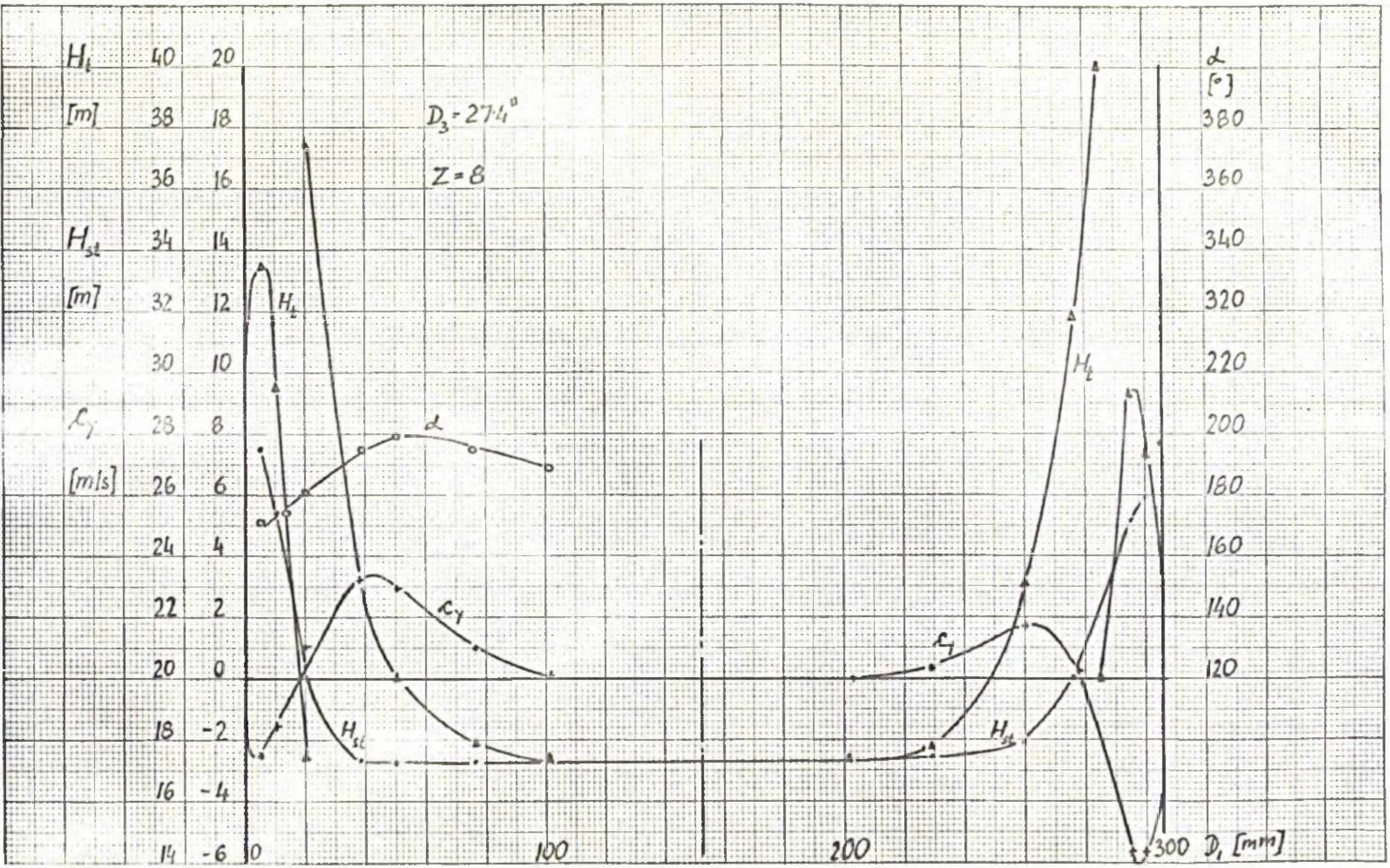

FIG. 20-14 SUCTION

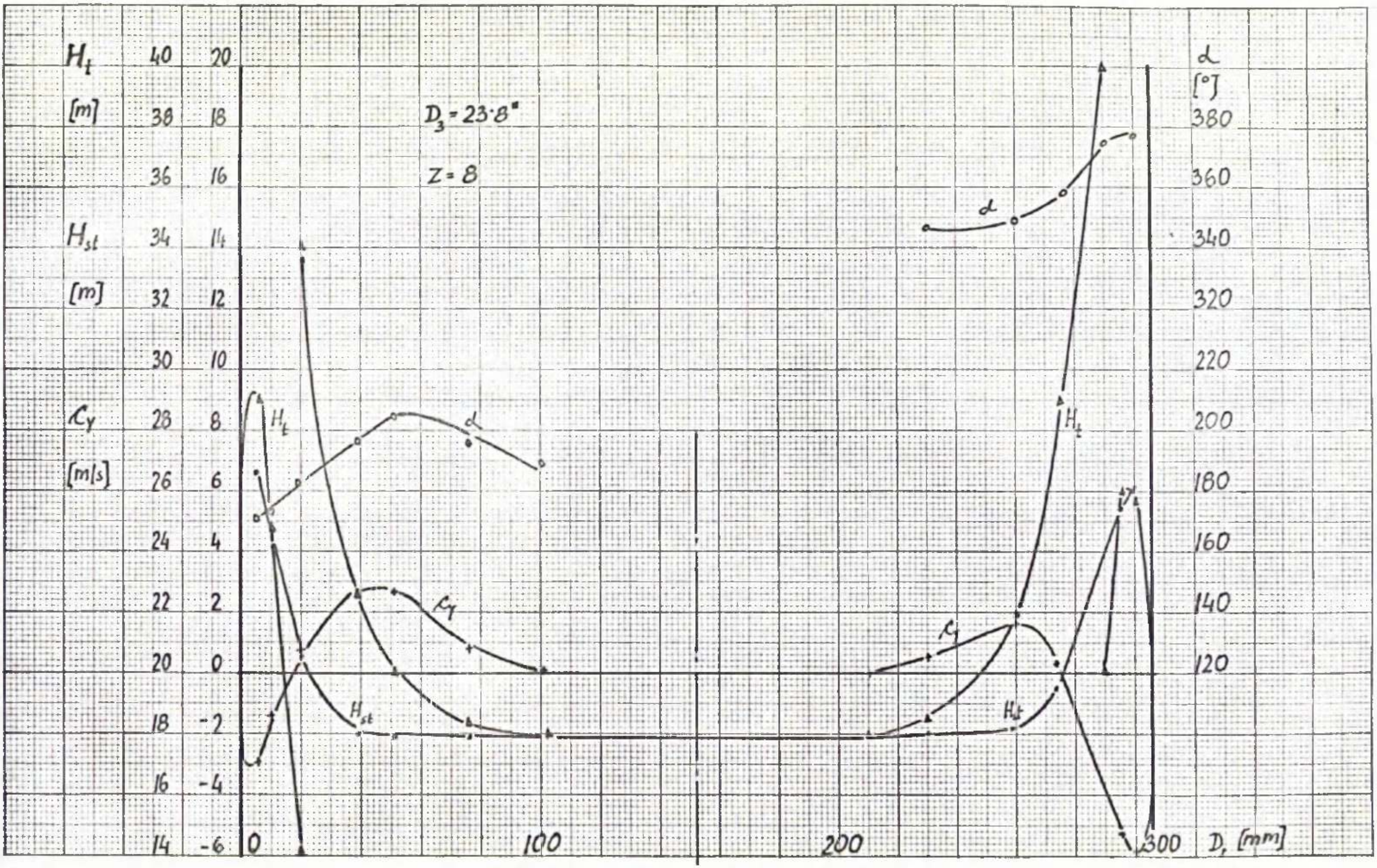

FIG 20-15 SUCTION

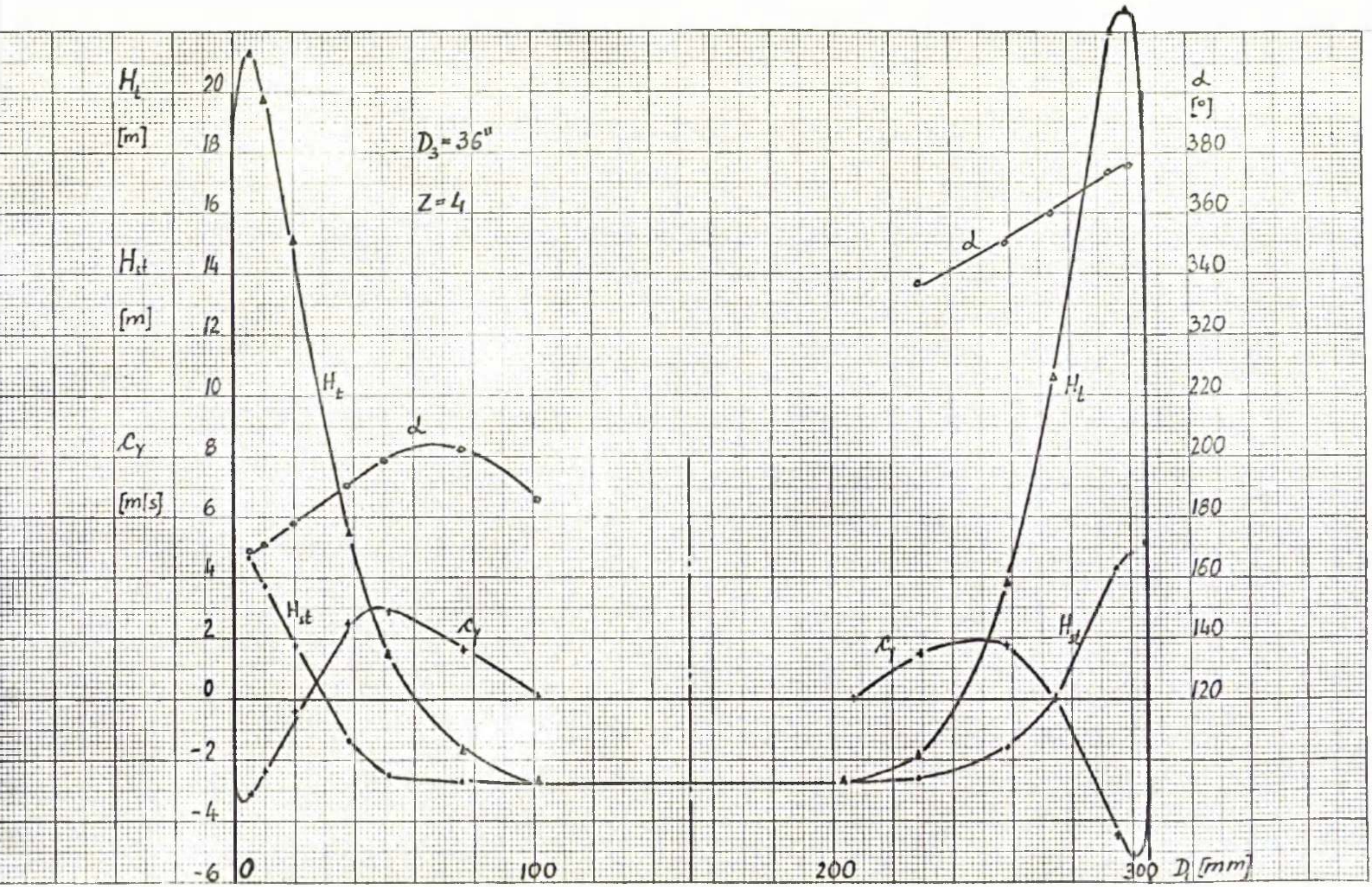

FIG. 20-16 SUCTION

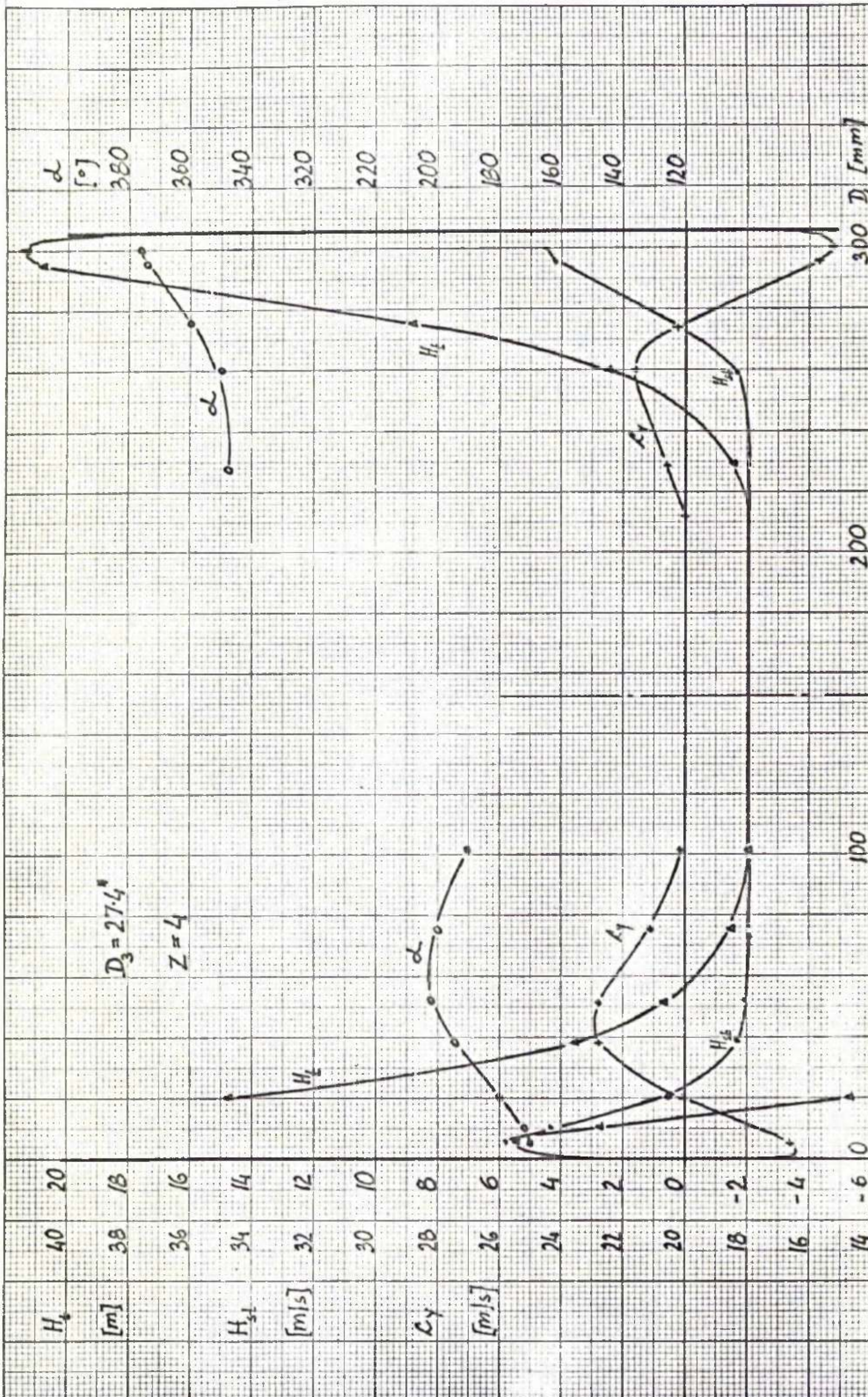

FIG. 20-17 SUCTION

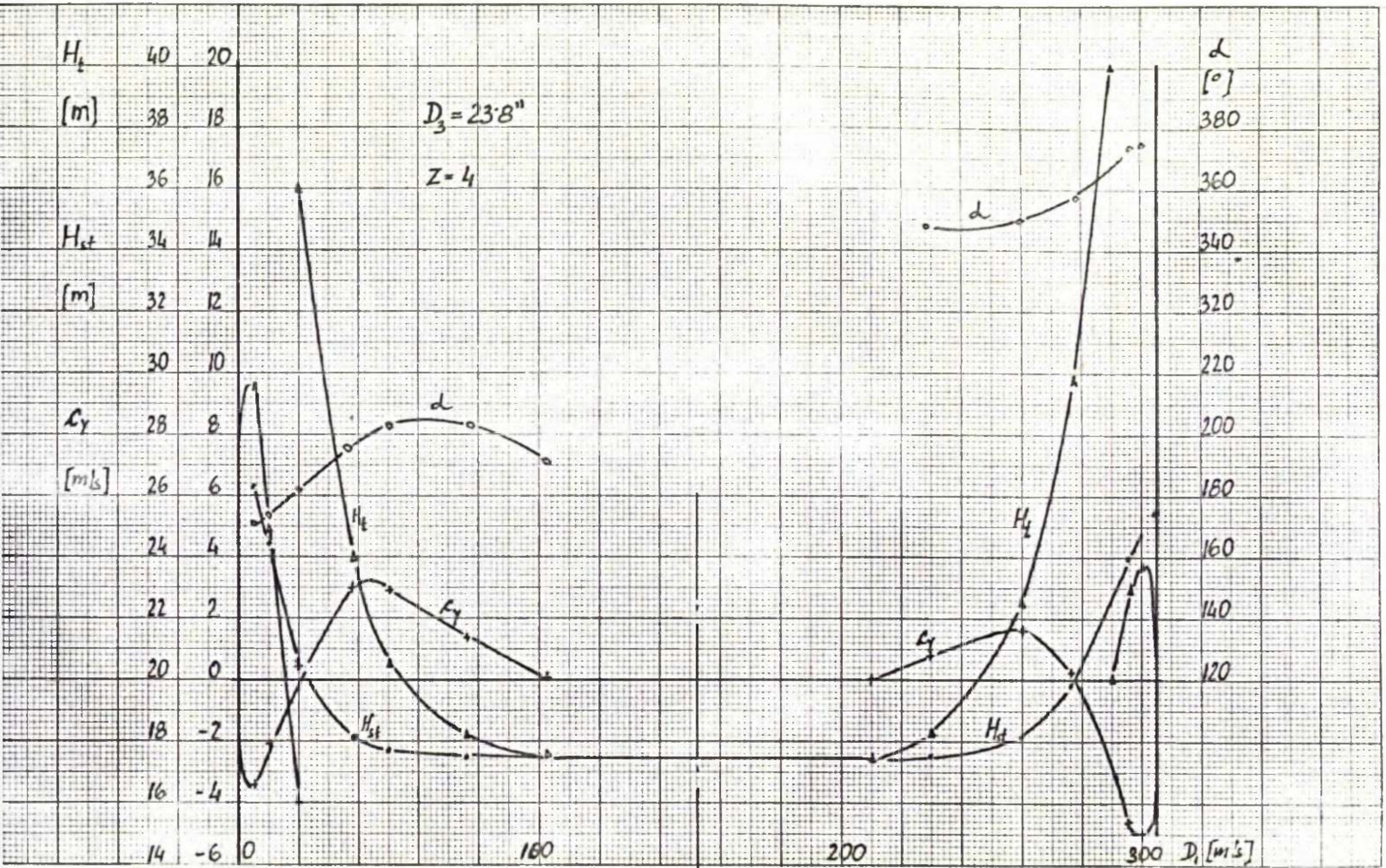

FIG. 20-18 SUCTION

impellerwise and moves away from the pump.

The nature of the velocity field and pressure distribution was found to be symmetrical about the pipe axis. The symmetry of the velocity field and pressure distribution was retained although considerable variations in suction diameter, number of blades and volute ring diameter were made.

The size of the core gradually increased with increase of the inlet diameter. Some data of the core ratio for different diameter ratio are shown below:

Diameter ratio D_1/D_2	Core ratio D_c/D_1
0.35	0.2
0.40	0.27
0.60	0.35

By plotting the foregoing values it can be seen that the core ratio D_c/D_1 approaches an asymptotical value and almost reaches its maximum at $D_1/D_2 = 0.6$.

The influence of the number of blades and volute ring diameter on the size of the core is nearly negligible.

Thus, the conclusion can be drawn that at constant speed the size of the core depends on the diameter of the suction nozzle.

Since in the region of the core there is no flow the total suction head and static suction head are equal.

The inner annulus represents the area where the axial component C_y of the absolute velocity C is directed towards the pump. The area of the inner annulus multiplied by the axial velocity component Cy yields the flow rate passing through the suction nozzle towards the pump.

The flow rate passing through the inner annulus depends very much on the suction diameter of the pump and little change is noticed when the number of blades is changed.

The ratio of the flow rate in the inner annulus for the 7" and 12" pipe diameter is in the order of 1:3. This ratio varies with the volute ring diameter and becomes smaller if the volute ring diameter is reduced. See figure 21.

The outer annulus represents the area where the axial component Cy of the velocity C is directed away from the pump. The product of both gives the flow rate passing through it.

The equation of continuity was satisfied by finding that both flow rates in the inner and in the outer annulus were equal, and so the conclusion drawn above for the flow rate in the inner annulus can be adopted for the flow rate in the outer annulus respectively.

Referring to the angle of the absolute velocity in the inlet traverse plane I, there is a good indication that the angle remains fairly constant for any alteration in geometry of the pump. The absolute angle of velocity in the outer annulus is in the range 0° to 15°. With regard to the absolute angle of the velocity in the inner annulus, the angle varies approximately from 0° to 30°.

The angle α plotted against pipe diameter forms a smooth curve with an interruption in the middle of the pipe where the core is formed.

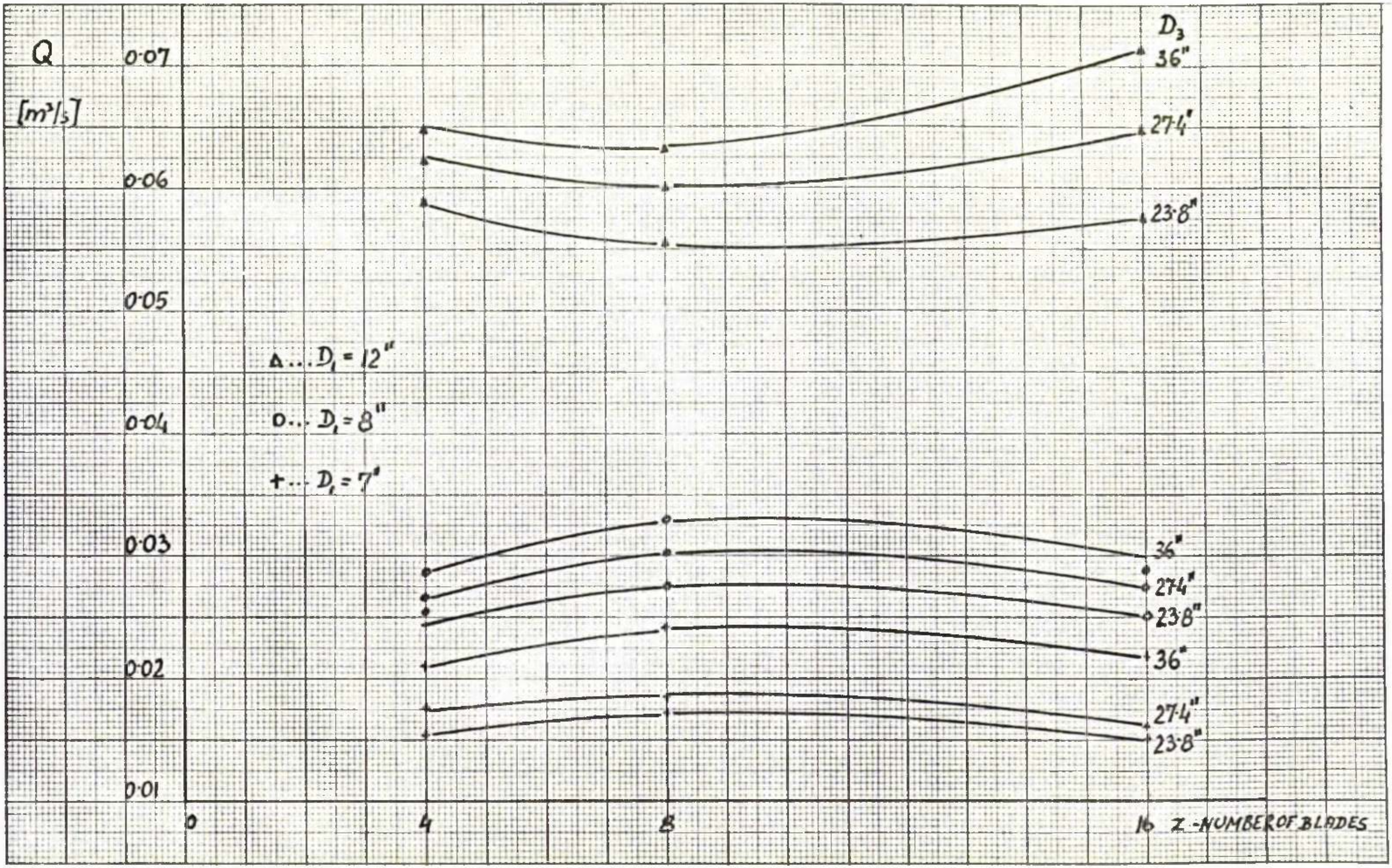

FIG. 21 SUCTION : FLOW RATE

The distribution of the total head across the suction diameter varies very rapidly. From its maximum value near the wall it falls steeply towards the centre of the suction pipe. Besides, the total head changes its value from positive to negative relative to atmosphere. A similar distribution can be found for the static head although in a different scale.

At the point where the static head becomes zero the axial velocity component Cy alters its direction by 180°. Alternatively, the conclusion can be drawn that points of zero static head along the suction pipe form a cylindrical surface which represents the boundary between inner and outer annulus.

Similarly, the points where the static head and total head lines cross represent the surface of the core. The core is obtained by linking the points of equal static and total head together along the suction pipe.

The conclusion can be made that the surface formed by the total pressure approximates that obtained from a forced vortex.

To get additional experimental data for the above statement the measurements were made in three different planes I, II, III along the suction nozzle. See figure 22 and figure 15. Similar patterns of hydraulic parameters were revealed in each plane with some reduction in head and velocity with distance from the pump.

An interesting behaviour of the suction head in the inner annulus was observed when the geometry of the pump was altered. Figure 23 shows the suction head plotted on a base of number of blades.

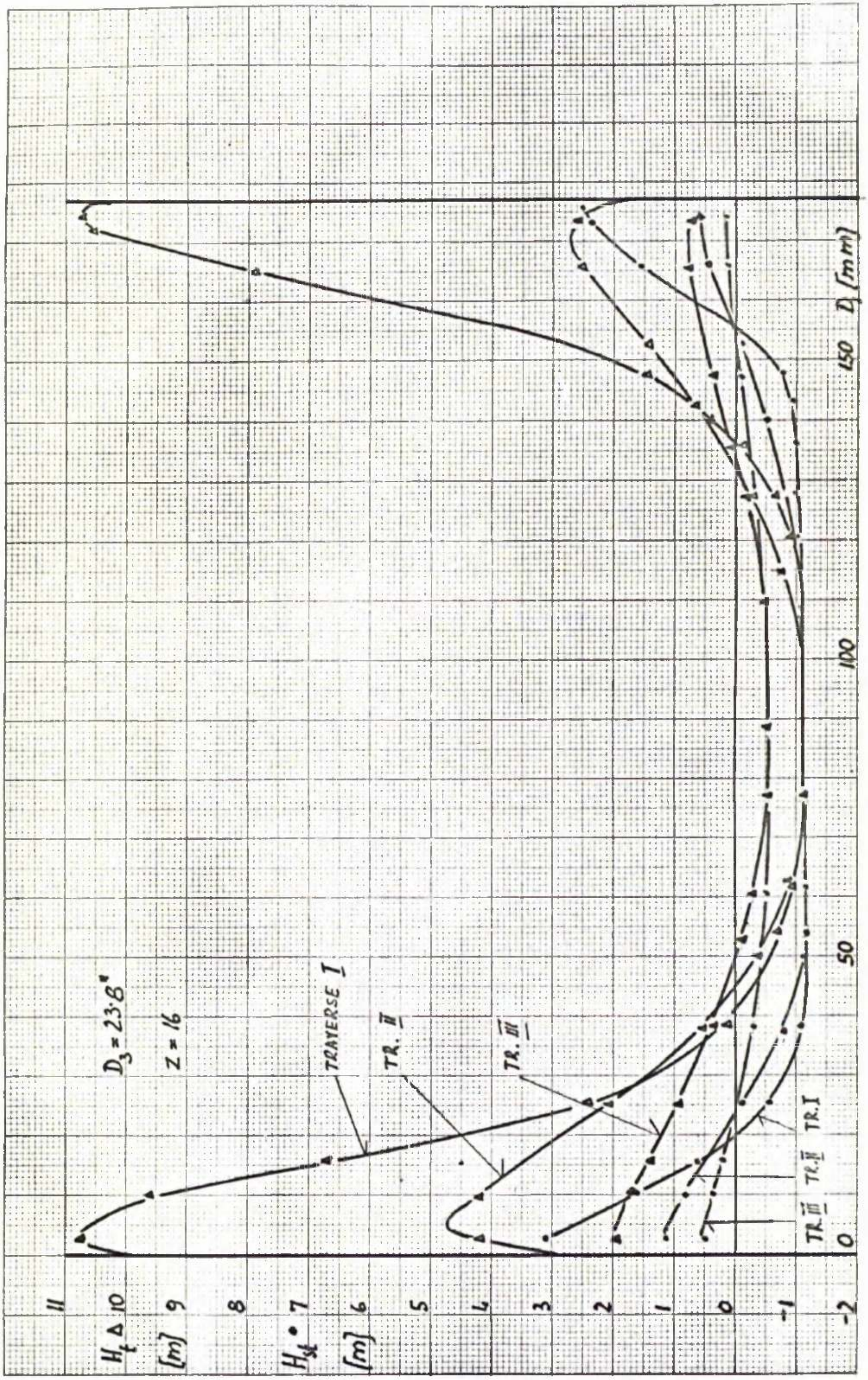

FIG. 22 DECAY OF HEAD ALONG THE SUCTION PIPE

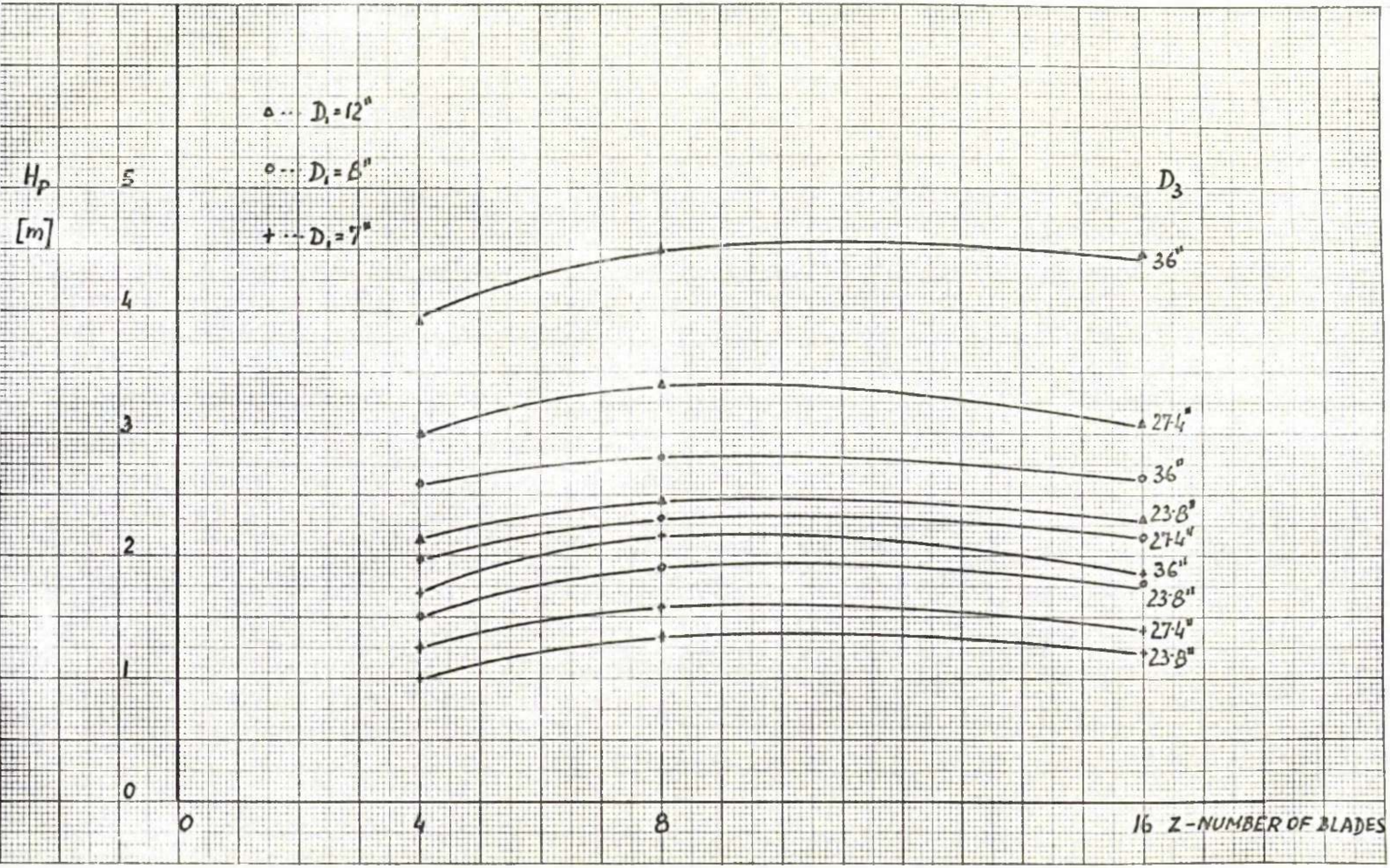

FIG. 23 SUCTION : PUMP HEAD

An optimum in suction head is found in a range of number of blades between $z = 8$ to 10. A considerable increase in suction head is shown for any number of blades when the diameter of the casing is enlarged. A great increase in suction head is also noticed if the inlet diameter is enlarged, and this applied regardless of the number of blades in the impeller.

Modification in geometry of the pumps affects directly the total head in the outer annulus. The changes of total head are shown in figure 24 for different numbers of blades, different inlet diameters and different diameters of casing. A study of the curves showing the change in the total head for different geometrical variables, shows that there is a similar behaviour to that found in the inner annulus.

The suction head characteristics are generally flat, but a sharp drop in total head is observed at $z = 4$ number of blades.

6.3 Discharge

Since the cylindrical casing and impeller are symmetrical about the axis of rotation there is no fundamental reason why the data obtained at any other point having the same radius around the impeller should be different.

Thus the readings taken at only one point at the radius $R = 280$ [mm] were considered adequate. Several readings were taken across the width of the casing.

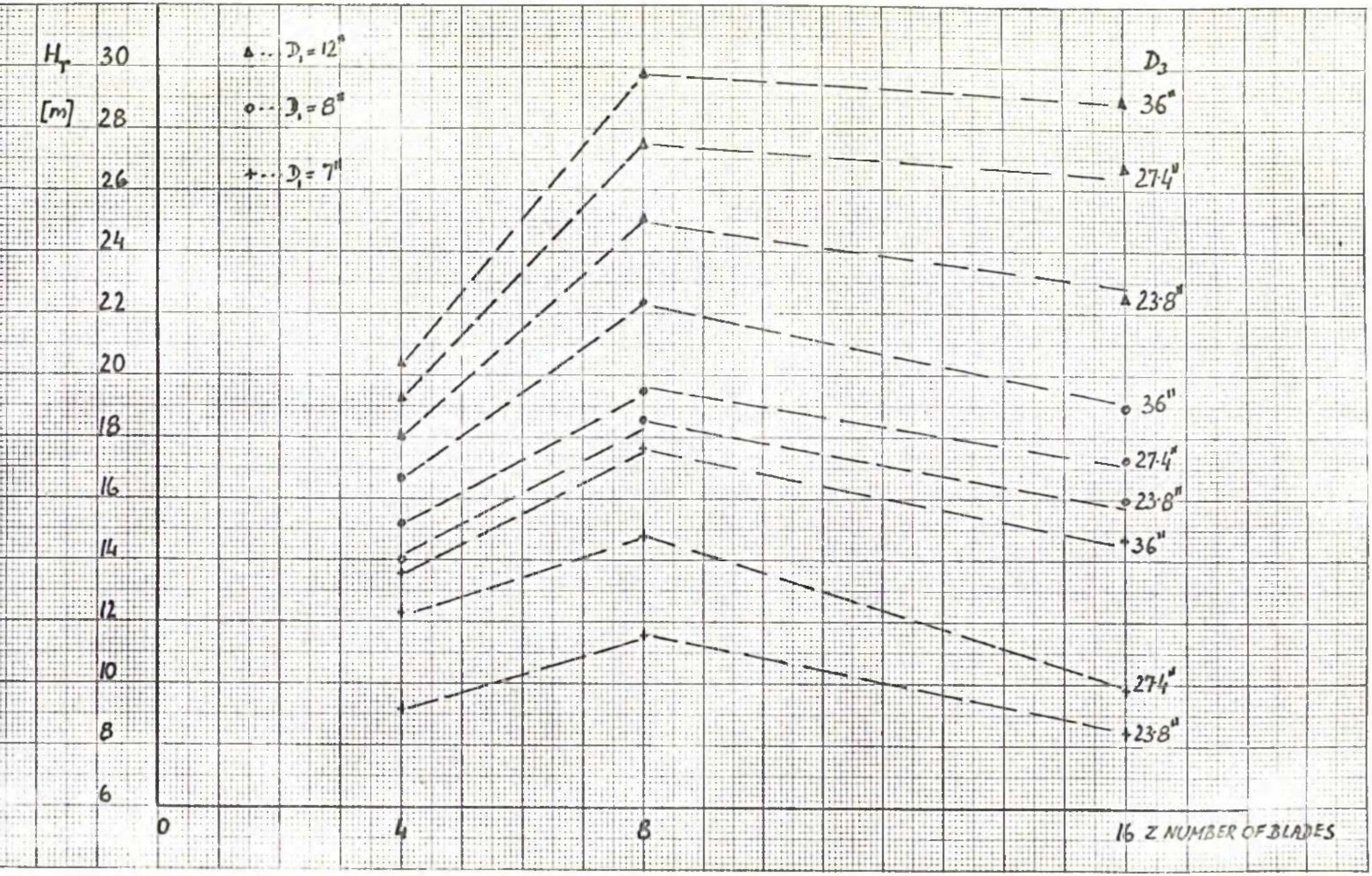

FIG. 24 SUCTION : TURBINE HEAD

Although the discharge was totally blocked visual observation indicated that a certain flow was entering and leaving the casing. Later that indication proved to be true by the results obtained from the cylindrical probe. See figure 25(1) to 25(18).

The surprising fact, although not unexpected, was revealed half of the area where measurements took place was taken up by outward flow and the other half by inward flow.

The total area where the recirculatory flow occurs is split into three sections.

a) The middle section

b) The two side sections with one close to the back shroud and the other close to the front shroud.

The middle section itself takes half of the total area and is slightly off centre. The displacement mostly depends on the diameter of the volute ring D_3 and inlet diameter D_1 but there is little change in position when the number of blades is varied.

If the diameter of the volute ring was changed from D_3=23.8"; 27.4" to 36" and if the impeller remained unchanged the displacement of the middle section was gradually reduced and for volute ring D_3 = 36" it almost disappeared.

By keeping the diameter of the volute ring D_3 constant and varying the inlet diameter from D_1 = 7"; 8" and 12" the maximum middle section displacement occurs at D_1 = 12". This seems to be particularly significant for the volute ring diameter D_3 = 23.8". The displacement almost vanishes at the diameter D_3 = 36".

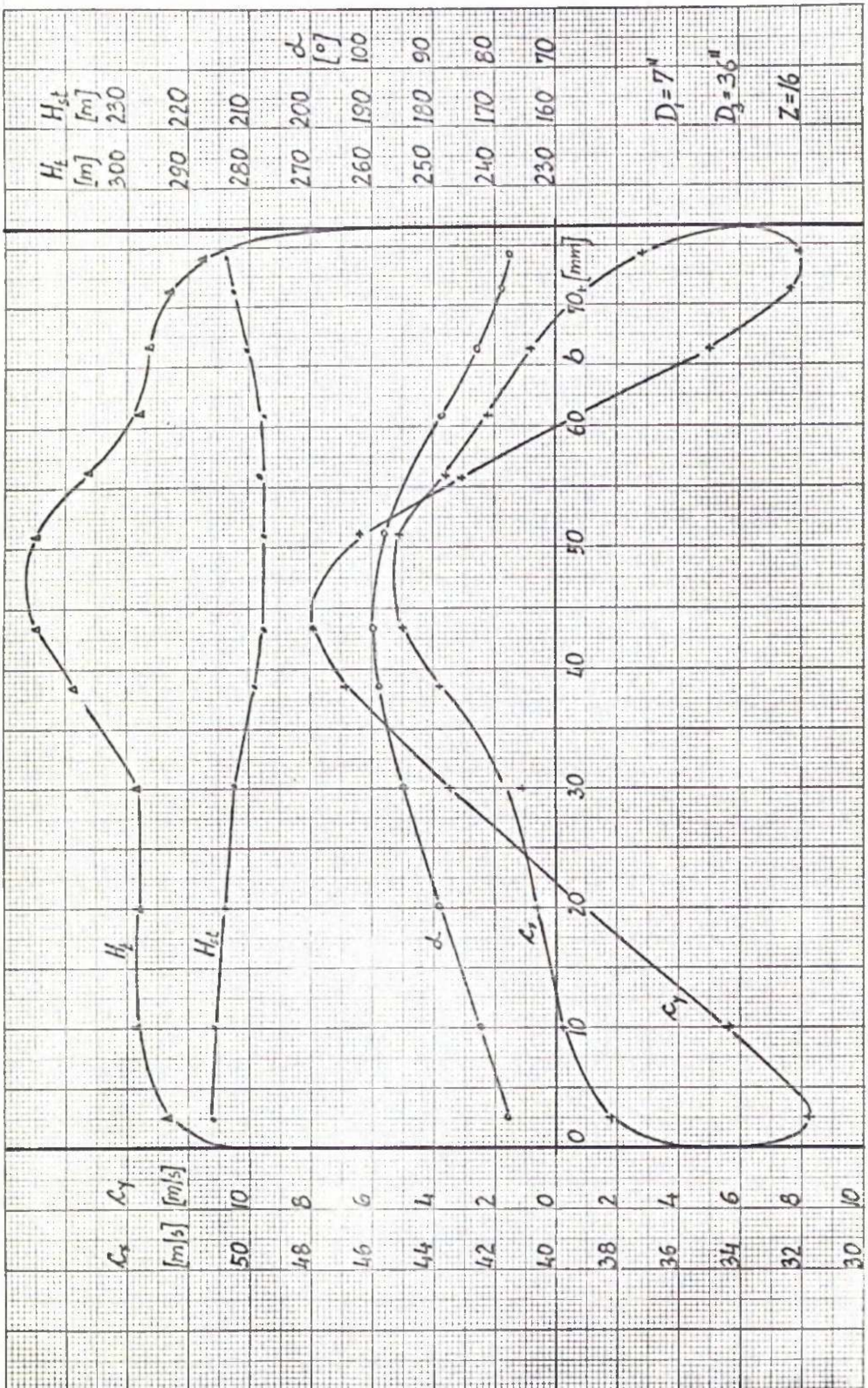

FIG. 25-1 DISCHARGE

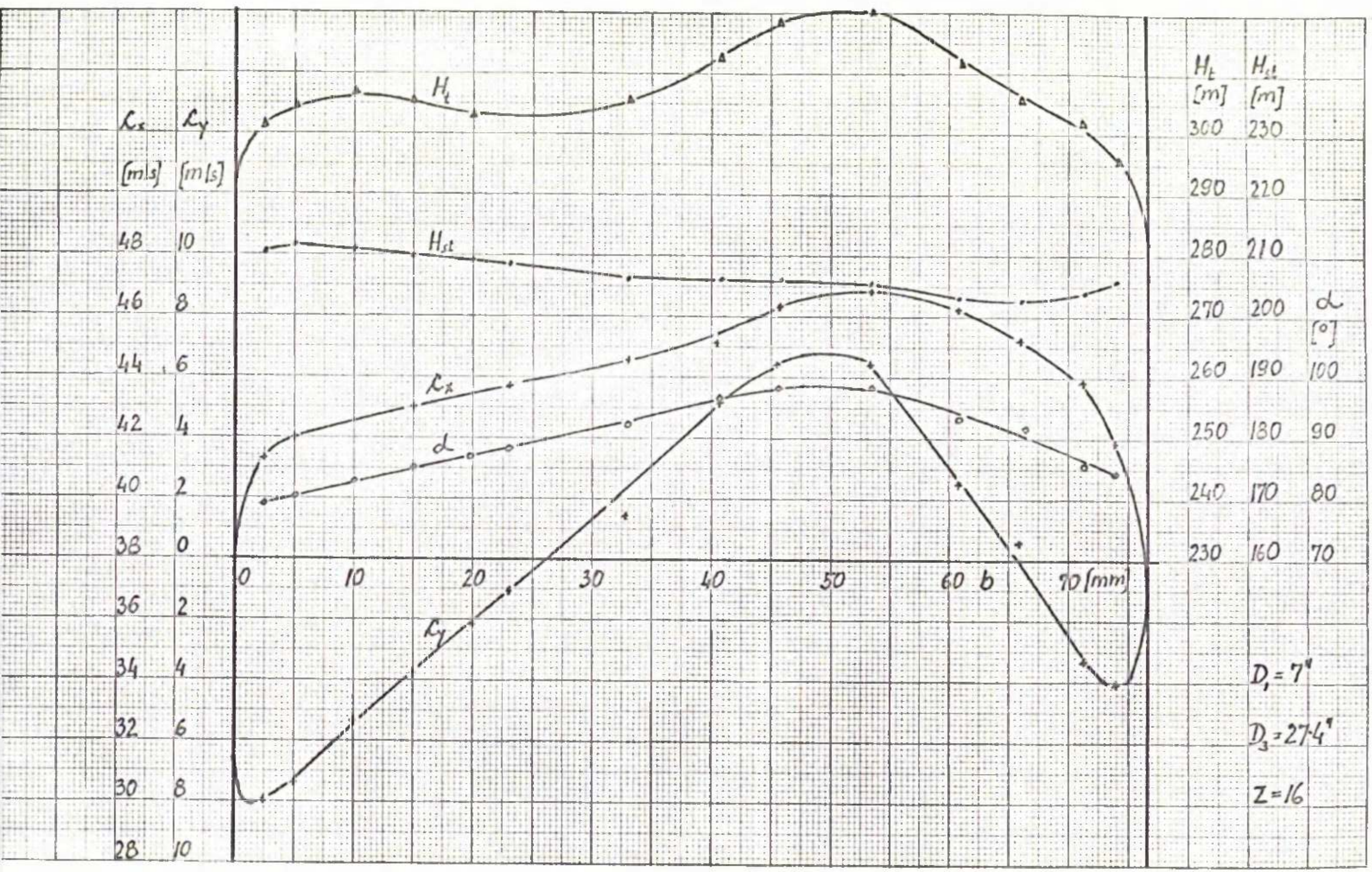

FIG. 25-2 DISCHARGE

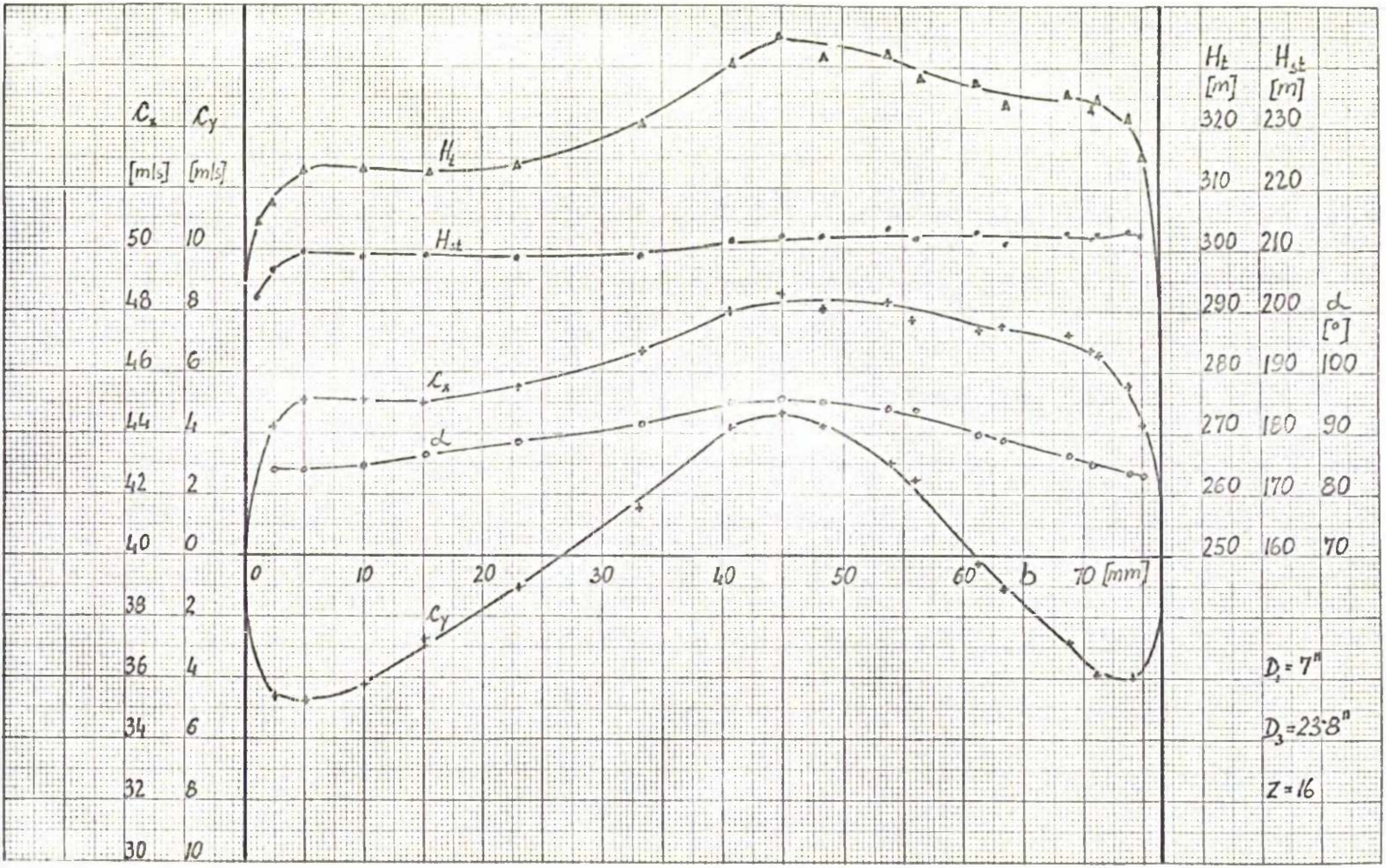

FIG. 25-3 DISCHARGE

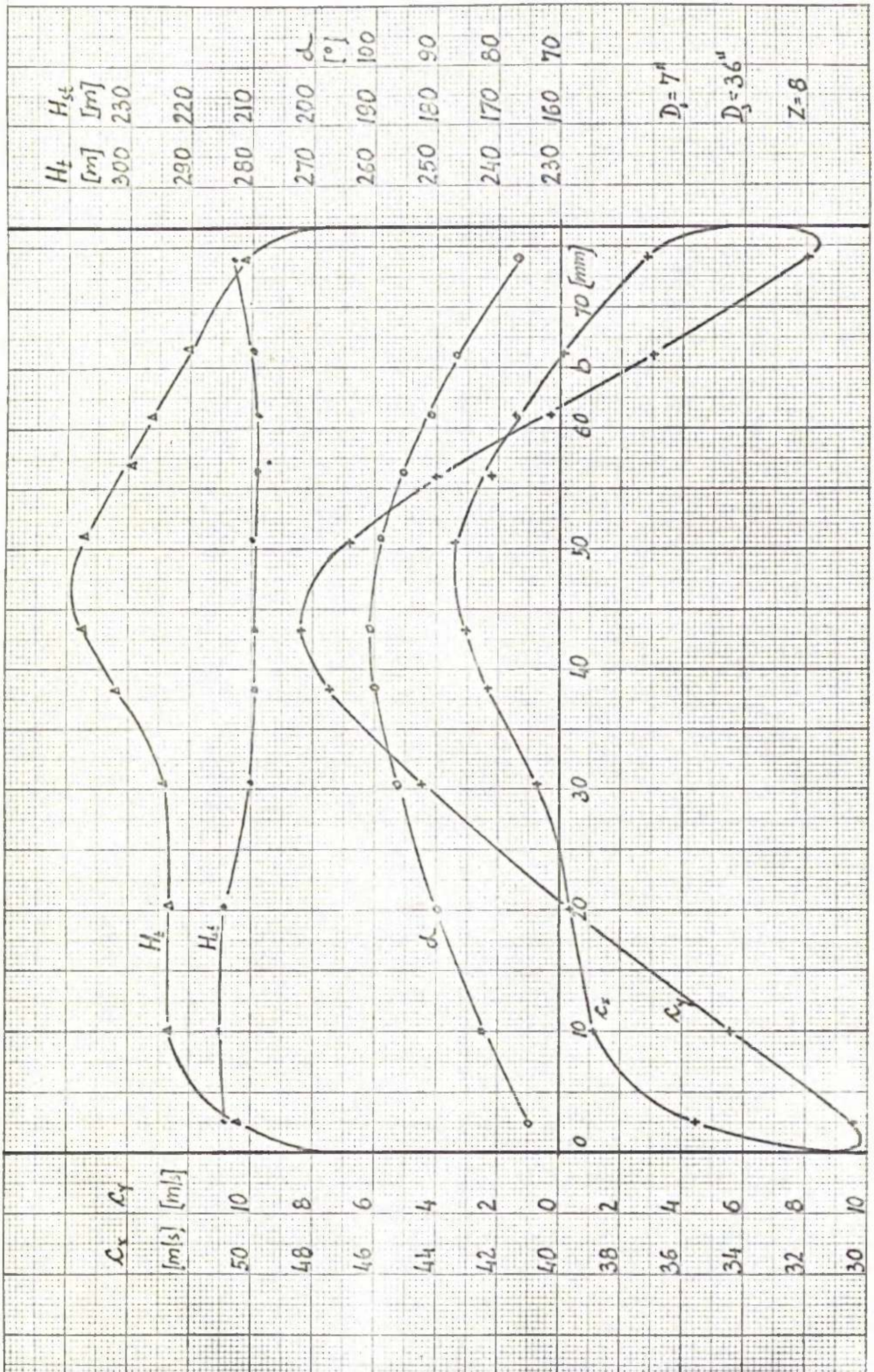

FIG. 25-4 DISCHARGE

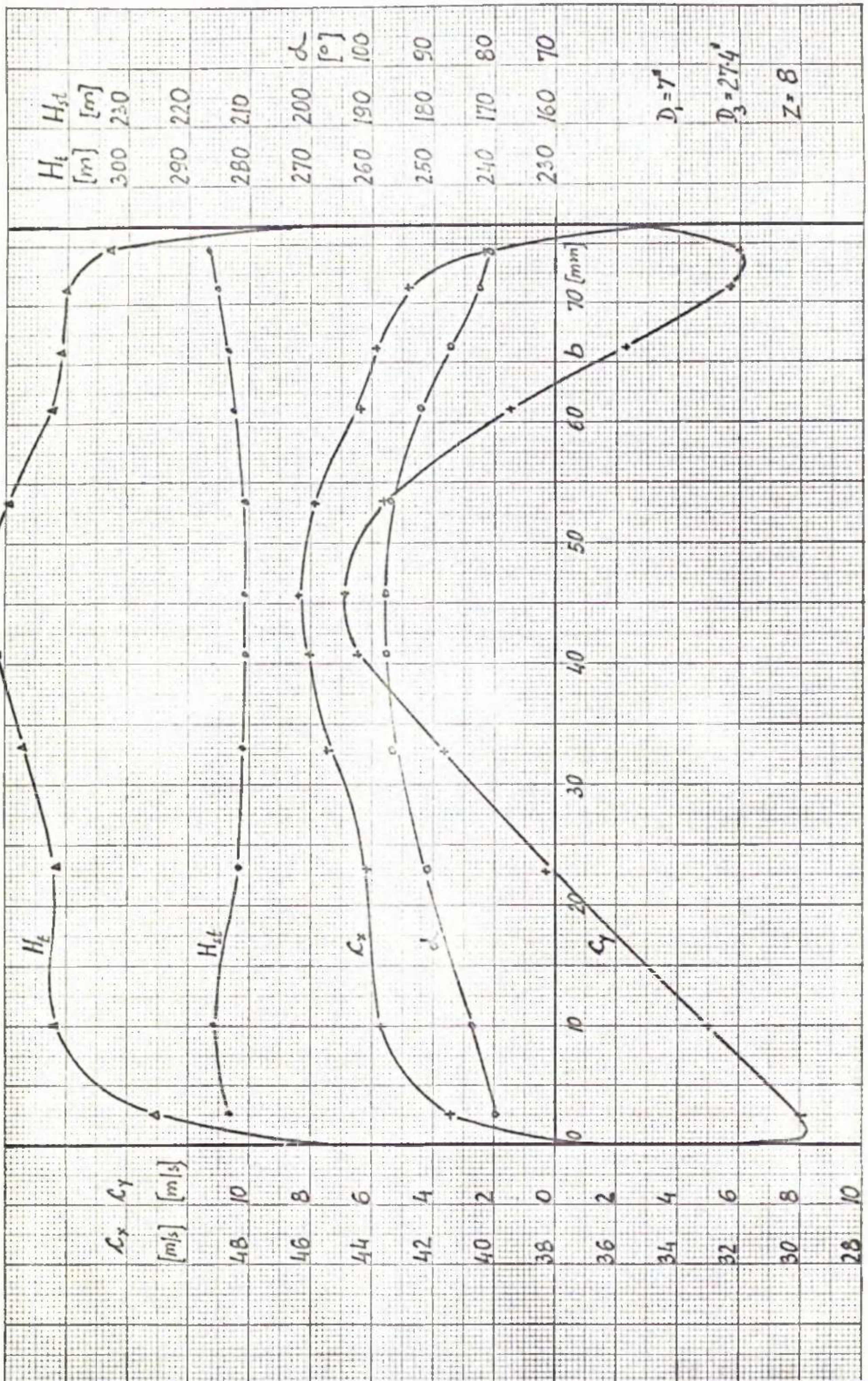

FIG. 25-5 DISCHARGE

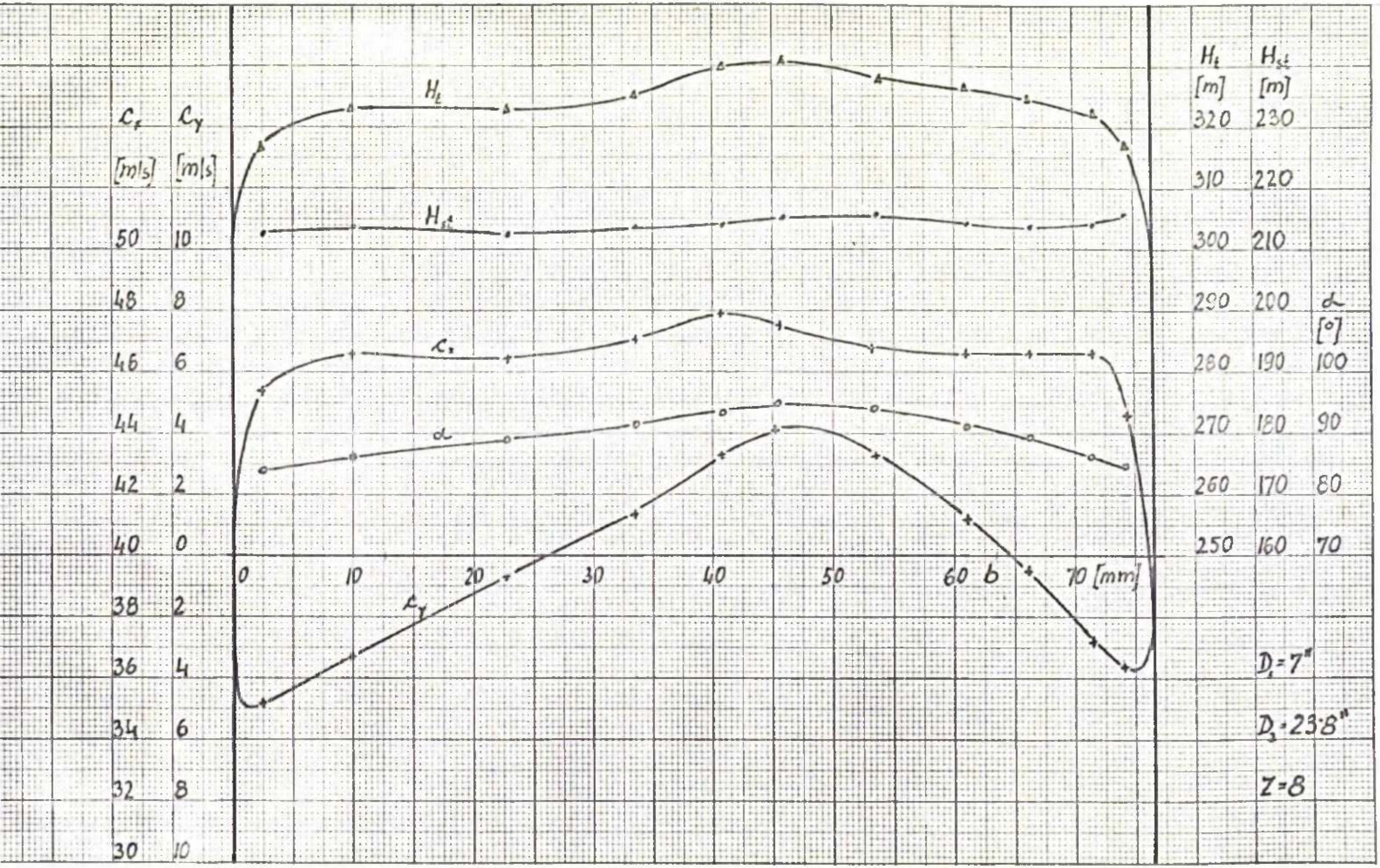

FIG. 25-6 DISCHARGE

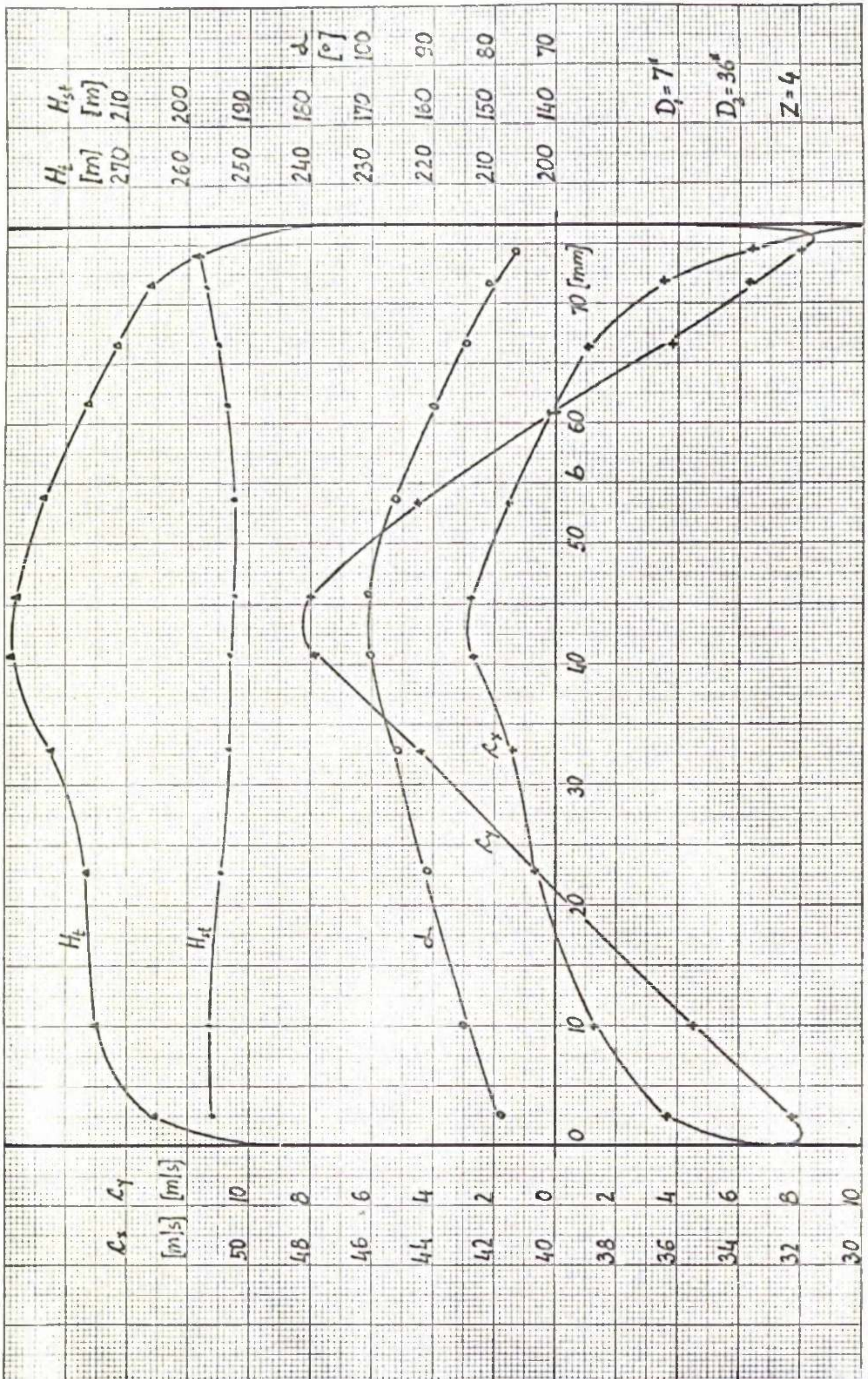

FIG. 25-7 DISCHARGE

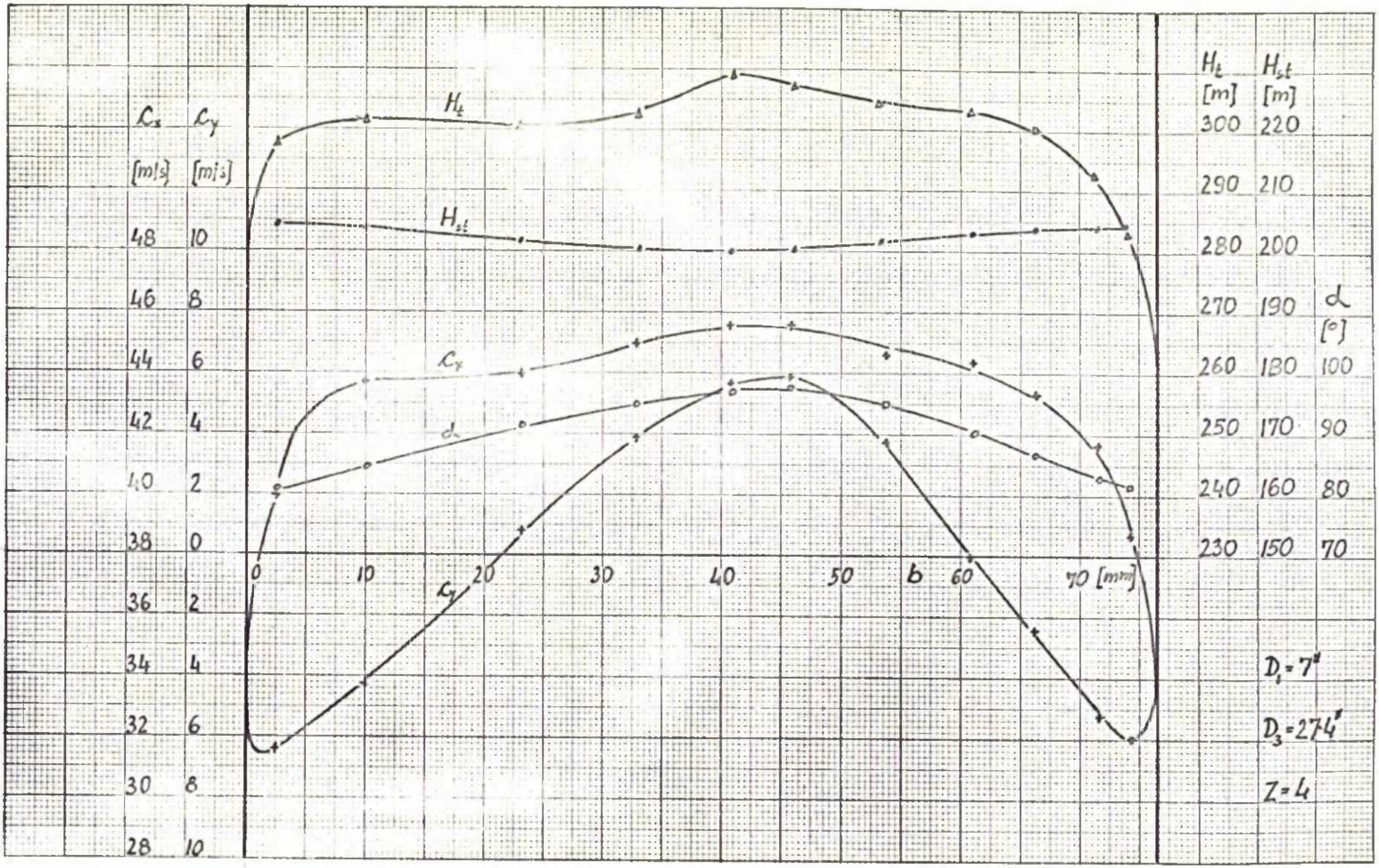

FIG. 25-B DISCHARGE

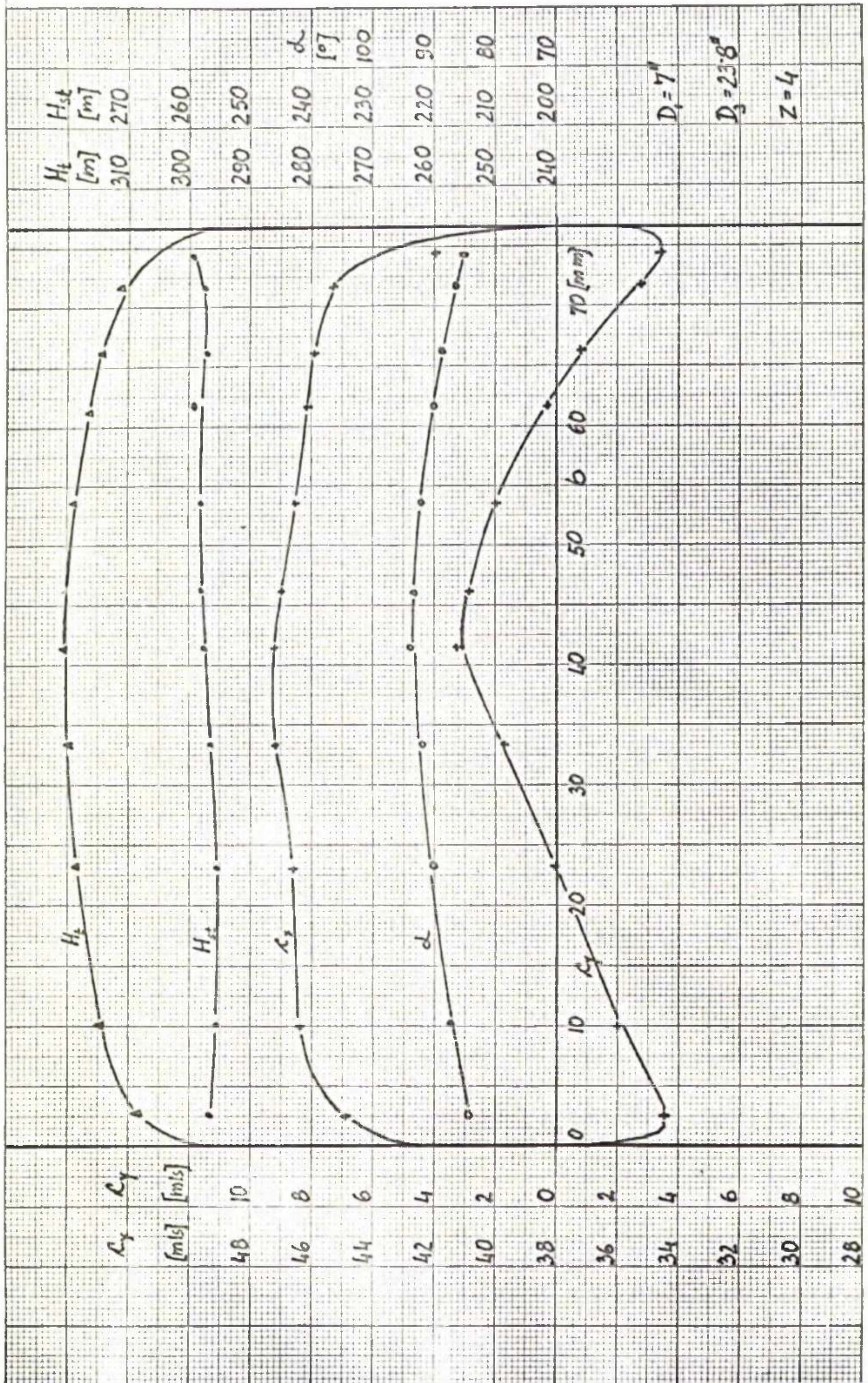

FIG. 25-9 DISCHARGE

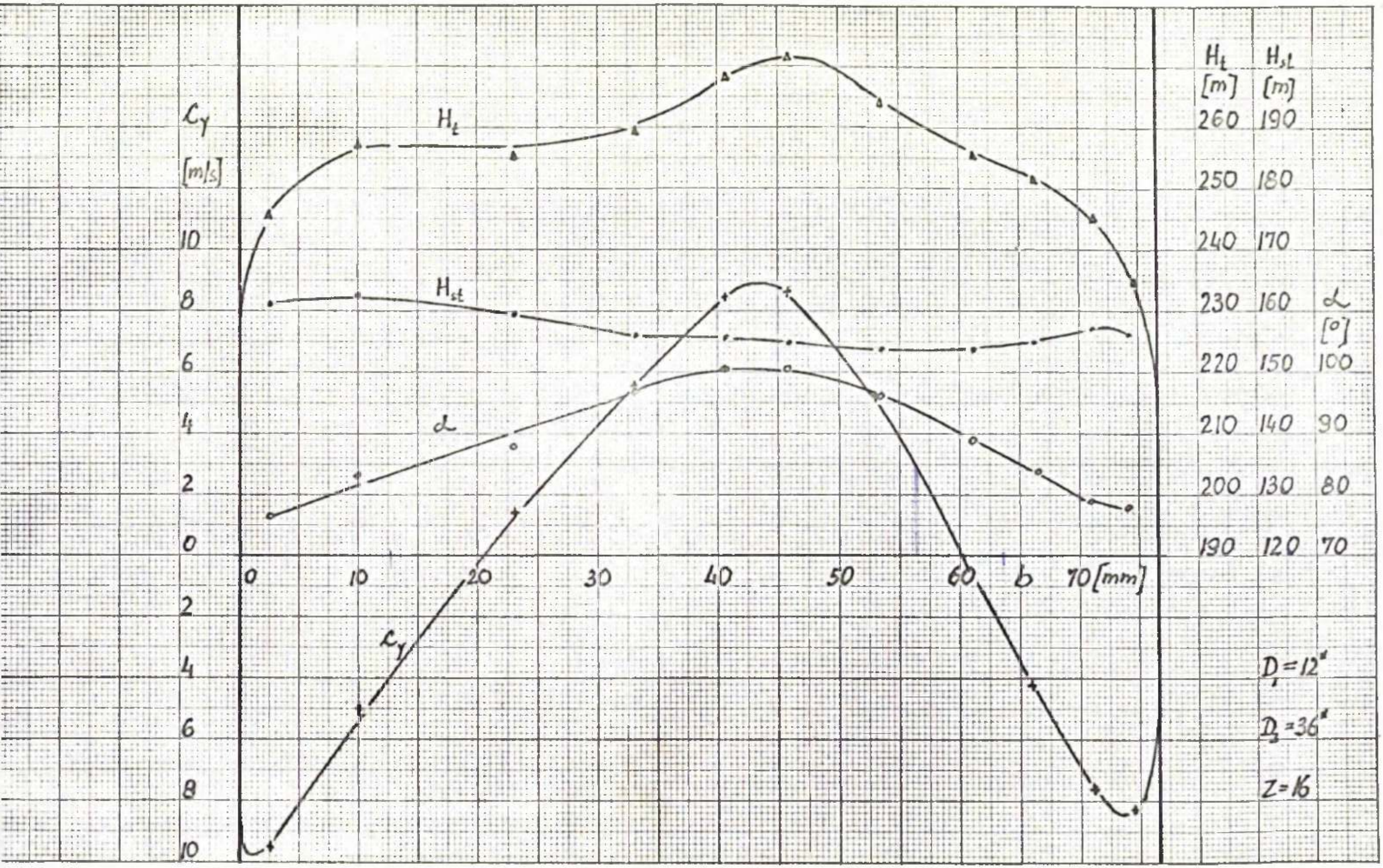

FIG. 25-10 DISCHARGE

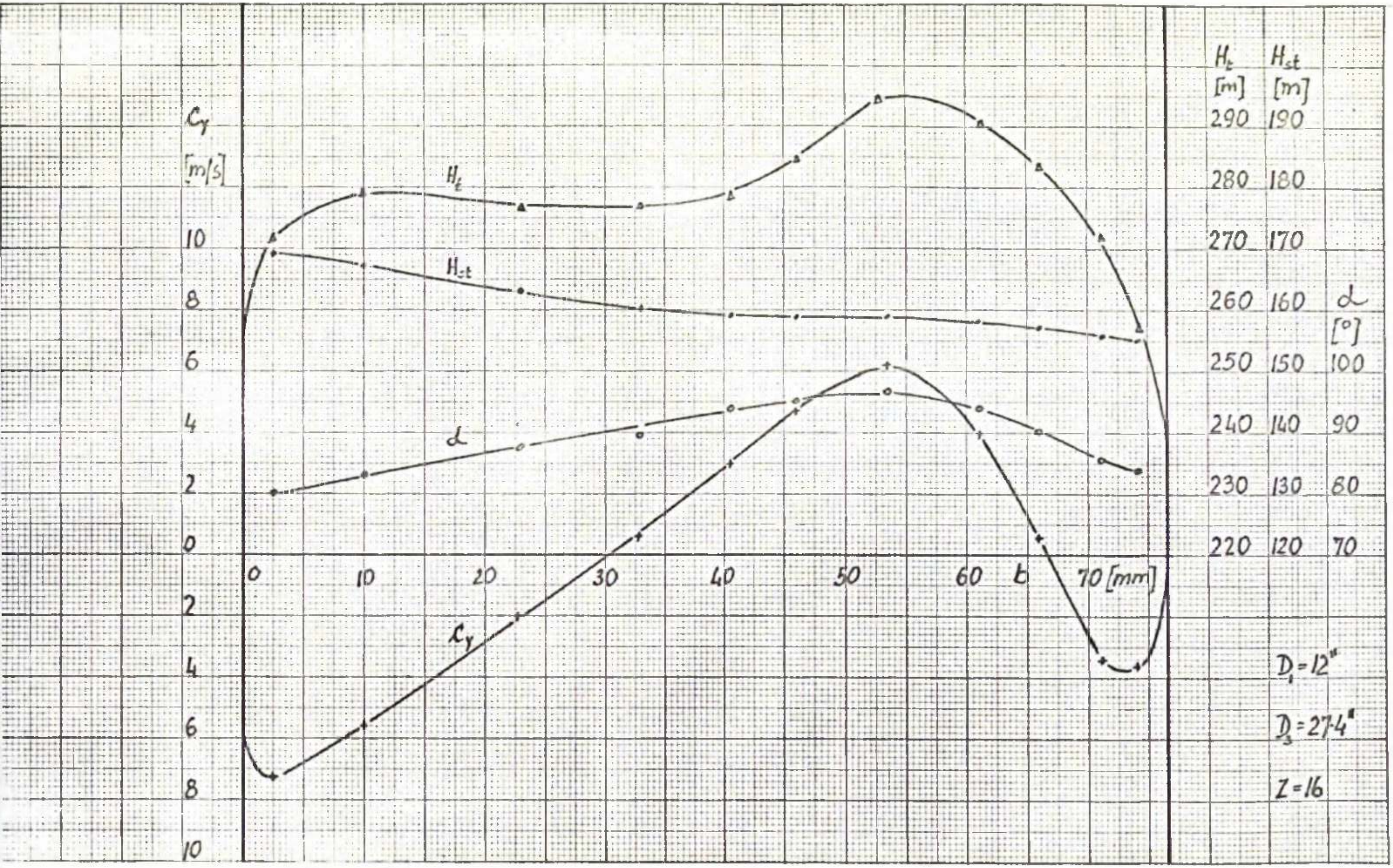

FIG. 25-11 DISCHARGE

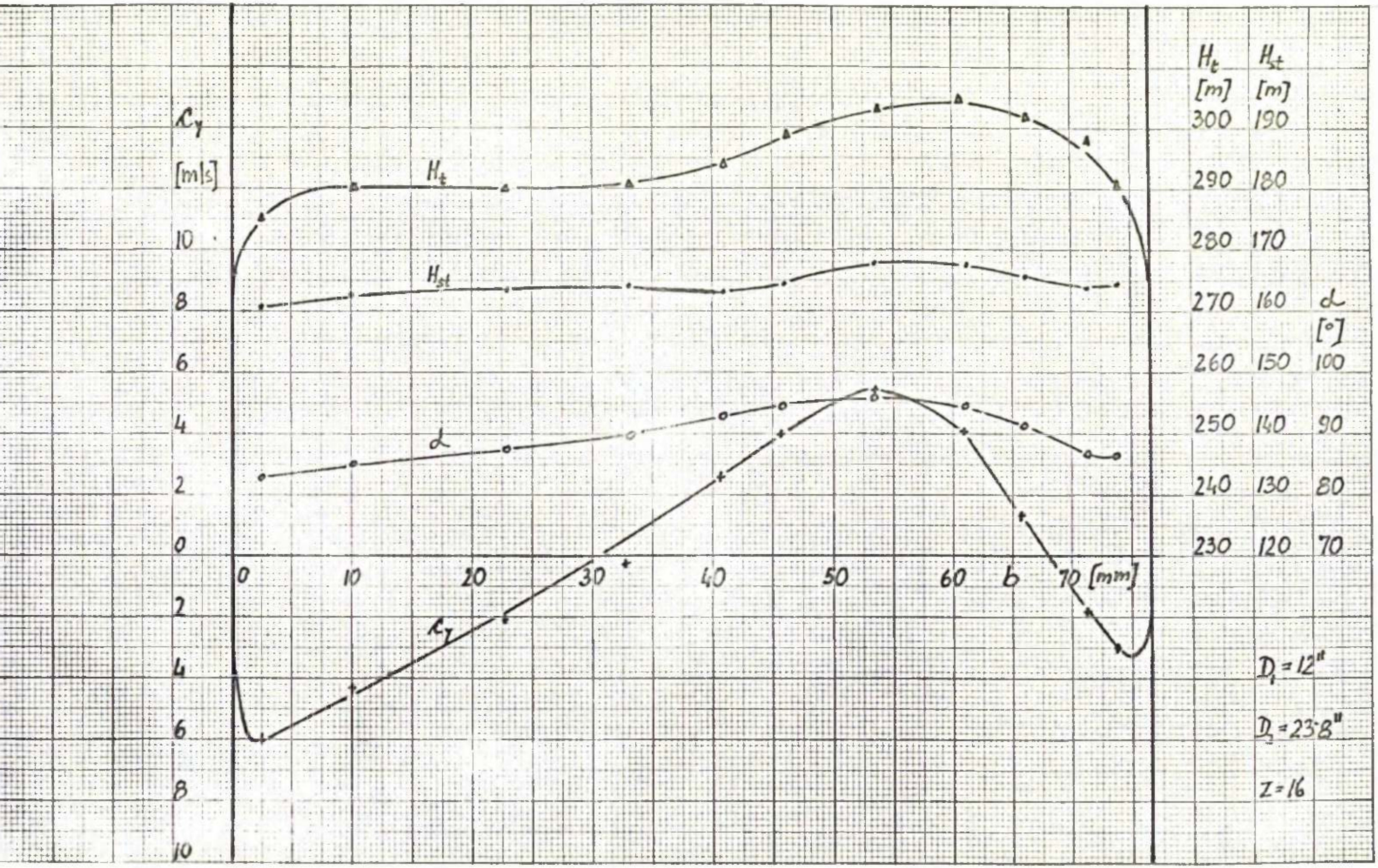

FIG. 25-12 DISCHARGE

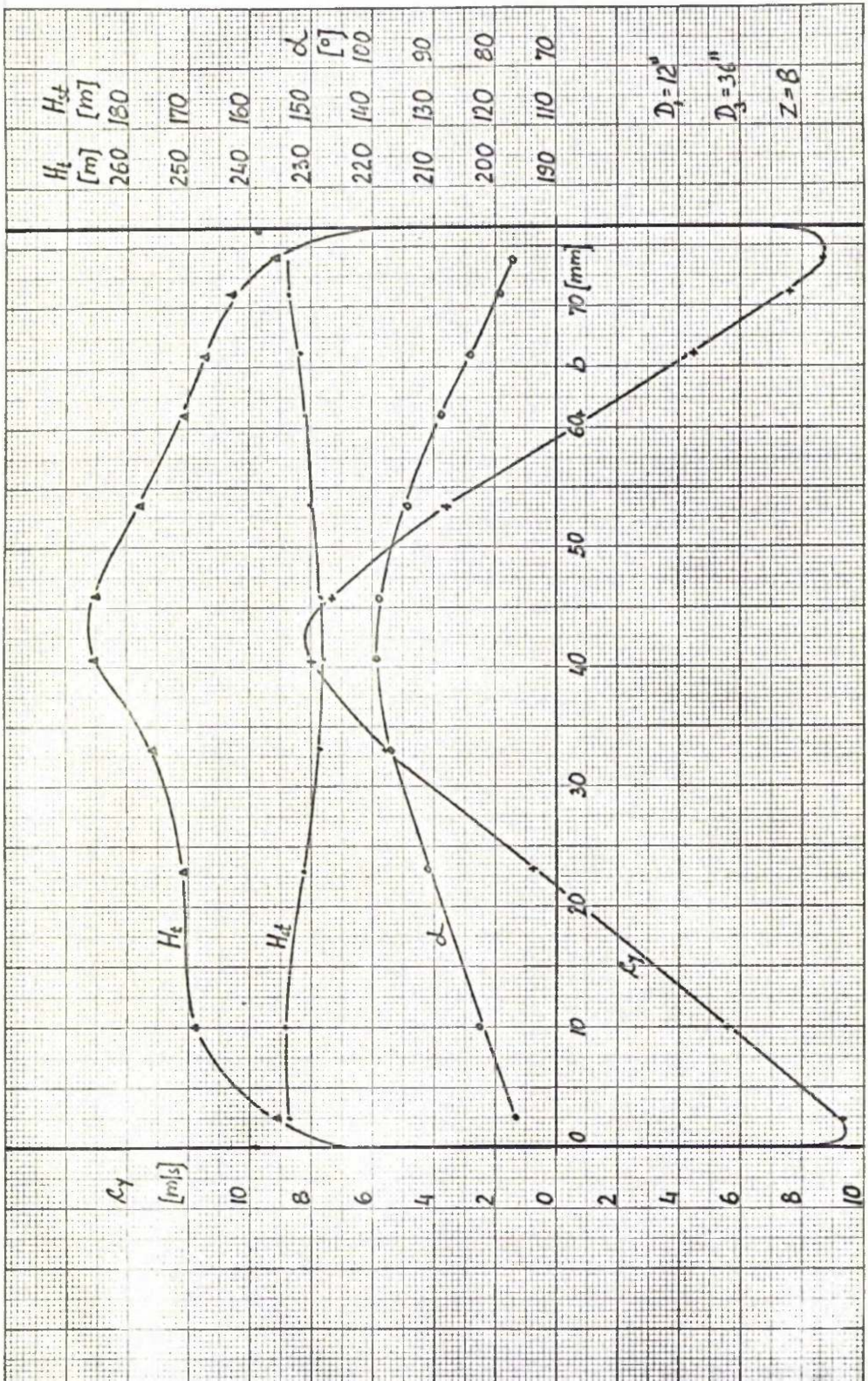

FIG. 25-13 DISCHARGE

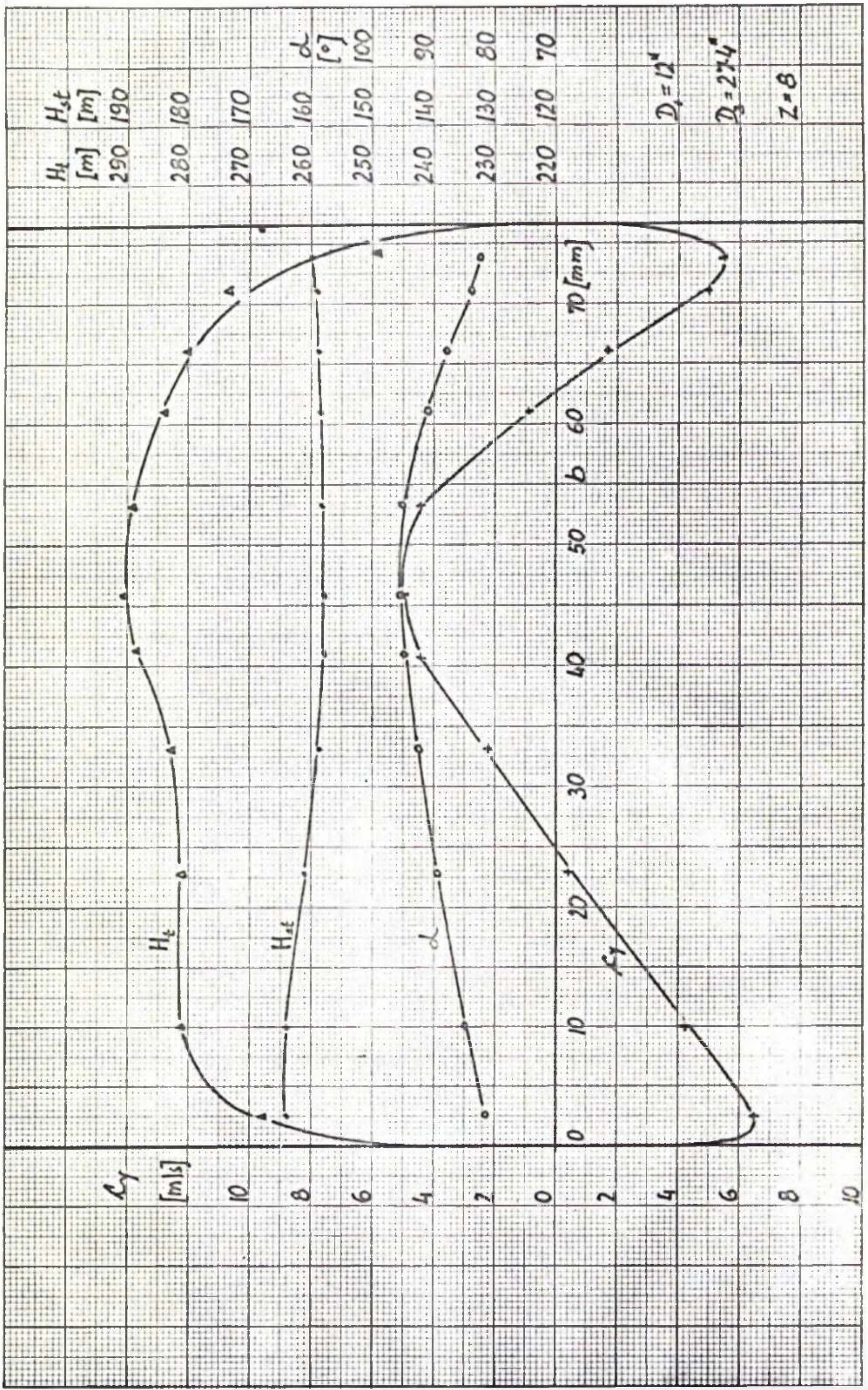

FIG 25-14 DISCHARGE

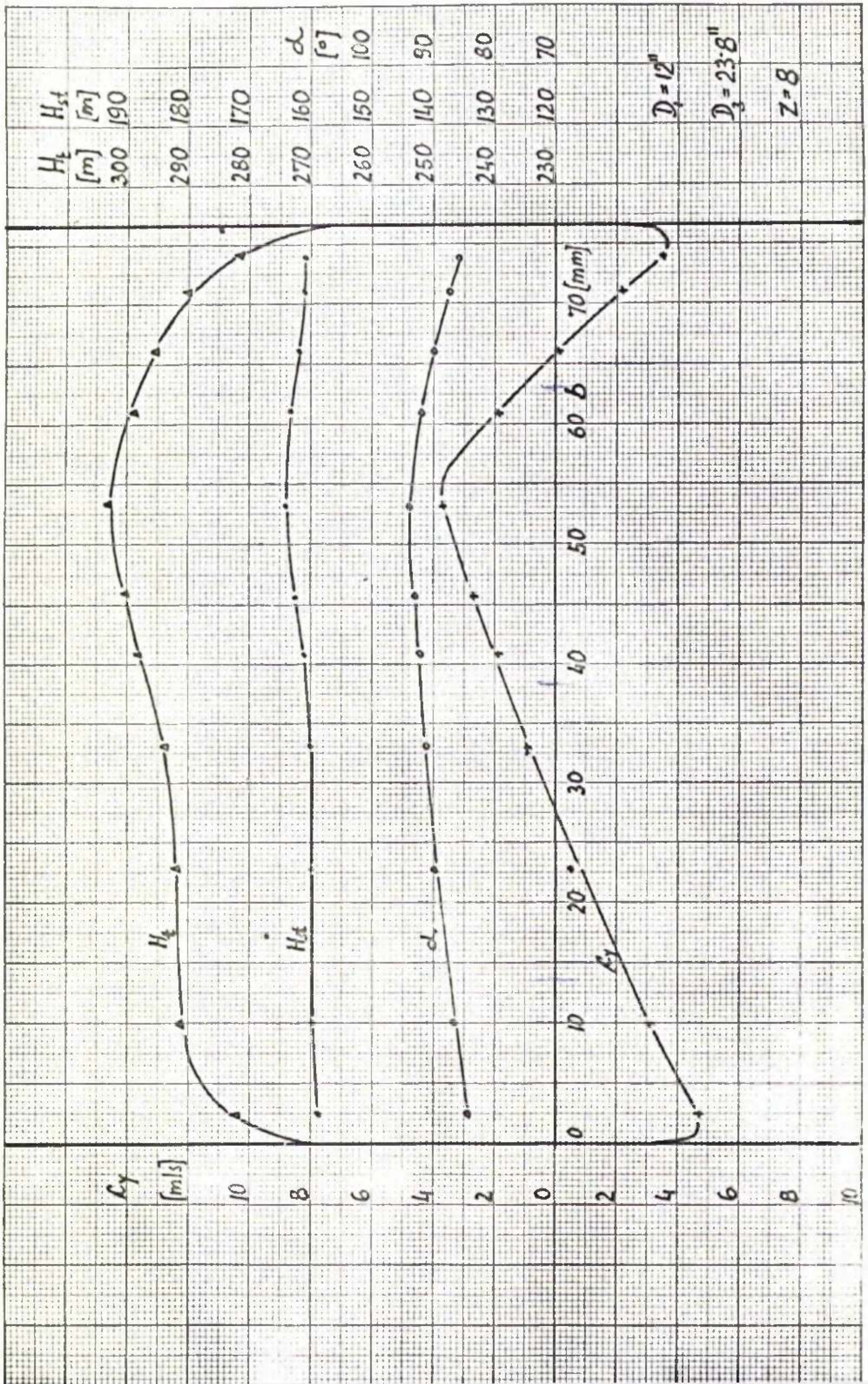

FIG. 25-15 DISCHARGE

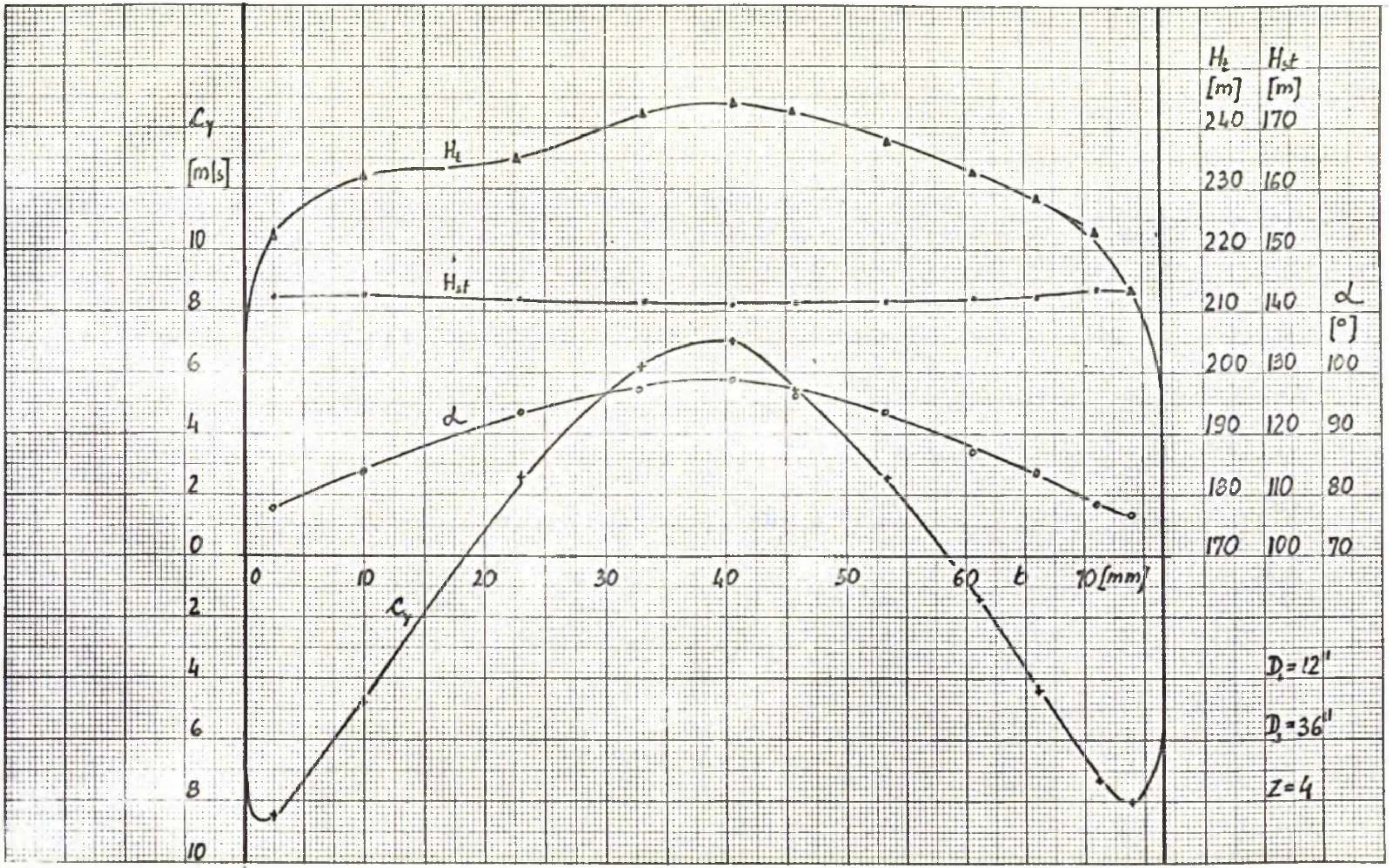

FIG. 25-16 DISCHARGE

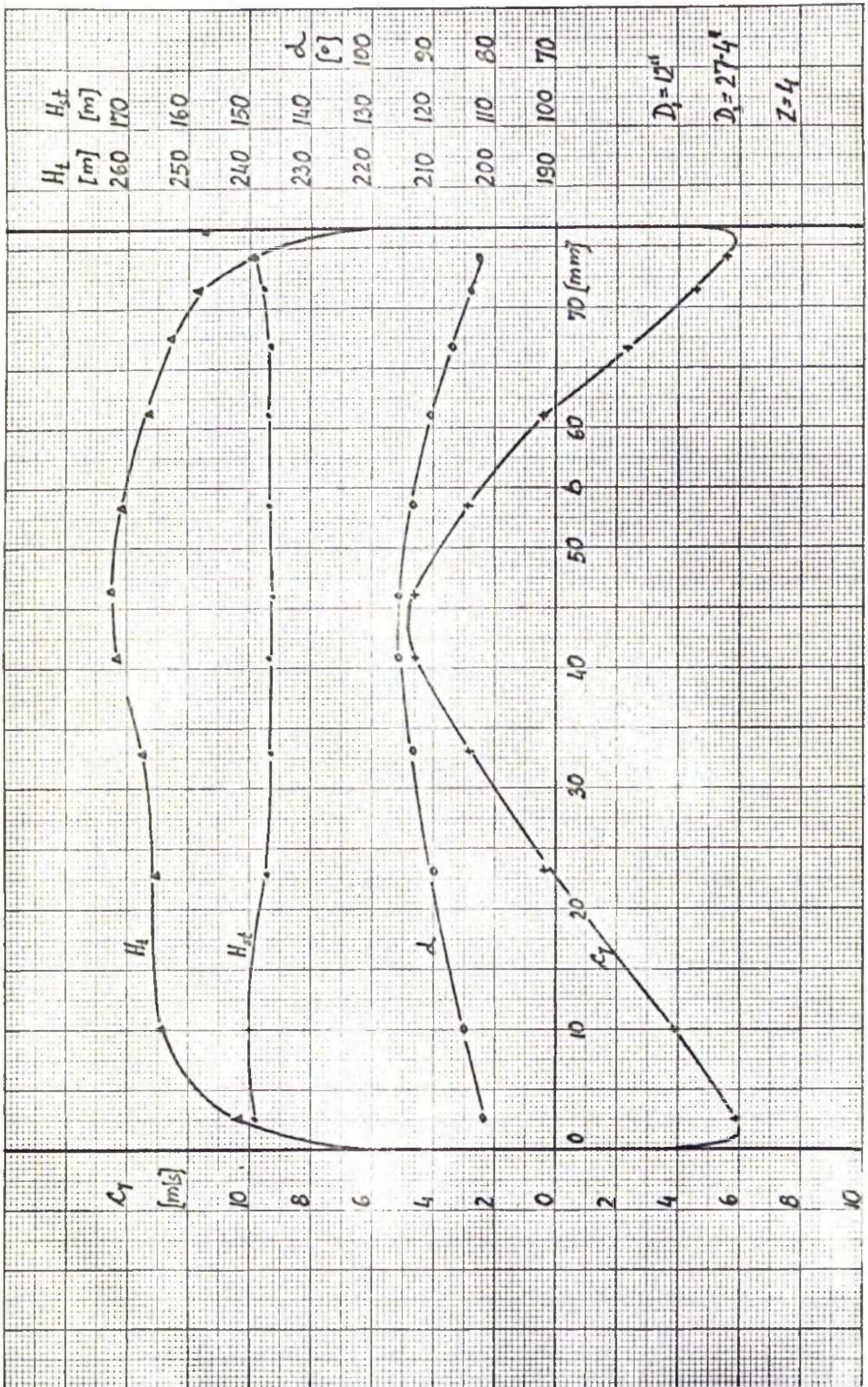

FIG. 25-17 DISCHARGE

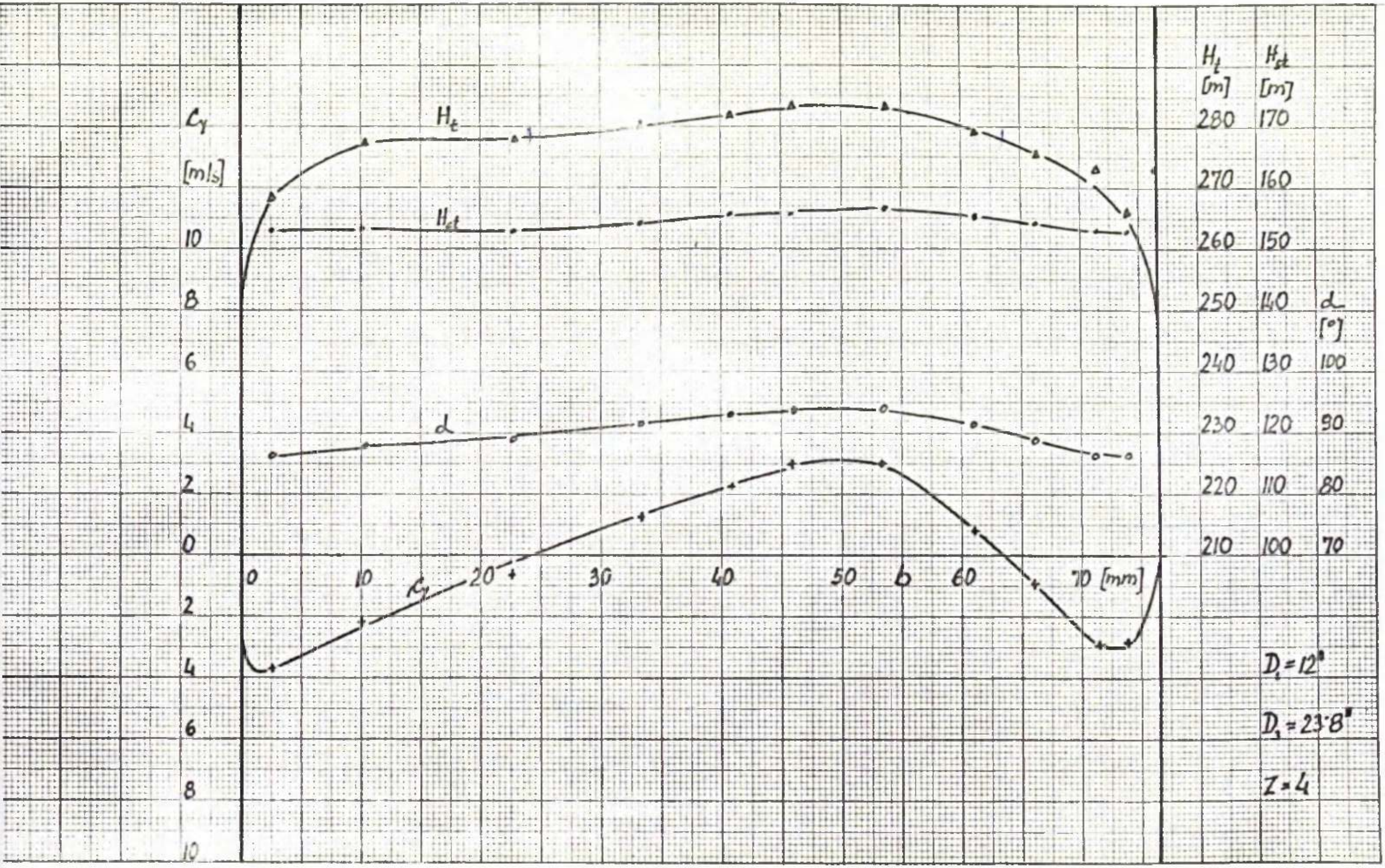

FIG. 25-18 DISCHARGE

The other half of the total area taken by the two side sections is not equally divided into two partitions. The partition near to the front shroud is always smaller than that near to the back shroud for any variation in geometry of the pump.

How both partitions vary if the inlet diameter D_1 and the number of blades Z are changed is seen from the example listed below. The volute ring diameter D_3 was kept constant.

$D_3 = 27.4''$

Z	$D_1 = 7''$ f_1/f_2	$D_1 = 12''$ f_1/f_2
16	0.397	0.305
8	0.62	0.575
4	0.728	0.67

where f_1 - area of the partition close to the front shroud

f_2 - area of the partition close to the back shroud

However, if the diameter of the casing is enlarged the ratio f_1/f_2 will increase.

Analysis of the flow phenomena at the discharge of the impeller indicated no effect of inlet diameter D_1 on flow rate. See figure 26.

However, the diameter of the casing D_3 and the number of blades Z, show considerable influence on flow conditions at the discharge. By increasing the diameter of the casing and the number of blades the flow rate was increased and reached its maximum at $D_3 = 36''$ and at $Z = 16$.

The experiments satisfied the equation of continuity by showing that the flow rate in the middle section was equal to the sum of the flow rates in the two side sections.

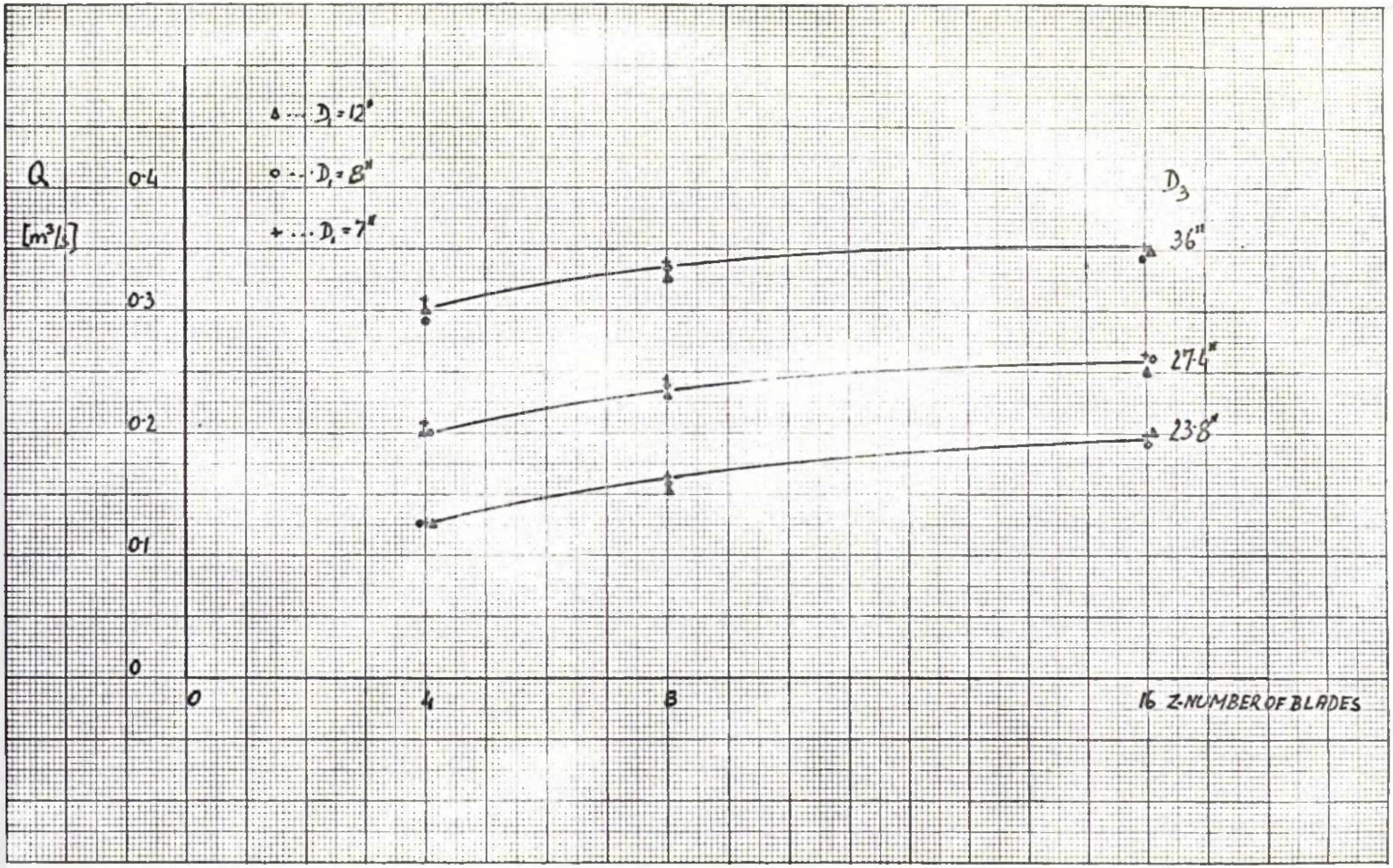

FIG. 26 DISCHARGE: FLOW RATE

The static head distribution measured across a width of the volute was found to be almost constant with a slight decrease in the region where inward flow occurred. The inlet diameter was the only parameter which affected the static head distribution. The experiments showed that on increase of inlet diameter the static head decreased.

The total head distribution in the measured section was fairly constant apart from the region where inward flow took place. In that region, measurements indicated a great increase in the total head.

The meaning of the total head will now be considered from two different aspects:

a) The total head in the casing

b) The total head which will be split into two sections namely the regions of inward and outward flow.

Referring to (a), the average total head showed a certain drop in head if the volute ring diameter or inlet diameter were increased. The drop in total head was most marked for the number of blades, $z = 4$, at the volute ring diameter $D_3 = 36"$ and at the inlet diameter $D_1 = 12"$.

The behaviour of the average total head in the region of inward and outward flow can be seen in figures 31 and 32. The relationship between the total head in the casing (fig.30) and the total head related to the region of inward and outward flow is as follows:

$$H_{td_{casing}} = \frac{H_{td_{inward}} + H_{td_{outward}}}{2}$$

The comments on item (b) from the physical point of view will be given later in chapter 7.

The angle α of the absolute velocity C at the discharge side of the impeller is very sensitive to the diameter of the volute ring D_3. The other geometrical variables do affect the angle α but in lesser degree. Variation in the angle α was from 0^o to 10^o in the region of the inward flow and from 0^o to -10^o in the region of outward flow. Those figures changed with the geometry of the pump and had the lowest variation at $D_3 = 23.8"$ and $z = 4$ where $\alpha = \pm 4^o$.

The plot showing distribution of the angle α across the measured section has a smooth shape with its maximum somewhere in the middle of the section and its minimum near the side walls.

6.4 Power

Although high accuracy of power measurement cannot be claimed, the results obtained are thought to be fairly reliable. In figure 27 the power consumption is plotted against number of blades.

The variation of power consumption is very significant when the volute ring diameter D_3 or the inlet diameter D_1 are increased. The number of blades z does not affect the power consumption very much although a maximum can be noticed between $z = 8$ to 10.

The friction losses are shown in figure 28 for inlet diameters

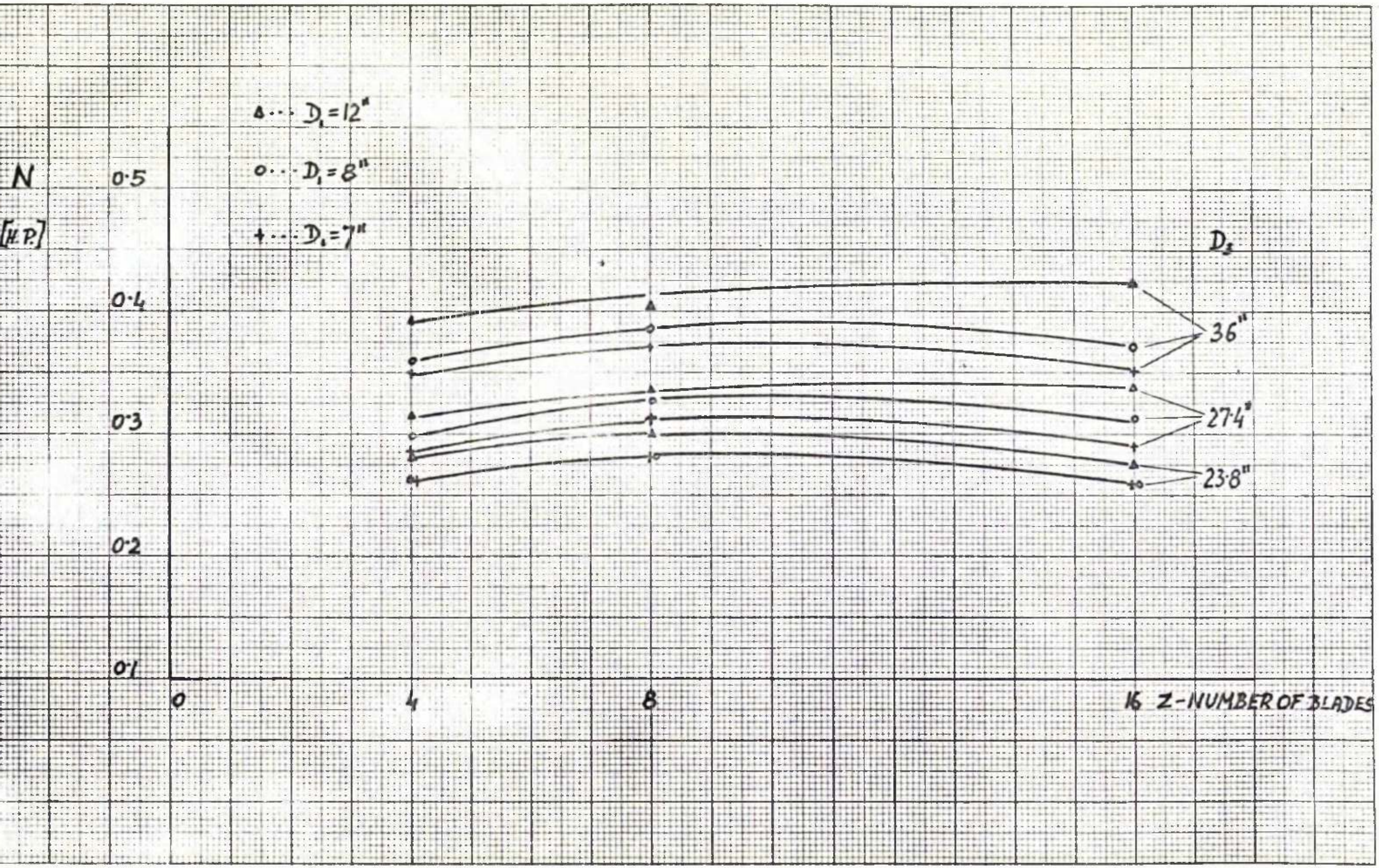

FIG. 27 TOTAL POWER CONSUMPTION

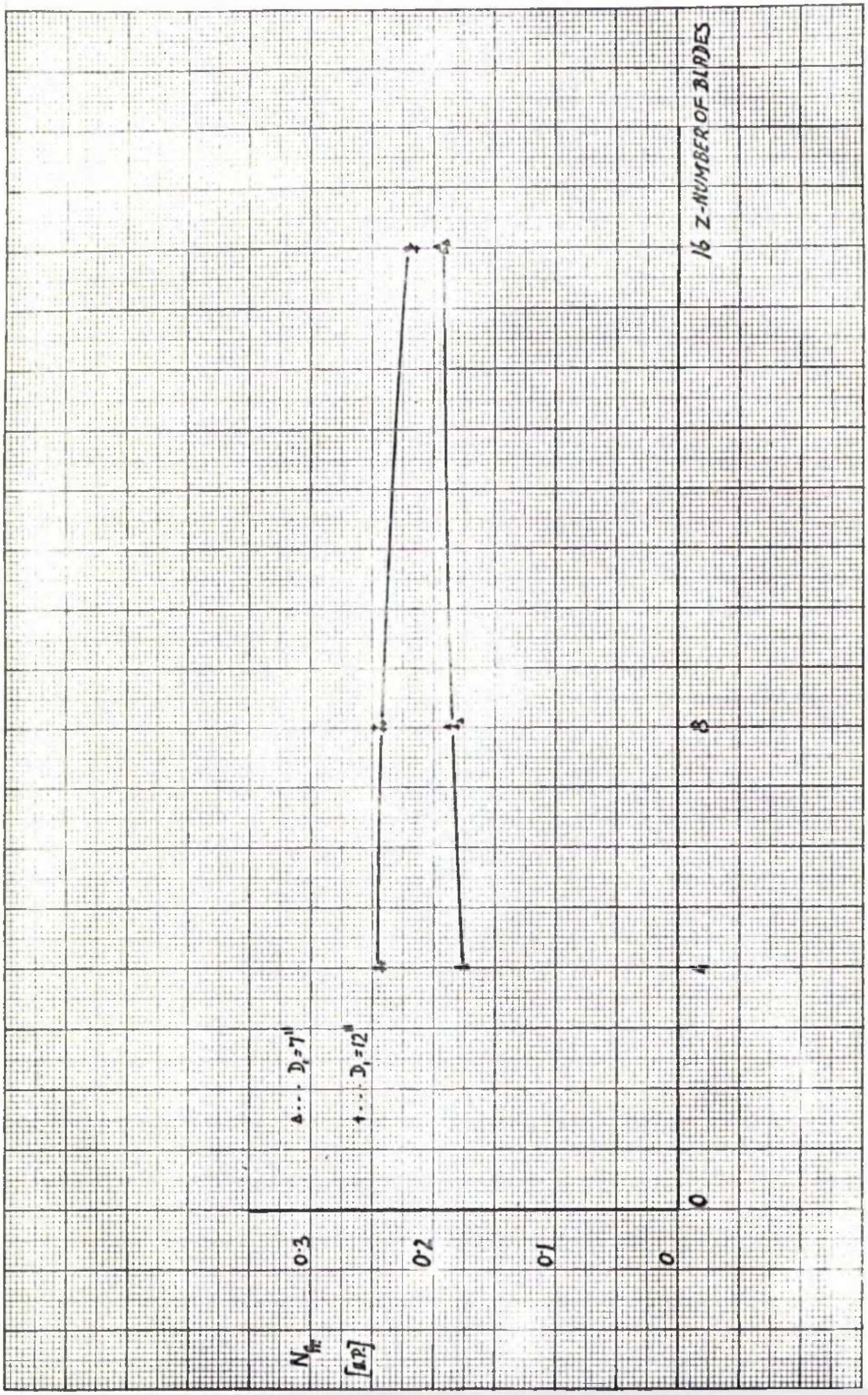

FIG. 28 POWER CONSUMPTION DUE TO FRICTION

$D_1 = 7"$ and $D_1 = 12"$. The friction losses for the inlet diameter $D_1 = 8"$ were not measured and were taken equal to the friction losses for $D_1 = 7"$.

When the friction losses were measured the outlet of the impeller was blocked by means of sellotape.

7. ANALYSIS OF RESULTS

7.1 Pump action - turbine reaction

The phenomenon which for a long time has not been explained and fully analysed is recirculation. Lack of information as to what happens at the inlet and at the discharge when $Q=0$ was the main drawback.

Many questions arise even if the problem is simplified as follows. Since the discharge is zero the output power is zero then the input power should be equal to the sum of the mechanical loss, the disc friction loss and the leakage loss. But in fact the measured input power is greater than this.

Detailed analysis of energy and flow conditions reveals the "mechanism" of flow phenomena at $Q=0$.

The experiments verify that considerable flow exists at the discharge of the impeller. Flow through the impeller and through the measured area can be divided into two components:
a circular flow around the axis of rotation and a through-flow. This flow definition is schematically shown in figure 29, where the resultant velocity is divided into two component Cx and Cy.

In addition, the physical meaning of the resultant velocity is changed if the angle α changes its sign from positive to negative.

When the resultant velocity leaves the impeller and the angle

PUMP VELOCITY TRIANGLE

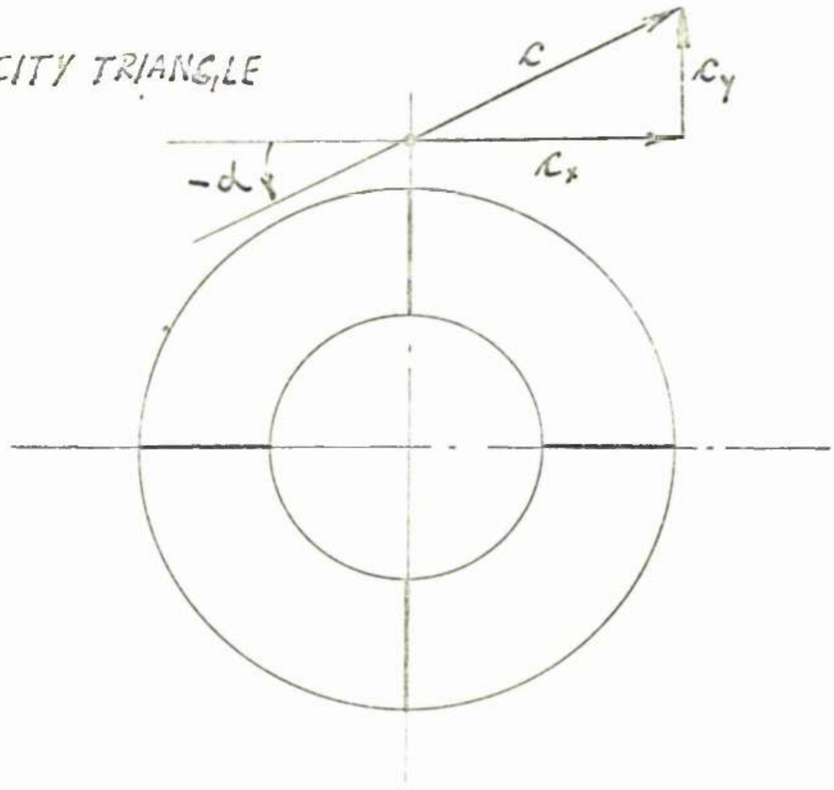

TURBINE VELOCITY TRIANGLE

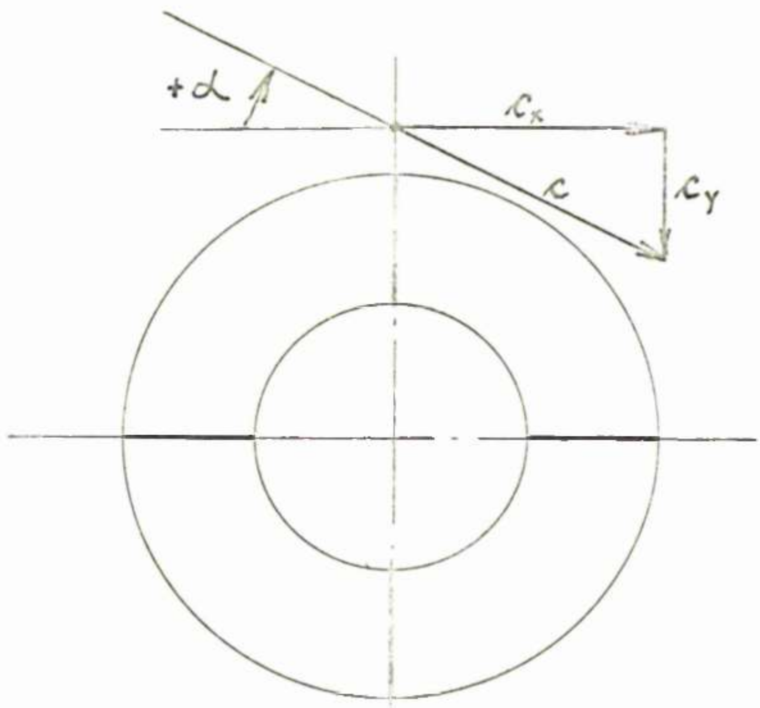

FIG. 29

is negative such a velocity triangle is usually referred to as the pump velocity triangle.

If the resultant velocity enters the impeller at the discharge and the angle α is positive such a velocity triangle is called turbine velocity triangle.

Since the two types of velocity triangle appear to exist at the discharge, although at different places, indication is given that the impeller itself works under two different physical conditions.

To understand the phenomena better the actual impeller may be thought of as divided into two separate "impellers".

a) The impeller having pump velocity triangles

b) The impeller having turbine velocity triangles

From the foregoing reasoning the straightforward conclusion can be made:

a) Part of the impeller acts as a pump

b) Part of the impeller acts as a turbine

c) Both actions happen in the same impeller at the same time

The pump action area corresponds to the region of inward flow and the turbine reaction area corresponds to the region of outward flow.

In general, the middle part of the impeller acts as a pump and the two side parts act as a turbine. Similarly, the average total head at discharge can be divided into two parts as regards the position of inward and outward flow area:

a) The average pump total head

b) The average turbine total head

To support the above conclusions power exchange will be analysed and the full meaning of the above statement will be revealed.

The power applied to the fluid by the impeller:

$$N_p = \gamma_d \cdot Q_d \; H_d - \gamma_s \cdot Q_s \; H_s \qquad 7.1$$

and the power returned to the impeller

$$N_t = \gamma_d \cdot Q_d \; H_d' - \gamma_s \; Q_s \; H_s' \qquad 7.2$$

where Q_d – the circulatory flow at discharge

Q_s – the circulatory flow at suction

γ_d – the specific weight of air at discharge

γ_s – the specific weight of air at suction

H_d – the total head at discharge belonging to the region of inward flow

H_d' – the total head at discharge belonging to the region of outward flow

H_s – the suction head belonging to the region of inward flow

H_s' – the suction head belonging to the region of outward flow

The difference between the power applied to the fluid field and the power returned to the impeller yields part of the power which is supplied to the impeller.

$$\Delta N = N_p - N_t$$

$$= (\gamma_d Q_d H_d - \gamma_s Q_s H_s) - (\gamma_d Q_d H'_d - \gamma_s Q_s H'_s)$$

$$= \gamma_d Q_d (H_d - H'_d) - \gamma_s Q_s (H_s - H'_s) \qquad 7.3$$

In the above equation it was assumed that the discharge flow $Q = 0$.

Several conclusions can be drawn from equation 7.3 by analysing it and introducing different fluid conditions:

a) The first condition

The recirculatory flow Q_d and Q_s exist but the term

$H_d - H'_d = 0$

and

$H_s - H'_s = 0$

It follows that

$H_d = H'_d$

and

$H_s = H'_s$

This would be an ideal case and there would be no losses either at the discharge or at the suction. The power applied to the fluid would be returned by the reverse flow which produces a turbine reaction on the impeller.

It would follow that

$\Delta N = 0$

b) The second condition

The recirculatory flows Q_d and Q_s exist and the terms

$H_d - H_d \neq 0$

and

$$H_s - H_s' \neq 0$$

This was the situation which occurred in the experiments discussed in this thesis and the following additional conditions were found:

$$H_d > H_d'$$

and

$$H_s < H_s'$$

The power applied to the fluid becomes:

$$N_p = (\gamma_d \; Q_d \; H_d - \gamma_s \, Q_s \; H_s) \qquad 7.4$$

and power returned to the impeller is

$$N_t = (\gamma_d \; Q_d \; H_d' - \gamma_s \, Q_s \; H_s') \qquad 7.5$$

where the difference is equal to the part of the power applied to the shaft.

$$\Delta N = N_p - N_t \qquad 7.6$$

Equation 7.4 represents the pump action on the fluid and equation 7.5 the turbine reaction of the fluid on the impeller.

Equation 7.6 fully explains why the power applied to the shaft is greater than the power needed to cover the friction and mechanical losses.

c) The third condition

A certain discharge flow Q is assumed, accompanied by a recirculatory flows Q_d and Q_s. Although no experiments have been made for this situation some preliminary conclusions can be drawn.

Thus,

$Q \neq 0$ and $Q < Q_n$

where Q_n is the nominal flow at design point.

Equation 7.3 has been changed and the new form is arrived at:

$\Delta N = Q$ (term in equation 7.7 represents $H_d' - \gamma_s Q_s \; H_s'$)   7.7

The first term in equation 7.7 represents the power which is necessary to energize the fluid and the second term shows the power return to the impeller.

It is clear that by increasing the flow rate Q the first term will increase and the second term will decrease. The part of the power applied to the shaft will be higher than the power expressed by equation 7.6.

d) The fourth condition

The discharge flow Q reaches the flow predicted at the design point i.e. Q_n and the recirculatory flow almost disappears. The part of the power applied to the shaft becomes:

$$\Delta N = Q \; (\gamma_d \, H_d \; - \; \gamma_s \, H_s) \qquad 7.8$$

Analysing the foregoing deductions some objections could be made concerning the experimental condition. Namely, the suction conditions were not measured at the very entrance of the impeller.

The author believes that by measuring the suction conditions nearer the impeller entrance (which would be technically very difficult) the last term in equation 7.3 would be slightly changed but the physical meaning of the problem would remain unaltered.

The above analysis does not show what the total power applied to the shaft was used for. Only one part of the total power and its physical meaning has been explained and examined.

It is evident that an additional type of energy dissipation is taking place inside the pump that cannot be ignored. There is no doubt regarding the mechanism which causes a large proportion of the power dissipation. Although energy has been dissipated from the hydraulic point of view, it has in fact been transformed into heat energy. Since no fluid could escape from the system to carry away heat with it, the result was that the air and the pump rapidly became hotter.

The direct measurement of energy transferred into heat is very difficult. For that reason the total power applied to the shaft will be divided into separate terms.

$$N = \Delta N + N_{fr} + N_{heat} + N_{mech.}$$

where N = total power applied to the shaft

ΔN = part of the power applied to the impeller, see equation 7.3

N_{fr} = friction losses

N_{heat} = heat losses

$N_{mech.}$ = mechanical losses

The first term ΔN has been already defined. The second term N_{fr} involves the losses caused by friction when the outlet of the impeller was blocked. The third term represents the heat loss. Most of the mechanical losses were eliminated before any experiments took place. The remainder of the mechanical losses was very small.

It consisted of friction loss between the shaft and the narrow felt ring and may be neglected without much error.

The difference of power

$$N - N_{fr} = \Delta N + N_{heat} \qquad 7.10$$

represents the input power and at the same time shows the effectiveness of the system.

The strong influence of the geometry of the pump on power consumption is observed. To understand this phenomenon the hydraulic parameters corresponding to a certain pump have to be analysed separately. In addition, a detailed study of the total head distribution and the recirculatory flow has to be made.

In figure 30 it is shown that the highest discharge total head is obtained in the smallest volute ring. By using these experimental data the conclusion can be made that the maximum total head would be obtained in the volute ring when the diameter was equal to the diameter of the impeller. It is understood that the total head so obtained would not be equal to the theoretical total head. Due to the losses at the inlet and in the impeller channel, the theoretical total head would be even greater.

The study of the recirculatory flow shown in figure 26 supports the above conclusion. In the large volute ring the recirculatory flow was found to be bigger. This phenomenon is reflected in the reduction of the total head at the discharge.

Studying the results plotted in figure 30 a reduction of the

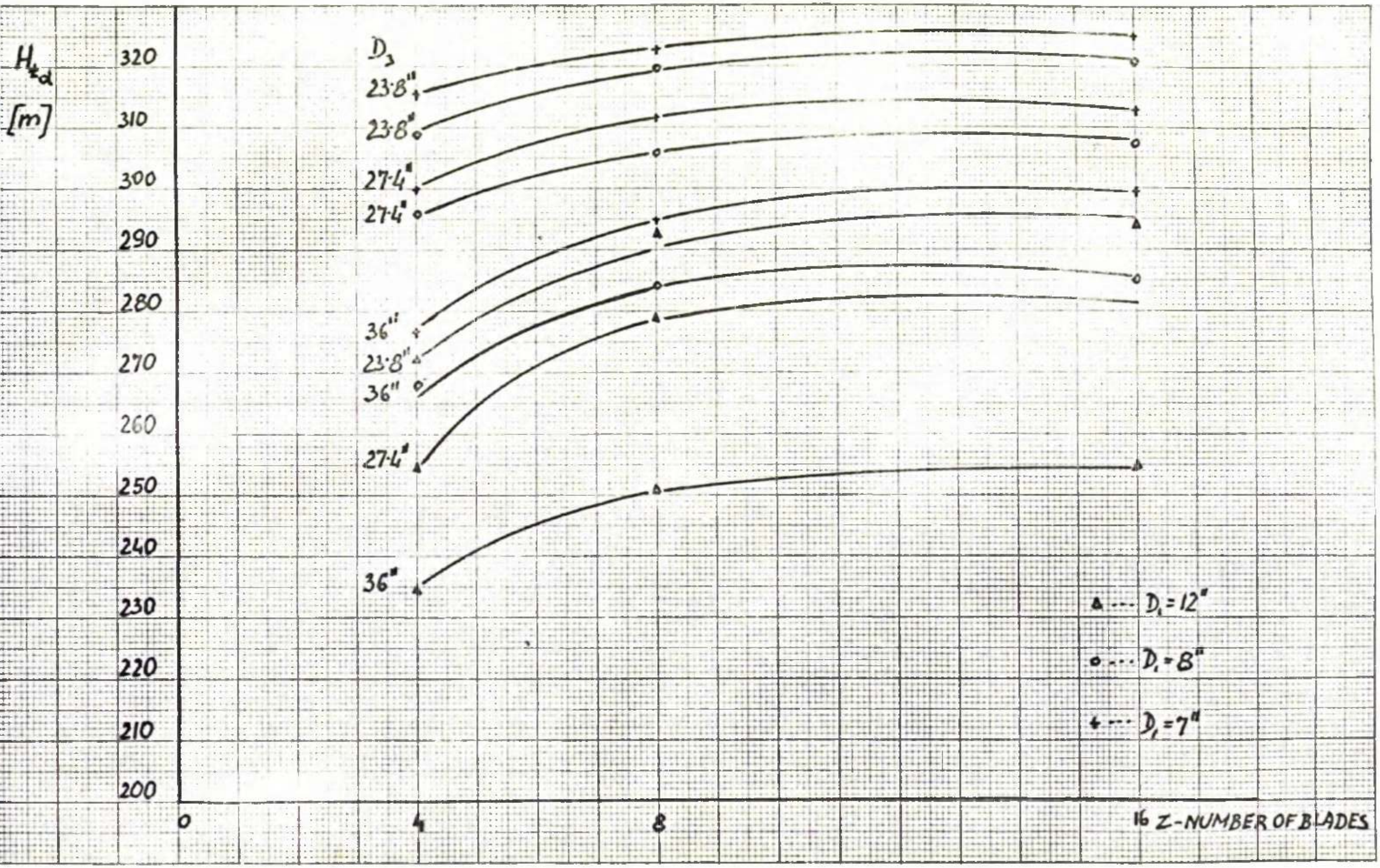

FIG. 30 DISCHARGE HEAD - CASING

total head is noticed when the number of blades is $Z = 4$. This indicates that additional losses must exist in the impeller channel thus reducing the discharge total head.

It is believed that a strong relative circulation is formed in the impeller channels. If an impeller channel were filled with fluid and closed at both ends, there would be an eddy rotation in a direction opposite to that of the impeller. Since the conditions reported in this work are very similar to the above assumption the explanation can be accepted. Also, it is reasonable to believe that relative eddy will be well spread through the impeller channel when the number of blades is small.

The conclusion can be drawn that the above reasoning shows the cause for a sudden drop in the total head for a small number of blades.

Figures 31 and 32 show the turbine and the pump total head at the discharge. Both parameters follow the same pattern as seen in figure 30. This is obvious since the total head plotted in figure (30) represents the mean value of the turbine and the pump total head.

Taking into account the discharge recirculatory flow and the total head caused by the pump action and turbine reaction, the output power characteristics at discharge are obtained.

The pattern of output power characteristics is opposite to the pattern of the total head characteristics. The turbine and pump power characteristics are increased by increasing the diameter of the casing. This is due to the recirculatory flow which is

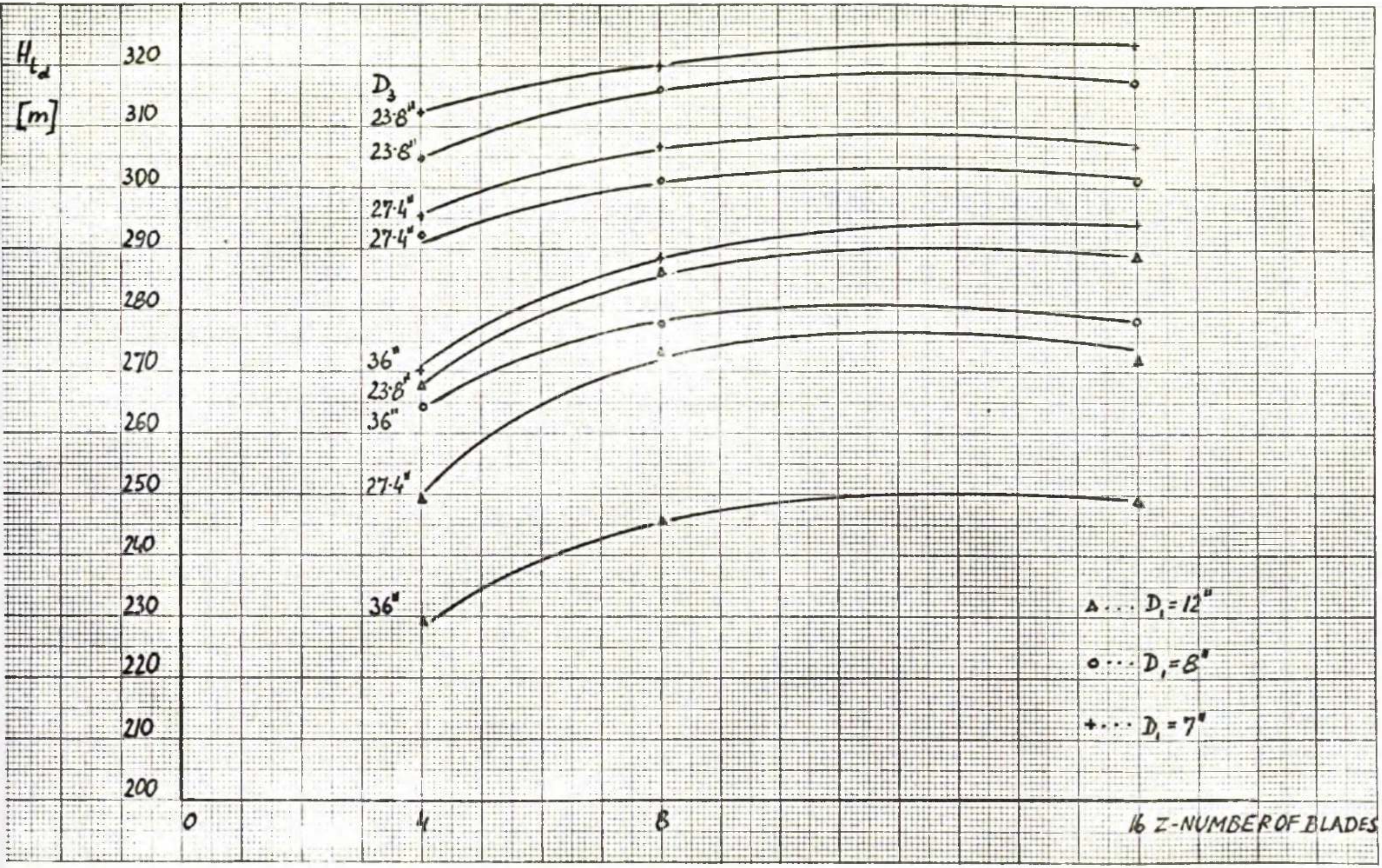

FIG. 31 DISCHARGE: TURBINE HEAD

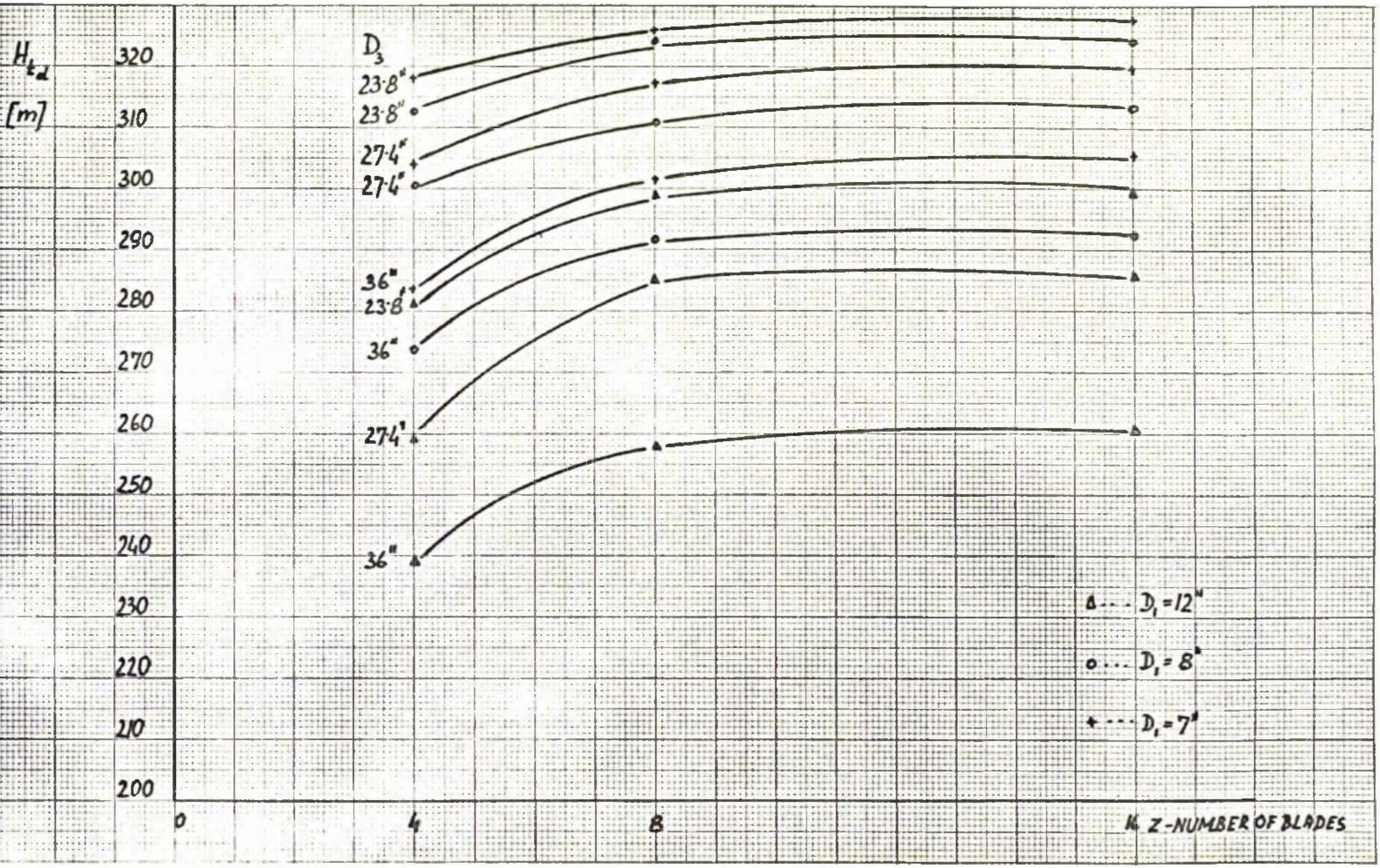

FIG. 32 DISCHARGE: PUMP HEAD

very much higher in a larger casing.

The effect of turbine reaction and pump action should be studied simultaneously. An incorrect conclusion may be drawn if for instance turbine reaction only is considered. It would follow that by increasing the casing diameter, the turbine reaction would be bigger and consequently the power applied to the shaft would be smaller. Such a conclusion is entirely wrong and experimental results confirm that the impeller running in the small casing consumes less power than the impeller running in the large casing. The exchange of power in the impeller and in the casing is far more economical when the smaller casing is used. In short, the "efficiency" of a small casing is higher. These results lead to the similar conclusion arrived at in equation 7.3.

In addition, the output power can be worked out from the data plotted in figures 26, 31, 32. It is found that the power characteristics follow the pattern of the flow characteristics as shown in figure 26.

Studying the behaviour of the recirculatory flow at the discharge, figure 26, no significant differences were observed when the diameter of the suction pipe was changed. This strongly indicates that two separate vortices exist at the suction and at the discharge side.

In figures 23 and 24, the suction pump head and the turbine head are plotted. The turbine head (figure 24) is much higher than the pump head. The turbine head at the suction of the impeller is considered as a loss and cannot be used. On the other hand, the turbine head at the suction side of the impeller can be used as a measure of the efficiency of the turbine reaction.

The behaviour of flow characteristics at the inlet, see figure 21, shows the significant influence of suction pipe diameter. A sudden change in the shape of the flow characteristic, particularly at 12" suction pipe diameter, is probably due to the basic feature of the impeller. The impeller with the larger diameter ratio D_1/D_2 gives a higher specific speed. This is due to a change in the flow which alters the pattern of the impeller characteristics.

Considering the recirculatory flow at the discharge and at the suction, at both sides the same indication is shown with regard to the influence of the volute ring diameter. When the small ring was fitted the recirculatory flow diminished and with the large ring the recirculatory flow was increased considerably.

The conclusion can be made that the pump, when fitted with a large volute ring, was less "throttled" than when used with a small one. Thus, the casing did affect the flow conditions at the suction and at the discharge irrespective of whether the flow lines at both sides were linked or not.

The velocity diagrams obtained by experiments at the discharge and suction indicate a flow motion which is depicted in figure 2. Two separate vortices were found. One close to the back shroud which is spread only along the impeller channel and the other one close to the front shroud extending far along the suction pipe. The extension of the second flow pattern depends on the shape of the suction pipe, the friction and viscous forces governing along the suction pipe.

The question which immediately arises is, where does the back flow have its source? Two explanations can be found which in some cases can be linked together. It is obvious that across the clearance between the fixed volute ring and rotating impeller a high pressure drop exists which can cause the back flow. The clearance itself could be reduced with a more expensive design to the range where no leakage would exist. So the problem of clearance, from a purely hydraulic point of view, is of no importance. But it is understood that the question of clearance as far as the fan is concerned is very important when any results near $Q = 0$ are analysed.

The other source of flow is inside the impeller where inward and outward flow could take place. The experiments confirm that such a flow exists in both directions. The fluid flows through the passage and since there is no external sink it follows that the fluid must find its way back through the rotor channels. The flow taking place from a high pressure region to a lower one explains the work which must be done on the rotor. As a result of the backward flow through the rotor, the turbine reaction and its power applied to the impeller is created.

The performance of the flow conditions along the suction pipe is very much affected by the friction losses. Neglecting friction effect the whirl would continue to spread along the suction pipe unless external forces were called into play. However, due to viscosity the energy of the recirculatory flow is quickly destroyed and brought to rest. The decay of recirculation along the suction pipe clearly shows how powerful the viscous forces are and how rapidly the recirculatory flow dies out. See figure 22.

It is obvious that both the inward and outward flows are influenced by viscous forces and affect each other. This effect can be termed "viscous induction". The distribution of flow along the suction pipe in both annuli can be explained by viscous forces. In figure 33 the flow lines along the suction pipe are depicted and the entire suction pipe is divided into numerous partitions. At sections more distant from the pump less flow passes and finally the position is reached where no flow exists. At that point the energy of the recirculatory flow is entirely destroyed by the viscous forces and by friction on the wall.

The total head plot along the suction pipe reveals the same phenomenon.

Change in total head along the suction pipe at different radii shows how the total head diminished. At a certain section along the suction pipe where the total head becomes equal to the static head, no flow exists. To destroy the recirculation in the suction nozzle a straightener was positioned at the entrance to the impeller. The straightener, with outside diameter 12" had four blades and its

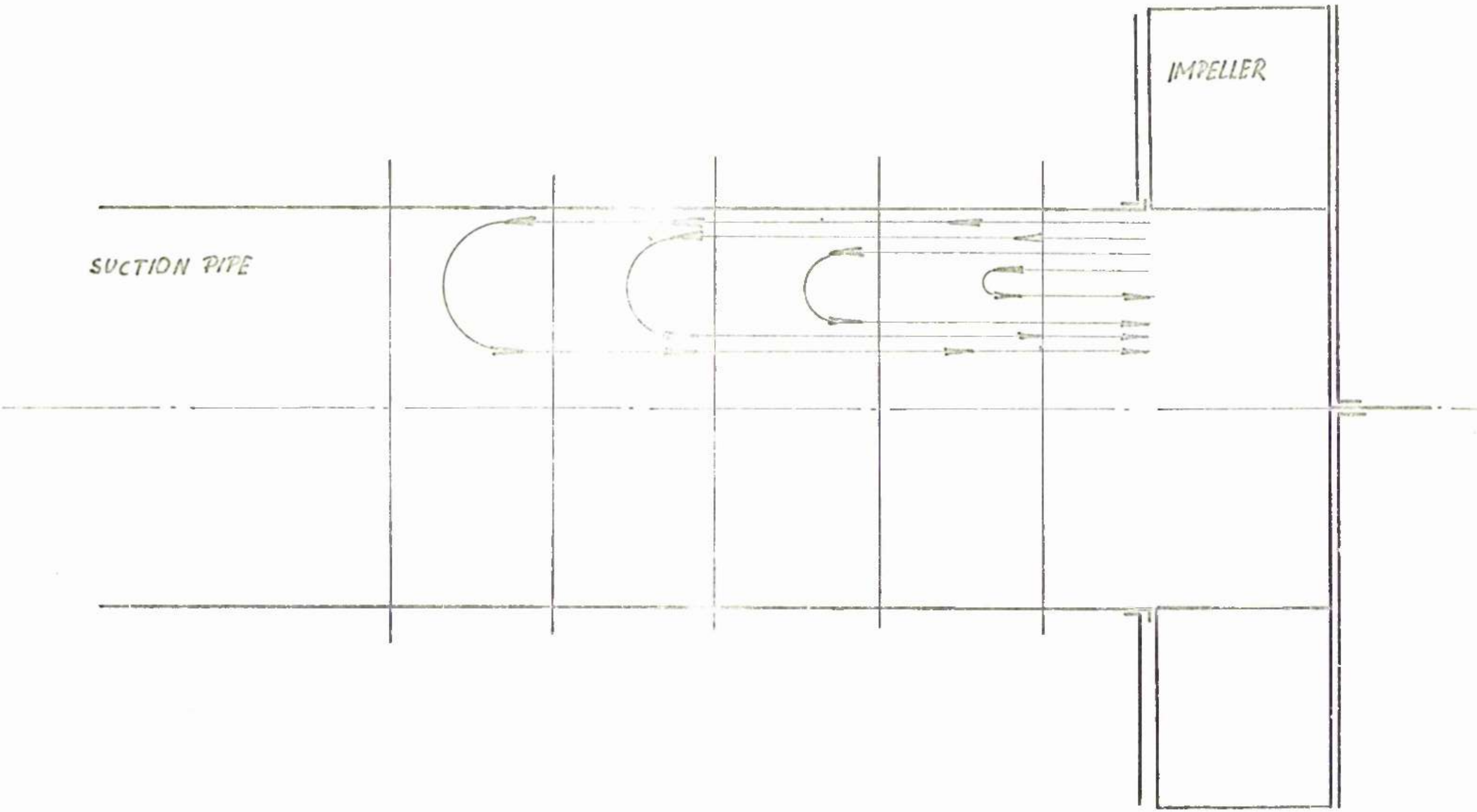

FIG.3 FLOW DISTRIBUTION ALONG THE SUCTION PIPE

chord length was 8". The idea was to see if there would be any change in the total head at the discharge of the impeller. Experiments were made for the following dimensions of impeller:

$D_1 = 12"$ the suction nozzle diameter

$D_2 = 20"$ the impeller diameter

$D_3 = 36"$ the volute ring diameter

$Z = 16$ the number of blades

To see the influence of the position of the straightener on the discharge conditions, the straightener was placed at three different positions with its exist edge close to:

a) the back shroud of the impeller

b) the front shroud of the impeller

c) $0.5 \times D_1$ away from the front shroud of the impeller

Considering position "a" no difference was observed in total head at the discharge regardless of whether the straightener was fitted or not.

Referring to the positions "b" and "c" some points of the total head were scattered but all were in the range of less than 1.5% of the value obtained without straightener which could be due to the technique of measurement. The conclusion can be drawn that at $Q = 0$ the presence of a straightener in the positions mentioned above does not influence the total head at the discharge of the impeller. But, it has to be kept in mind that at any discharge flow where $Q > 0$ the position of the straightener is very important.

Some additional tests were made where the number of blades was changed to $Z = 8$ and with the straightener's exit edge placed at the front shroud of the impeller. No change in total head was noticed at the discharge of the impeller. Although the above-mentioned tests do not give a complete indication that the suction conditions are independent of discharge phenomena, the strong possibility exists that this is so.

More tests with a straightener fitted in the suction pipe should be made to prove the above statement. The author believes that the geometry of the pump plays a very important role.

7.2 Head coefficient at zero flow

The head coefficient ψ expresses the head as a fraction of the maximum theoretical head at zero capacity.

$$\psi = \frac{H}{\frac{u_2^2}{g}} \qquad 7.11$$

The same definition can be applied for the head coefficient at zero discharge but the following notation will be used:

$$\psi = \frac{Ho}{\frac{u_2^2}{g}} \qquad 7.12$$

The Euler's equation gives the head coefficient for any flow rate:

$$\psi = 1 - \phi \cot \beta_2 \qquad 7.13$$

At zero flow equation 7.13 becomes

$$\psi_o = 1 \qquad 7.14$$

where the effect of relative eddy is given by the unique value. This happens when the rotor is in the completely "shut off" condition i.e. when the rotor is shut off from the volute by the insertion of the wrapper around the periphery.

According to Busemann's original equation where the relative eddy formation was taken into account, the head at zero flow is given by:

$$H_o' = h_o \frac{u_2^2}{g} \qquad 7.15$$

The factor h_o depends on the geometry of the impeller i.e. the diameter ratio, the number of blades and the outlet angle.

All the results presented in this thesis will be based on the definition given by the equation 7.12.

The present experiments show that, at no through flow, the discharge is almost independent of the suction conditions. That is the reason why only the discharge total head was taken into account in equation 7.12.

Of course it must be understood that when the suction diameter was altered, the pump was under different conditions and the total head changed.

In figure 34 it is seen that the head coefficient increases when the number of blades is increased. Besides, the head coefficent increases as the volute ring diameter or the suction pipe diameter are

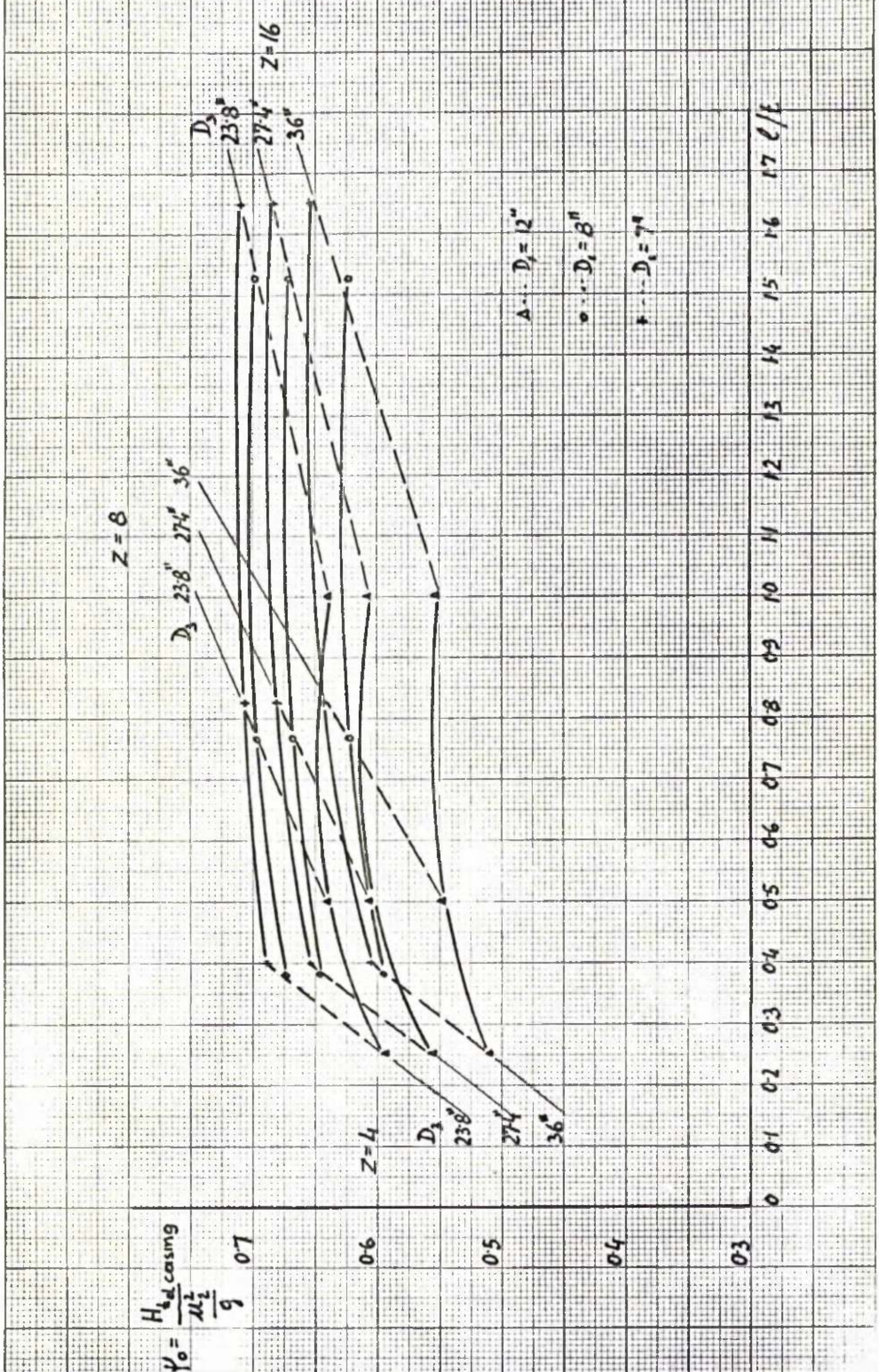

FIG. 34 DISCHARGE COEFFICIENT

decreased.

The explanation for the total head variation already given in chapter 7.1 can be accepted for the head coefficient, with some additional conclusions. Since the discharge angle of the absolute velocity C in the larger casing is bigger than in a small one, the tangential component of the absolute velocity becomes smaller and consequently so does the head coefficient.

The increase in head coefficient obtained by reducing the suction pipe diameter can be explained if one can imagine that the suction diameter is greatly reduced or if a plate with a small hole in the middle is fitted in the suction pipe. Under these conditions any recirculation would be prevented along the suction pipe and the total discharge head would be increased. This is what is observed to happen when the suction pipe diameter is reduced.

A more comprehensive view of the total head coefficient was shown when ψ was plotted against the ratio of the chord length "l" to the vane spacing "t". See figure 34. Straight lines were obtained when the points of the head coefficient referring to the same number of blades and to the same casing were linked together.

In figure 35 the same graph is given to a different scale for volute ring diameter D_3 = 36" only. The lines for a constant number of blades z and a constant suction pipe diameter D_1 are shown. By means of interpolation, additional z -lines and D_1 - lines are obtained which reveal the behaviour of the head coefficient when other parameters are changed. When the l/t ratio is fixed the number of blades z and the suction pipe diameter D_1 can be chosen to

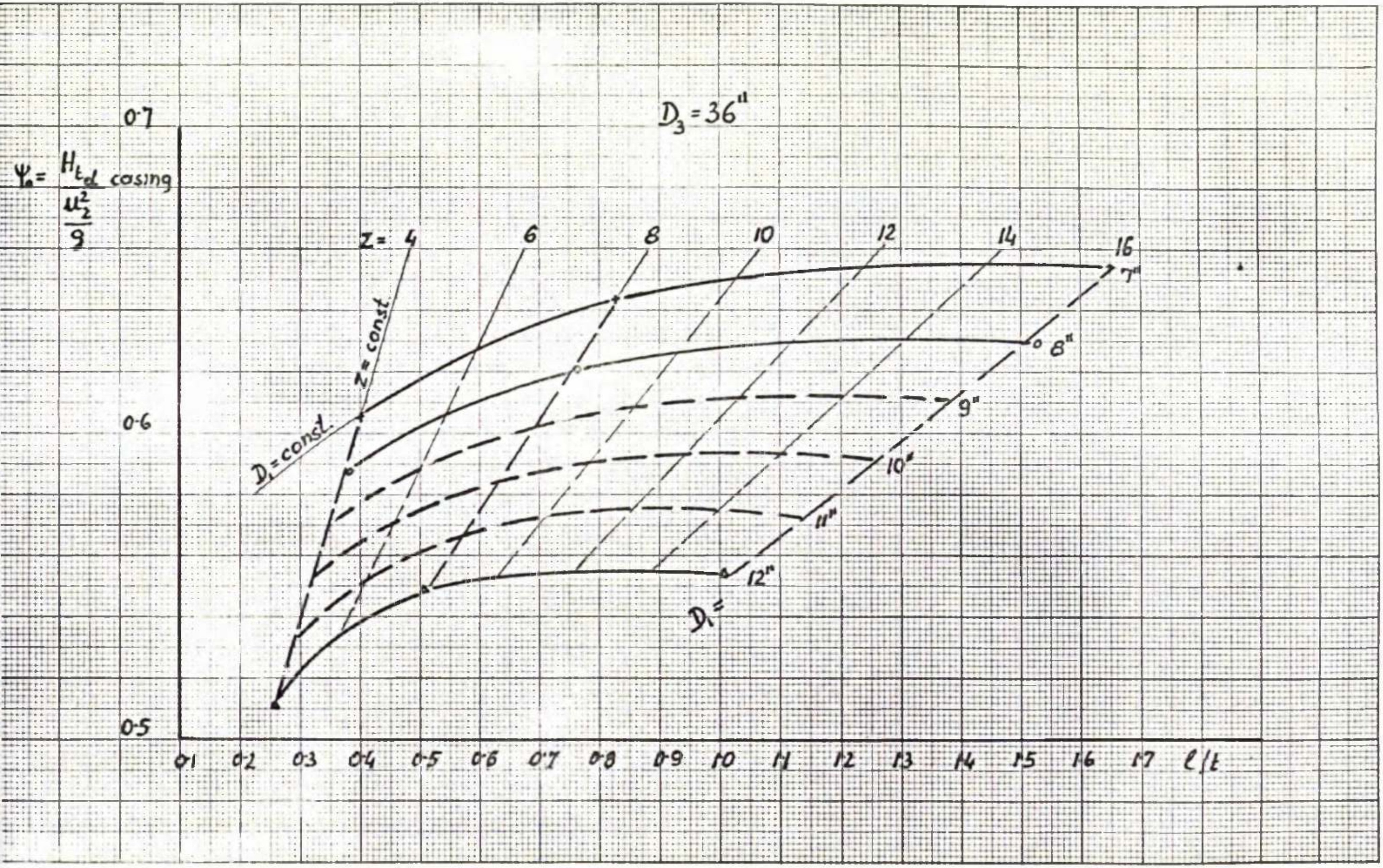

FIG. 35 DISCHARGE COEFFICIENT

suit the desired head coefficient. Although the present tests were made in the cylindrical casing with an impeller having straight radial blades, the head coefficient should not differ greatly from the real value which would be obtained with a spiral casing.

Closely linked to graph 35 is graph 36 where the head coefficient is plotted against the power coefficient.

The ideal head-power characteristic of these impellers is a straight line parallel to the power axis. If the power used to overcome disc friction losses is subtracted, the experimental head-power characteristic shows a certain slope.

Generally, two head-power characteristics are obtained, one for the number of blades $Z = 4$ and the other for the number of blades $z = 8$ & 16. Studying the first characteristic for $Z = 4$, we see that the relationship between the head and power coefficient remains linear regardless of change in the suction pipe diameter or the volute ring diameter. When 8 or 16 blades are used the head coefficient becomes higher, the points are more scattered but all fall within $\pm$ 15% of the mean curve.

At zero power, the head coefficient for $Z = 4$ is equal to $\psi = 0.7$ and for $Z = 8$ & 16 is equal to $\psi = 0.74$. These figures should be very near to the theoretical value of the head coefficient.

The difference in the slope between the theoretical and the experimental head-power characteristics is due to several causes.

One reason for a greater slope is that the flow returning to the impeller returns part of its momentum so that the torque supplied

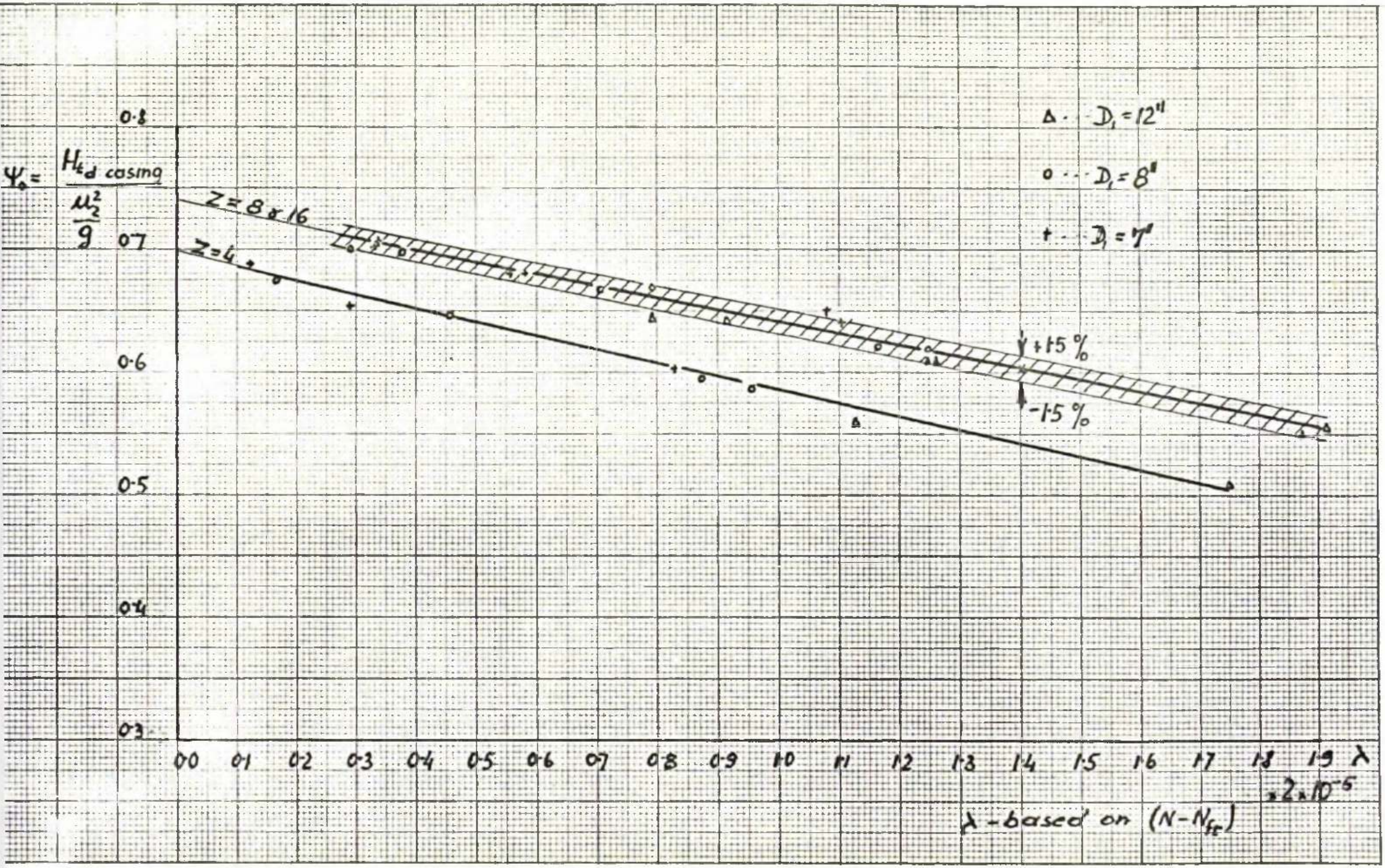

FIG. 36 DISCHARGE v POWER COEFFICIENT

to the shaft is diminished accordingly.

The other reason for this greater slope is that the flow out of the impeller has to return to it and the discharge area is shared equally between inward and outward flow.

7.3 Conclusions drawn from experiments

The following conclusions can be made, based on the experiments:

i) There is a considerable flow through the impeller running at zero discharge and this is why the head generated with the valve closed never attains the theoretical zero flow head of the impeller.

ii) The results prove that two types of flow exist, a flow leaving the impeller and a flow returning into the impeller.

iii) The discharge area where the flow occurs is equally shared between inward and outward flow.

iv) The equation of continuity is satisfied at the suction and at the discharge, although different flow rates were found at each side.

v) A strong indication is given that two separate regions of whirl exist, one at the suction and the other at the discharge.

vi) The decay of recirculation along the suction pipe is very rapid and mostly depends on the viscous forces and partly on friction losses at the wall.

vii) The impeller acts partly as a pump and partly as a turbine. The turbine reaction is very large and reduces the input power considerably.

viii) The input power (less disc friction losses) is spent on losses caused by recirculatory flow and on covering the heat losses.

ix) The geometry of the pump plays an important role in the hydraulic parameters.

a) The circulatory flow increases and the total head decreases in the larger casing.

b) Reduction of the number of blades or increasing the suction pipe diameter causes a drop in the total head.

c) The suction pipe diameter shows negligible effect on the discharge flow.

d) The pump suction head is almost indppendent of the number of blades, but shows a great increase if the volute diameter and/or the suction pipe diameter are increased.

e) The turbine head has a similar behaviour at the suction side to the pump suction head, with the exception that the turbine head was very large.

f) The power applied to the shaft increased when the volute ring diameter, the suction pipe diameter or the number of blades were increased.

g) The head coefficient was found to have a linear relationship with the power coefficient. Two curves were obtained, one referring to the impeller with four blades and the other to the impeller with eight and sixteen blades.

7.4 Theoretical results

The theory developed in chapter 3 is based on two-dimensional ideal fluid motion. The object of developing the theory of the flow in hydrodynamic runners is primarily to derive the information necessary for calculating the runner head from the Euler equation.

How the hydraulic parameters are influenced by the geometry of the pump is shown in figure 37 where the numerical results are plotted.

The velocity distribution around the tip of the impeller is periodic and its period depends on the factor $\frac{2\pi}{Z}$ i.e. the number of blades. For this reason the absolute velocity C expressed non-dimensionally was plotted against $\frac{2\pi}{Z}$.

In figure 37 the velocity distribution expressed as $C/\omega R_2$ is shown for $Z = 4$ and $D_1 = 7''$. In addition the C_{u_2/u_2} coefficient was worked out for the same impeller and plotted in figure 38.

Since the velocity distribution is periodic, it is only necessary to plot and obtain the entire picture of the velocity field for one period.

It was found that by increasing the number of blades, the absolute velocity at the impeller tip was increased and by reducing the diameter ratio an increase in the absolute velocity was obtained. The absolute velocity changes its direction and in half of the area of the impeller channel the angle of the absolute velocity is positive and in the other half the angle is negative. The flow rate evidently follows the same pattern. The conclusion can be drawn that the flow rate in

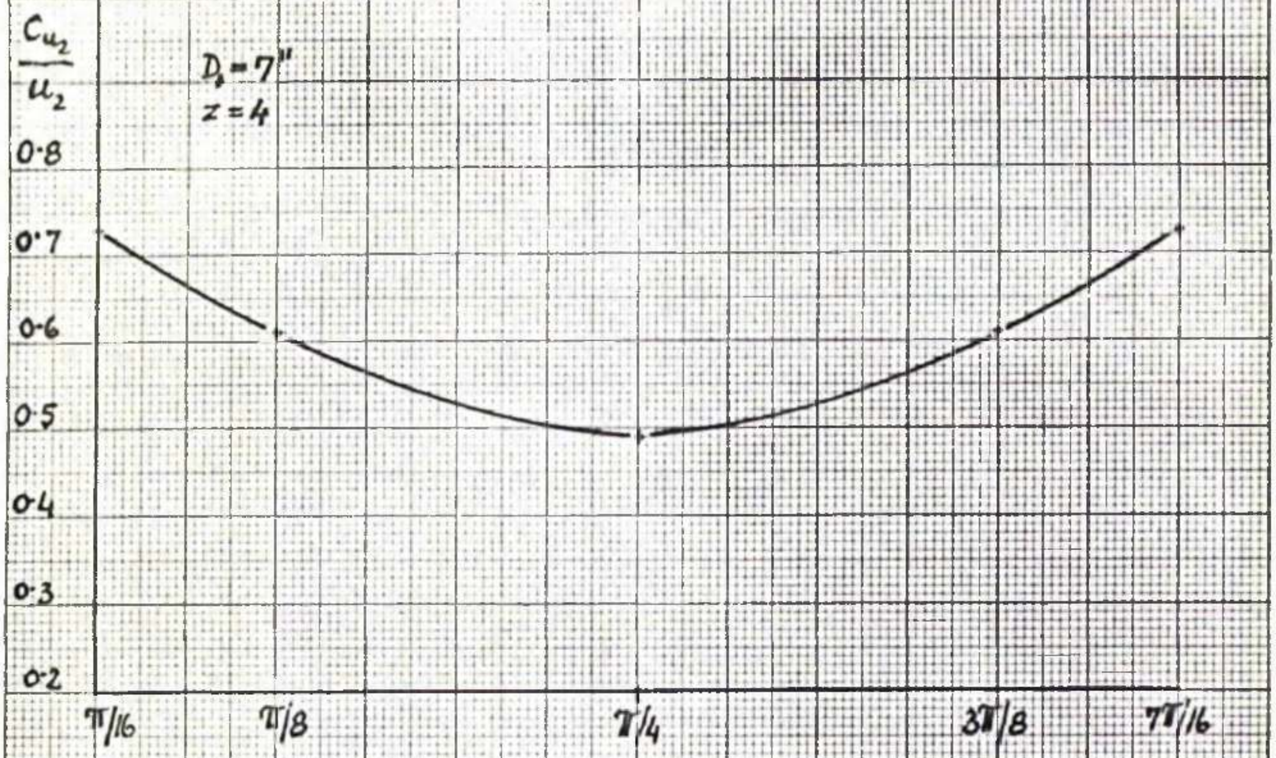

FIG. 38 C_{u_2}/u_2 DISTRIBUTION

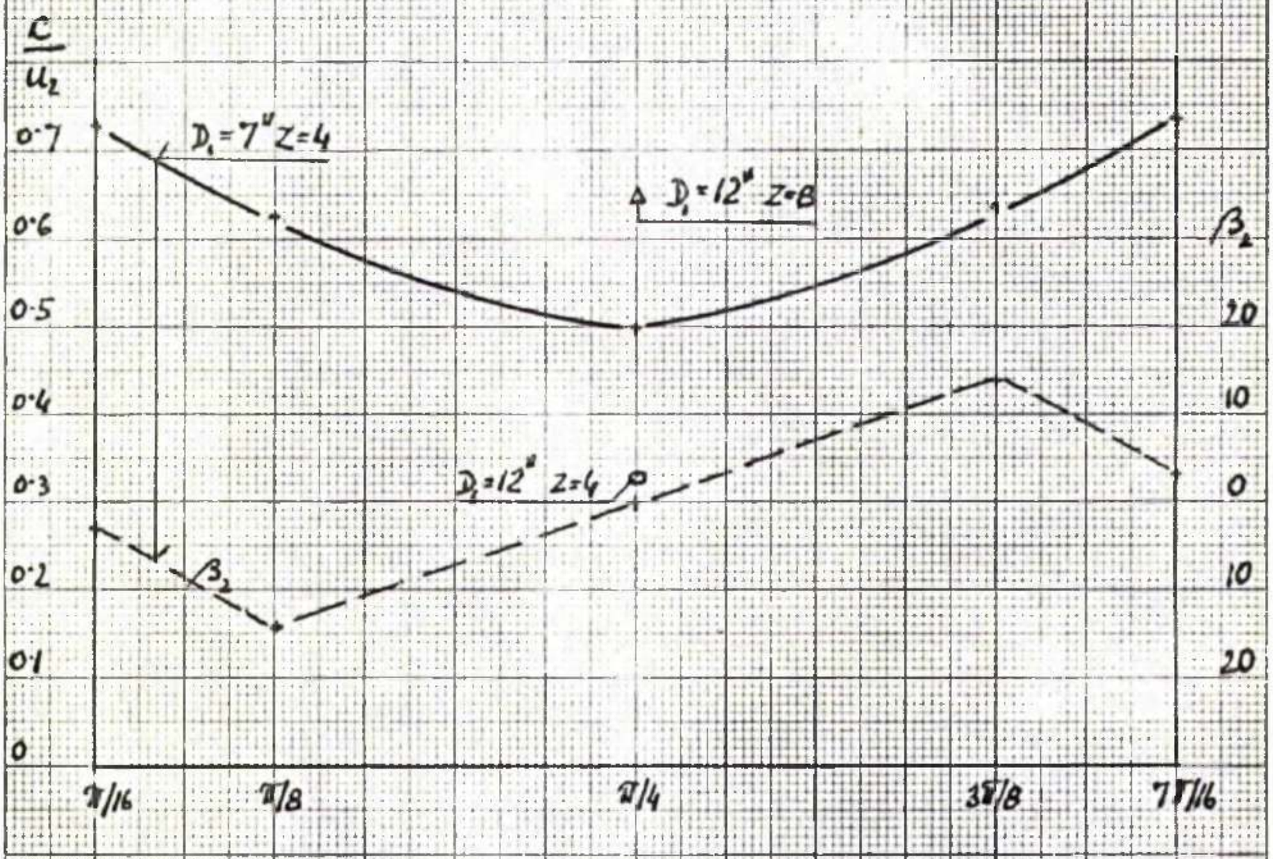

FIG. 37 C/u_2 DISTRIBUTION

the impeller channel is divided into two regions. In one of these the flow leaves the impeller and in the other region the flow enters the impeller. Two separate systems appear to exist which results in the period nature of the flow.

Experiments did not show any indication that such flow exists in the plane perpendicular to the shaft of rotation. No pulsation of the total or static pressure was observed when discharge conditions were checked. One explanation which could be given is that the frequency was too high to be registered by the cylindrical probe.

The basic effect of the diameter ratio and number of blades on the head coefficient is the same as that which was found by experiment. That does not prove that the theory entirely explains the experimental results. The results obtained by theory are referred to the plane perpendicular to the shaft of rotation and the results obtained from the experiments were measured in a plane parallel to the shaft.

In the theory undertaken in chapter 3 the friction effect and the hydraulic losses are not introduced.

The influence of the friction effect can be obtained from the assumption that a certain velocity distribution is given. This does not show the reduction in head of the pump which results from the frictional resistance against the flow through the machine and which is measured by the hydraulic efficiency η_h.

The total head reduction of a centrifugal impeller is given by the product $\eta_h \cdot \psi_{fr} \cdot \psi_i$ where ψ_i denotes an ideal head coefficient applying to the flow of a frictionless fluid. The friction head coefficient ζ_{fr} is based on the discharge velocity profile.

The experimental curve of the velocity distribution at the discharge approximates to sinusoidal shape, particularly when the largest volute ring is used. Using this fact the velocity distribution across the width of impeller can be described by the equation:

$$Cm_2 = Cm_{max} \sin f \qquad 7.16$$

On the assumption that the angular momentum of the fluid at the inlet is zero, the angular momentum at the discharge of the impeller becomes:

$$M_2 = \frac{\gamma}{g} R_2 \int_0^f c_{u_2} c_{m_2} df \qquad 7.17$$

where $c_{u_2} = u_2 - c_{m_2} \cot\beta_2$ 7.18

and f - outlet area.

The equation 7.18 is introduced into equation 7.17

$$M_2 = \frac{\gamma}{g} R_2 \int_0^f \left(u_2 c_{m_2} - c_{m_2}^2 \cot\beta_2 \right) df \qquad 7.19$$

The equation 7.19 was solved by Wislicenus (Ref.4) for similar conditions and its deduction is shown in Appendix 7.1.

The angular momentum is

$$M_2 = \frac{\gamma}{g} Q R_2 \left(u_2 - c_{m_{av}} \frac{\pi^2}{8} \cot\beta_2 \right) \qquad 7.20$$

and the corresponding head

$$H^x = \frac{u_2}{g}\left(u_2 - c_{m_{av.}} \frac{\pi^2}{8} \cot\beta_2\right) \tag{7.21}$$

where

$$\zeta_{fr} = \frac{\left(u_2 - c_{m_{av.}} \frac{\pi^2}{8} \cot\beta_2\right)}{\left(u_2 - c_{m_{av.}} \cot\beta_2\right)} \tag{7.22}$$

It is obvious that in equation 7.20 the angle β_2 was taken to be constant. But the experiments showed that the angle β_2 varied across the whole discharge area and equation 7.21 in the present form cannot be accepted. Besides, the supposition of a sinusoidal distribution of the velocity at discharge is only approximate and cannot be generally applied.

In addition, two different hydraulic systems exist in one impeller, namely those of pump and turbine. This fact which is confirmed by experiments, cannot be solved by the theoretical approach. On the other hand the hydraulic efficiency η_h at $Q = 0$ still remains to be found.

All these facts point to the conclusion that the theoretical approach to determination of the flow and total head distribution, under conditions as complicated as those at $Q = 0$, is not sufficient.

The theory does give some information about the influence of the geometry of the pump on the flow and total head conditions and some details of the nature of the flow but this knowledge seems to be inadequate.

Appendix 7 - I

Impeller discharge area is given by

$$f = 2\pi R_2 b_2$$

where b_2 represents the axial width which can be measured by the co-ordinate X.

One can write

$$df = 2\pi R_2 dX$$

Furthermore, a new axial co-ordinate is introduced,

$$\xi = \pi \frac{X}{b} \qquad \text{so that} \qquad dX = \frac{b}{\pi} d\xi$$

and

$$df = 2R_2 b_2 d\xi \qquad 7.23$$

In equation 7.16 Cm_{max} is replaced by Cm_{av}

$$C_{m_{av}} \cdot b_2 = \int_0^b C_{m_2} dX = \frac{b}{\pi}\int_0^b C_{m_2} d\xi = \frac{C_{m\,max}\; b}{\pi}\int_0^\pi \sin\xi . d\xi$$

so

$$Cm_{max} = \frac{\pi}{2} Cm_{av}$$

and

$$Cm_2 = Cm_{av} \frac{\pi}{2} \sin\xi \qquad 7.24$$

By substitution of the expressions 7.23 and 7.24 into equation 7.19 one obtains

$$M_2 = 2\frac{\gamma}{g} R_2^2 b_2 \left(u_2 C_{m_{av}} \frac{\pi}{2}\int_0^\pi \sin\xi . d\xi - C_{m_{av}}^2 \frac{\pi}{4} \cot\beta_2 \int_0^\pi \sin^2\xi . d\xi \right)$$

from which equation 7.20 is deduced.

8. FUTURE RESEARCH

Looking at the work which has been done already it is seen that only the first step has been made. Many parameters which influence the flow head characteristic were omitted and simplified. Only one type of impeller blade with constant width of impeller channel has so far been investigated.

Before any general conclusion could be made, experimental results for different blade shape and different impeller channel should be obtained. Such work would show the influence of these parameters on the head coefficient. It is obvious that such information would still be basic information revealing the flow condition in the volute ring and could not be applied to a spiral casing such as is usually used in pump design. Therefore, it would be essential to carry out this experiment with a spiral casing at $Q = 0$ and at Q

Having obtained such data it is believed that sufficient information would be available to link the design point with the point where $Q = 0$.

In the future the author intends to do part of this work.